Distribution Agreement

In presenting this thesis or dissertation as a partial fulfillment of the requirements for an advanced degree from Emory University, I hereby grant Emory University and its agents the non-exclusive license to archive, make accessible, and display my thesis or dissertation in whole or in part in all forms of media, now or hereafter known, including display on the world wide web. I understand that I may select some access restrictions as part of the online submission of this thesis or dissertation. I retain all ownership right to the copyright of the thesis or dissertation. I also retain the right to use in future works (such as articles or books) all or part of this thesis or dissertation.

Signature:

_____	_____
Kevin O'Halloran	Date

Controlling the Synthesis of New Polyoxometalates and Removing Their Crystallographic Disorder

By

Kevin P. O'Halloran
Doctor of Philosophy

Chemistry

_____

Craig L. Hill
Advisor

_____

Karl S. Hagen
Committee Member

_____

Cora E. MacBeth
Committee Member

Accepted:

_____

Lisa A. Tedesco, Ph.D.
Dean of the James T. Laney School of Graduate Studies

_____

Date

Controlling the Synthesis of New Polyoxometalates and Removing Their Crystallographic Disorder

By

Kevin P. O'Halloran
Bachelor of Science, University of Kansas, 2006

Advisor: Craig L. Hill, Ph.D.

An abstract of
A dissertation submitted to the Faculty of the
James T. Laney School of Graduate Studies of Emory University
in partial fulfillment of the requirements for the degree of
Doctor of Philosophy in Chemistry
2011

Abstract

Controlling the Synthesis of New Polyoxometalates and Removing Their Crystallographic Disorder

By Kevin P. O'Halloran

Crystallographic disorder encompasses a wide range of frequently-encountered problems in many areas of chemistry. These problems include, but are not limited to, positional disorder, occupational disorder, solvent disorder, libration and twinning. Often, crystallographic disorder is discovered in the early stages of investigation and further efforts with that system are abandoned because the pertinent questions cannot be answered at the resolution provided by a disordered crystal structure. Therefore, this problem deserves quite a bit of attention. In the field of polyoxometalates (POMs), several of these disorder problems are routinely encountered. Many times they are satisfactorily addressed, but other times the data is abandoned because of poor resolution. Therefore, we sought to address this problem for a particular class of POMs where discrete positional disorder is currently limiting research progress. We chose mono-substituted derivatives of three archetypal POMs: Keggin-, Wells-Dawson- and Knoth-type structures. To achieve this, we introduced a covalently-bound phenyltin unit into the polyanion structure and crystallized the resulting complexes (Chapter 1). The results show that the phenyl group effectively removes crystallographically-imposed symmetry elements that cause positional disorder in the unit cells.

The controlled synthesis of molecules is a fundamental principle of many areas of chemistry. In this process, chemical reactions are planned and carried out in a stepwise, logical manner; a process to which many achievements in chemistry owe their discovery. However, many POM complexes are still formed serendipitously from a mixture of various starting reagents. Therefore, the field of POMs would benefit from a controlled synthesis method. This prompted us to develop such a method by the stepwise removal of a tungsten unit from a POM and subsequent replacement with a new metal ion. We achieved this by the hydrolytic decomposition of a polytungstate with the judicious adjustment of pH value and crystallization conditions (Chapter 2). The results show that this method successfully generated three new complexes and may create opportunities for new complexes in POM research.

New polyoxometalates are continually being discovered with applications in various emerging fields of research. Often these POMs contain multiple d-electron-transition metals. We have prepared and characterized six such POMs (Chapter 3).

Controlling the Synthesis of New Polyoxometalates and Removing Their Crystallographic Disorder

By

Kevin P. O'Halloran
Bachelor of Science, University of Kansas, 2006

Advisor: Craig L. Hill, Ph.D.

A dissertation submitted to the Faculty of the
James T. Laney School of Graduate studies of Emory University
in partial fulfillment of the requirements for the degree of
Doctor of Philosophy in Chemistry
2011

Acknowledgments

I would like to extend my sincere thanks to many people who have helped me through this doctoral program. I thank Dr. Craig Hill for working so hard to provide me with the opportunity to conduct exciting research at Emory. I thank my committee members Dr. Karl Hagen and Dr. Cora MacBeth for their generous contributions to my chemical knowledge. I thank all the current and former Hill group members for their exchange of ideas and assistance. I thank all of our collaborating authors on many research projects. I thank my family for supporting me through this entire process. And I thank God, in whom all things are possible.

Table of Contents

CHAPTER ONE: REMOVING COMMON CRYSTALLOGRAPHIC DISORDER IN THREE DIFFERENT MONOSUBSTITUTED POLYOXOMETALATE SYSTEMS ……....1

1.1 ABSTRACT ……..…...1

1.2 INTRODUCTION ……..……...……2

1.3 RESULTS AND DISCUSSION ..…….……..……...…..7

1.4 EXPERIMENTAL ……...….19

General methods and materials ……..……..19

Synthesis of $((CH_3)_2NH_2)_4[Sn(C_6H_5)PW_{11}O_{39}]\bullet 5H_2O$ (**1**) …….…...22

Synthesis of $K_7[Sn(C_6H_5)P_2W_{17}O_{61}]$ (**2**) …….…..23

Synthesis of $((CH_3)_2NH_2)_7[Sn(C_6H_5)P_2W_{17}O_{61}]\bullet 20H_2O$ (**2'**) ……..…..23

Synthesis of $((CH_3)_2NH_2)_6K[Sn(C_6H_5)(H_2O)P_2W_{20}O_{70}(H_2O)_2]\bullet 11H_2O$ (**3**)……..…….…24

X-ray crystallography …….…….…….....25

1.5 CHARACTERIZATION DATA FOR COMPLEXES **1**-**3**…….…….…….....28

1.6 CONCLUSIONS ……..…..39

REFERENCES ……..…..40

CHAPTER TWO: CONTROLLED SYNTHESIS OF A UNIQUE $M_aM_bM_c(PW_9)_2$ SANDWICH-TYPE COMPLEX *VIA* AN UNPRECEDENTED SYNTHETIC ROUTE …….…….48

2.1 ABSTRACT ……...….48

2.2 INTRODUCTION ……..…….…49

2.3 RESULTS AND DISCUSSION ..……..……..…..51

2.4 EXPERIMENTAL ……..…….60

General methods and materials ……..……..60

Synthesis of $Rb_6K_5[Sn(C_6H_5)(H_2O)P_2W_{19}O_{69}(H_2O)]$ (**4**)……..…….61

Synthesis of $Rb_2K_6[(Sn(C_6H_5)(H_2O))_2P_2W_{19}O_{69}(H_2O)]$ (**5**)……...……62

Synthesis of $((CH_3)_2NH_2)Rb_4K_4[Cu(H_2O)Sn(C_6H_5)(H_2O)\text{-}P_2W_{19}O_{69}(H_2O)]$ (**6**)……..…….63

X-ray crystallography……...……...…….…….64

2.5 CHARACTERIZATION DATA FOR COMPLEXES **4-6**…….……..……..69

2.6 CONCLUSIONS ……..……...78

REFERENCES ……..……...79

CHAPTER THREE: MULTI-D-ELECTRON–CONTAINING POLYOXOMETALATES AS USEFUL COMPLEXES IN EMERGING RESEARCH AREAS……...…….…….82

3.1 ABSTRACT ……...…82

3.2 INTRODUCTION ……..…….……82

3.3 RESULTS AND DISCUSSION ..……..85

3.4 EXPERIMENTAL ……101

General methods and materials ……..101

Synthesis of $[(\alpha\text{-}P_2W_{15}O_{56})Mn^{III}_3Mn^{IV}O_3(CH_3COO)_3]$ (**8a**) by the generation of the Mn_4O_3 cluster *in situ*…….…..103

Synthesis of $[(\alpha\text{-}P_2W_{15}O_{56})Mn^{III}_3Mn^{IV}O_3(CH_3COO)_3]$ (**8a**) by fragmentation of $Mn_{12}O_{12}$…….……..103

Synthesis of $K_2Na_{14}[Mn_4(H_2O)_2(P_2W_{15}O_{56})_2]$ (**9**)……...104

Synthesis of $((CH_3)_2N)_4Na_6[O(FePW_{11}O_{39})_2]$ (**10**)……...…..105

Synthesis of $((CH_3)_2N)_7Na_3[O(FePW_{11}O_{39})_2]$ (**11**)……..…..……..105

Synthesis of $Cs_8Na_6[Pd^{II}_3(SiW_9O_{34})_2]$ (**12**)……..106

Synthesis of $K_{11}Na_3[Pd^{II}_3(SiW_9O_{34})_2]$ (**13**)……..107

X-ray crystallography……..…….…..107

3.5 CHARACTERIZATION DATA FOR COMPLEXES **8-13**……...……..113

3.6 CONCLUSIONS …….....120

REFERENCES ……...122

List of Figures

FIGURE 1.1. Combined polyhedral/ball-and-stick representations of polyanions **1a**, **2a**, and **3a** in complexes **1**, **2** and **3**……..…….……7

FIGURE 1.2. Thermal ellipsoid plot and numbering scheme for polyanion **1a** (plotted at 50% probability)…….…..…10

FIGURE 1.3. Packing of polyanion **1a** in the crystal lattice…...……12

FIGURE 1.4. Thermal ellipsoid plot and numbering scheme for polyanion **2a** (plotted at 50% probability)……..…...…….13

FIGURE 1.5. Packing diagram of **2**… ……..…..15

FIGURE 1.6. Thermal ellipsoid plot and numbering scheme for polyanion **3a** (plotted at 50% probability).……...……...…17

FIGURE 1.7. Packing of polyanion **3a** in the crystal lattice……....…18

FIGURE 1.8. FT-IR spectrum of **1**, 2% by weight in KBr……..…….28

FIGURE 1.9. ^{31}P NMR spectrum of **1** in D_2O…….…….29

FIGURE 1.10. TGA weight loss curve of **1**, 16.838 mg sample under inert atmosphere.…...……...…30

FIGURE 1.11. FT-IR spectrum of **2'**, 2% by weight in KBr……..……...…31

FIGURE 1.12. ^{31}P NMR spectrum of **2'** in D_2O…….…….…….32

FIGURE 1.13. TGA weight loss curve of **2'**, 16.8120 mg sample under inert atmosphere……...33

FIGURE 1.14. FT-IR spectrum of **3**, 2% by weight in KBr……..…34

FIGURE 1.15. ^{31}P NMR of **3** in D_2O……..……..35

FIGURE 1.16. TGA weight loss curve of **3**, 12.2783 mg sample under inert atmosphere……...…36

FIGURE 1.17. Combined polyhedral/ball-and-stick representation of **2a** showing the cation-π interaction of the phenyl ring with two potassium ions (K2 and K6)……..37

FIGURE 1.18. Cation-π interactions of K2 (top) and K6 (bottom) in **2**……..…38

FIGURE 2.1. Thermal ellipsoid plot and numbering scheme of the polyanion of **4** (plotted at 50% probability)…….....52

FIGURE 2.2. Thermal ellipsoid plot and numbering scheme of the polyanion of **5** (plotted at 50% probability)…….....56

FIGURE 2.3. Thermal ellipsoid plot and numbering scheme for the polyanion of **6** (plotted at 50% probability)…….....57

FIGURE 2.4. Schematic illustration of the $\{M_aM_bM_c(A\text{-}PW_9O_{34})_2\}$ sandwich-type structure.....59

FIGURE 2.5. FT-IR spectrum of **4**……...…69

FIGURE 2.6. ^{31}P NMR of **4** in D_2O.....…70

FIGURE 2.7. TGA weight loss curve of **4**…….....71

FIGURE 2.8. FT-IR spectrum of **5**....……...……72

FIGURE 2.9. ^{31}P NMR of **5** in D_2O……..…73

FIGURE 2.10. TGA weight loss curve of **5**…….……..…74

FIGURE 2.11. FT-IR spectrum of **6**…….75

FIGURE 2.12. ^{31}P NMR of **6** in D_2O…….....76

FIGURE 2.13. TGA weight loss curve of **6**.....……77

FIGURE 3.1. Ball-and-stick representation of **7** derived from X-ray data……...…86

FIGURE 3.2. Left: The cubane $[Mn^{III}_3Mn^{IV}O_3X]^{6+}$ motif (X: monoanion ligand) common to many Mn_4 SMMs. Right: Structure of polyanion complex **8** (plotted at 50% probability)……...…...…87

FIGURE 3.3. Temperature-dependence of xT for **8a** (0.1 T).……..89

FIGURE 3.4. Thermal ellipsoid plot and numbering scheme for the polyanion of **9** (plotted at 50% probability)…….....93

FIGURE 3.5. Combination polyhedral/ball-and-stick representation of the polyanion of **9**……..95

FIGURE 3.6. Thermal ellipsoid plot and numbering scheme for the polyanion of **10** (plotted at 50% probability)…….97

FIGURE 3.7. Thermal ellipsoid plot and numbering scheme for the polyanion of **11** (plotted at 50% probability)…….....97

FIGURE 3.8. Thermal ellipsoid plot and numbering scheme for the polyanion of **12** (plotted at 50% probability)…….99

FIGURE 3.9. Thermal ellipsoid plot and numbering scheme for the polyanion of **13** (plotted at 50% probability). …….100

FIGURE 3.10. In-phase ac magnetization component m' of **8a** (24.06 mg) for frequencies ranging from 10 to 1500 Hz between 1.8 and 5 K in the absence of a dc bias field, illustrating the lack of frequency dependency……..……113

FIGURE 3.11. Calculated energies of the zero field-split substates belonging to the ground state of **8a**……..…114

FIGURE 3.12. Arrangement of cluster anions in a unit cell of **8a**…..……115

FIGURE 3.13. ^1H NMR spectrum of **8a** in D_2O……116

FIGURE 3.14. ^{31}P NMR spectrum of **8a** in D_2O……117

FIGURE 3.15. TGA and simultaneous DTA graphs of **8a** (10 K/min, 60 ml N_2/min)……...118

List of Tables

TABLE 1.1. Bond distances and angles of the Sn centers in complexes **1**, **2** and **3**…11

TABLE 1.2. Crystal data and structural refinement for the X-ray structures of **1** and **2**……26

TABLE 1.3. Crystal data and structural refinement for the X-ray structure of **3**.……27

TABLE 2.1. Crystal data and structural refinement for **4a** and **4b**.....…67

TABLE 2.2. Crystal data and structural refinement for **5**.....68

TABLE 2.3. Crystal data and structural refinement for **6**.....69

TABLE 3.1. Bond distances and angles for **10** and **11**….....96

TABLE 3.2. Crystal data and structural refinement for **8** and **9**.……...110

TABLE 3.3. Crystal data and structural refinement for **10** and **11**……111

TABLE 3.4. Crystal data and structural refinement for **12** and **13**……112

List of Abbreviations

Å	Angstrom
a, b, c	unit cell axial lengths
bpy	bipyridine
br	broad intensity stretch (FT-IR)
°C	degrees Celsius
C	carbon
calcd.	calculated
CCD	charge-coupled device
CIF	crystallographic information file
cm^{-1}	reciprocal centimeter
DMA	Dimethylammonium, $(CH_3)_2NH_2^+$
eq., equiv.	equivalent
Fe	iron
F.W.	formula weight
F(000)	structure factor for the unit cell; it is equal to the total number of electrons in the unit cell
FT-IR	Fourier transform infrared spectroscopy
g	gram(s)
Ge	germanium
h	hour(s)
H	hydrogen
Hf	halfnium
Hz	Hertz
ICP-OES	Inductively coupled plasma emission spectroscopy
K	potassium
^oK	degrees Kelvin
L	ligand
m	medium intensity stretch (FT-IR)
M	molarity
mg	milligram(s)
MHz	megahertz
M.W.	molecular weight
min	minute(s)
mL	milliliter(s)
mmol	millimole
Mn	manganese
mol	mole
N	nitrogen
Na	sodium
nm	nanometer
NMR	nuclear magnetic resonance spectroscopy
O	oxygen
OAc	acetate
P	phosphorus

Pd	palladium
pH	potential of hydrogen, a measure of the acidity or alkalinity of a solution
Ph	phenyl, C_6H_5
POM	polyoxometalate
ppm	part per million
R	discrepancy index for crystal structure refinement
s	strong intensity stretch (FT-IR)
s, sec	second(s)
sh	shoulder (FT-IR)
Si	silicon
Sn	tin
TBA	tetrabutylammonium
TGA	thermogravimetric analysis
UV	ultraviolet
V	volume of the unit cell
vs	very strong intensity stretch (FT-IR)
W	tungsten
w	weak intensity stretch (FT-IR)
Z	number of molecules per unit cell
α, β, γ	interaxial angles between unit cell vector b and c, a and c, and a and b, respectively
δ	chemical shift (expressed in ppm for NMR)
ε	molar extinction (or absorption) coefficient, units $M^{-1}cm^{-1}$
θ	the glancing angle of the X-ray beam to the "reflecting plane"
λ	wavelength
μ	the total linear absorption coefficient (with unit of cm^{-1})
μL	microliter

Chapter 1: Removing Common Crystallographic Disorder in Three Different Monosubstituted Polyoxometalate Systems

1.1 Abstract

Three new phenyltin-substituted polyoxometalates, $((CH_3)_2NH_2)_4[Sn(C_6H_5)PW_{11}O_{39}]$ (**1**), $K_7[Sn(C_6H_5)P_2W_{17}O_{61}]$ (**2**), and $((CH_3)_2NH_2)_6K[Sn(C_6H_5)(H_2O)P_2W_{20}O_{70}(H_2O)_2]$ (**3**), have been synthesized and characterized by single crystal X-Ray diffraction studies, ^{31}P and ^{1}H NMR spectroscopies, and FT-IR spectroscopy. Significantly, the covalently-incorporated phenyltin group in all three complexes is not positionally disordered. This strategy solves a longstanding problem of crystallographic disorder in polyoxometalate chemistry. In the examples presented herein the $[Sn(C_6H_5)]^{3+}$ group can be unambiguously determined and refined anisotropically with full occupancy in X-ray crystallography, a result that is very unusual for mono-substituted polyoxometalates and in particular for polytungstates. Three factors account for the disorder-free nature of the mono-phenyltin-substituted polyanion structures: (1) the steric bulk and rigidity of the phenyl group, (2) hydrogen bonding and (3) cation-π interactions between the phenyl ring and counter cations. These results demonstrate the ability of a phenyl group to remove the crystallographically-imposed positional disorder nearly always seen in mono-substituted polyoxometalates, an attribute that usually renders structural and structure-related reactivity studies of this large class of polyoxometalates quite difficult.

1.2 Introduction

Polyoxometalates (POMs) are a large class of early d^0 transition metal-oxide clusters whose structural and dynamic properties model those of industrially important redox-active metal oxides including TiO_2 and CeO_2.[1-7] The high charge density values on the atoms of POMs make their alkali earth metal salts easily soluble in water and if the counter cations are exchanged for those containing alkyl chains they become soluble in organic solvents as well. Because of this wide range of solubility and the molecular aspects of POMs, they can be effectively studied by several structural methods including single crystal X-ray diffraction, neutron diffraction and a variety of spectroscopic techniques. Moreover, the physical and chemical properties of the individual POMs can be extensively tuned (e.g. by changing central heteroatoms or counter cations). This ensemble of attributes has made POMs studied for over 100 years and much more intensely investigated in recent years. Many d^n (where n = 1-9) transition-metal-substituted derivatives of POMs are effective catalysts for either homogenous or heterogeneous oxidations of organic substrates,[8-14] and recently, Ru-, Co- and Ir-substituted POMs have been shown to be fast and oxidation-resistant soluble catalysts for the oxidation of water to dioxygen.[15-19] The structural properties of POMs, as revealed by X-ray crystallography, are also of major fundamental interest. Transition-metal-substituted polyoxometalates have been shown to adopt the chirality of small organic molecules,[20] assemble into porous/open frameworks,[21] and effectively coordinate hydrogen peroxide[22] (an intermediate hypothesized in many important biological and oxidative pathways,[23] among others.

Defect (or lacunary) POMs can covalently incorporate d-electron or d^0 transition metal centers which re-forms their plenary structures. Monovacant polytungstates are good inorganic ligands for several reasons: (1) they and their mono-transition-metal-substituted derivatives are stable in both solid and solution phases; (2) they are tetra- or penta-dentate ligands which dictate large association constants with transition metal ions; (3) they are good σ-donating and π-accepting ligands able to stabilize high valent transition metal centers;[24-28] (4) their reactions with transition metal ions are predictable (there is only one coordination site, and their product complexes are stable in solution, etc.); and (5) they can accommodate a large variety of metal ions including p-, d- and f-block metal elements. For these and other reasons, monovacant polytungstates have been widely used to form mono-substituted POMs which typically are hydrolytically stable, oxidatively robust and effective catalysts for the oxidation of organic substrates including thiols, alkenes and alcohols[29-33] including some oxidations that proceed using only O_2.[9-14, 34-38]

However, largely due to the crystallographic disorder a longstanding problem in mono-substituted POM chemistry exists. As a result of crystallographically-imposed high symmetry elements few mono-substituted POMs have been structurally characterized, and as a result, little structural information of the substituted metal center is known. For example, mono-substituted complexes of the Keggin type, $[MPW_{11}O_{39}(H_2O)]^{n-}$ (M = transition metal or lanthanide metal center), which are the most widely studied class of metal-substituted POMs, typically crystallize in high symmetry (e.g. cubic) space groups because of the intrinsically high symmetry of the polyanion units themselves and the nearly identical geometrical features of the

substituted metal site versus the 11 tungsten sites in the polyanion. The substituted site is almost invariably twelve-fold positionally disordered over the 12 metal positions. As a result, the bond distances and angles around the substituted d^n transition metal site and the identity of any ligands on this site are very difficult to determine. This, in turn, makes it problematical to insightfully probe the key structural intermediates present in many reactions catalyzed by these metal-substituted POMs.[39] Additional data provided by EPR,[40] XANES and EXAFS,[41, 42] and 2D NMR spectroscopies[43] on mono-substituted Keggin POMs have helped characterized the structures of these fairly ubiquitous compounds but the lack of disorder-free crystal structures remains a major impediment to detailed studies. Many studies have focused on obtaining structures of positional-disorder-free-mono-substituted Keggin complexes by X-ray diffraction but with only very limited success which will be described below.

Several existing reports detail a transition metal occupying one unique site in dimers or trimers[44-50] as well as covalently-linked chains of Keggin units.[51-57] However, these examples do not represent true, isolated Keggin ions. Of the examples where the Keggin unit does exist as a single, isolated entity, nearly all exhibit disorder.[48, 55, 58, 59] A few studies have revealed isolated mono-substituted Keggin units with no positional disorder: Kortz and co-workers reported $[Ru(dmso)_3(H_2O)XW_{11}O_{39}]^{6-}$ (X = Ge, Si) which contains a chain of 5 sodium ions connecting two equivalent Ru-substituted Keggin units in the crystal lattice.[60] Peng and co-workers reported $[Co(H_2O)_4(4,4'\text{-bpy})]_2(4,4'\text{-Hbpy})_2[SiW_{11}Co(4,4'\text{-bpy})O_{39}]^{6-}$ (bpy = bipyridine) where the substituted Co atom is bound to a pyridine molecule that

exhibits π-π interactions with three $\{[Co(H_2O)_4(4,4'\text{-bpy})]^{2+}\}_n$ chains running parallel to the Keggin units.[61] Another example from Peng's group is $[PW_{11}O_{39}Co(pbpy)]^{5-}$ (pbpy = 5-phenyl-2-(4-pyridinyl)pyridine) which makes use of a long antenna ligand and extensive hydrogen bonding and π-π interactions to orient the polyanions in the crystal lattice.[62] Proust and co-workers showed a disorder-free Ru(*p*-cymene) unit in $[PW_{11}O_{39}\{Ru(p\text{-cymene})(H_2O)\}]^{5-}$ where the ruthenium is bound to two oxygen atoms of the POM framework and the authors describe this as an "end-on" coordination mode.[63] Drain, Francesconi and co-workers used a large bulky ligand, *meso*-tetra(4-pyridyl)porphyrin (tpyp), to obtain the complex $[Hf(tpyp)PW_{11}O_{39}]^{5-}$.[64] In this case the porphyrin ligand bound to the Hf atom forms hydrogen bonds with solvent molecules to achieve a disorder-free structure. These five examples represent rare cases of mono-substituted Keggins that do not display positional disorder of the incorporated transition metal center; the weak interactions in the crystal lattice and the steric nature of the bound ligand are responsible for breaking down the high symmetry elements.

For the Wells-Dawson structure, two possible isomers result from the removal of one $[W=O]^{4+}$ unit, either from the belt position (to give the α_1 isomer) or from the cap position (to give the α_2 isomer). The incorporation of a transition metal into the α_1 isomer usually results in positional disorder among the multiple positions in the belt except in cases where dimers or chains of polyanions form.[45, 52, 65-68] Similarly, a substituted transition metal in α_2 isomer is also usually positionally disordered among the three positions in the cap except where dimers or chains are formed.[65, 69-71] A di-

substituted, isolated α_2-P_2W_{17} was reported where the vacant site is occupied by two adjacent organosilyl groups resulting in a disorder-free complex.[72, 73]

The Knoth structure, $[P_2W_{21}O_{71}(H_2O)_3]^{6-}$, is abbreviated henceforth as $\{P_2W_{21}\}$ and consists of two symmetry-equivalent $[A\text{-}\alpha\text{-}PW_9O_{34}]^{9-}$ units linked by three $[O{=}W(H_2O)]^{4+}$ units.[74] When one of the three $[O{=}W(H_2O)]^{4+}$ units in the central belt is removed, the vacant site can be filled by a transition metal which is typically disordered over the three bridging sites due crystallographically-imposed symmetry elements. As a result, the structural information of the substituted transition metal center cannot be unambiguously determined.[75] To the best of our knowledge, no mono-substituted Wells-Dawson or Knoth-type structure has been isolated as a single unit without positional disorder of the substituted metal center.

To overcome these crystallographic challenges, we sought to incorporate a covalently bound phenyltin group into the polyanion unit to lower the crystallographic symmetry of the resulting complexes. The steric bulk and rigid nature of the phenyl group and its possible interaction with solvent molecules and counter cations in the crystal lattice can direct the orientation of the polyanion units. Phenyltin-, organotin- and phenylantimony-substituted POMs have been reported,[76-84] but all contain two or more organometal units per POM molecule. The originality of this report therefore is twofold: (1) three new POMs are reported that are the first examples of mono-substituted phenyltin POMs to be characterized by single crystal X-ray diffraction, and (2) these complexes each represent the only (or a rare) example of an isolated, mono-substituted and disorder-free polyanion in each of their respective families.

1.3 Results and Discussion

Synthesis

All three complexes are synthesized by using a general procedure involving the addition of a slight excess of $(C_6H_5)SnCl_3$ to the appropriate monovacant polytungstate in aqueous solution at room temperature. Tin oxide is produced as a side product and is filtered off after stirring the reaction mixture for 20 minutes. All three complexes show successful incorporation of the phenyltin group into the polyanion unit (Figure 1.1). The complexes in this chapter are designated by a number while their respective polyanions are designated by that number followed by a letter (for instance, **1a** is the polyanion in **1**.)

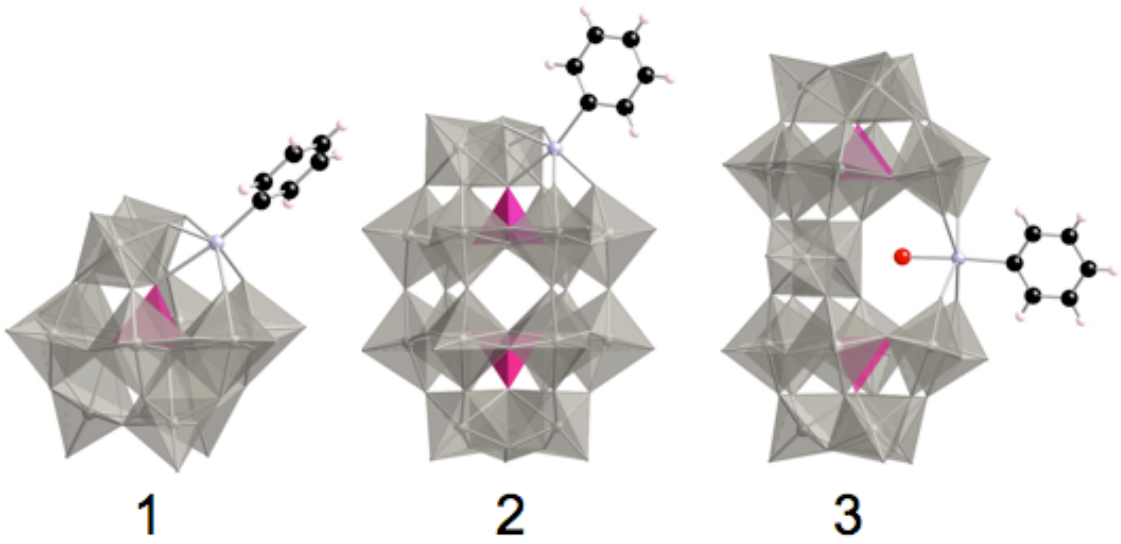

Figure 1.1. Combined polyhedral/ball-and-stick representations of polyanions $[Sn(C_6H_5)PW_{11}O_{39}]^{4-}$ (**1a**), $[Sn(C_6H_5)P_2W_{17}O_{61}]^{7-}$ (**2a**), and $[Sn(C_6H_5)(H_2O)P_2W_{20}O_{70}(H_2O)_2]^{7-}$ (**3a**) in complexes **1**, **2** and **3**. The WO_6 and PO_4 polyhedra are shown in gray and pink. The Sn, O, C and H atoms are shown in light blue, red, black and white, respectively.

The complex $((CH_3)_2NH_2)_4[Sn(C_6H_5)PW_{11}O_{39}]\bullet 5H_2O$ (**1**) is isolated as colorless prisms after the addition of dimethylammonium chloride (DMA^+Cl^-) and LiCl to the reaction mixture and evaporation at room temperature. The use of both DMA^+ and Li^+ in the crystallization process is important because the resulting polyanion $[Sn(C_6H_5)PW_{11}O_{39}]^{4-}$ is very insoluble in water as a DMA^+ salt whereas Li^+ increases its solubility in water. While Li^+ is not present in the final isolated product (all 4 DMA^+ cations were located in the X-ray structure and confirmed by elemental analysis), the presence of Li^+ slows precipitation of **1**, allowing for the formation of X-ray diffraction quality crystals. The ^{31}P NMR spectrum of **1** shows a singlet at -11.53 ppm which confirms the purity of its bulk sample.

The polyanion $[Sn(C_6H_5)P_2W_{17}O_{61}]^{7-}$ (**2a**) is synthesized by the addition of 1.1 equivalents of $(C_6H_5)SnCl_3$ to the α_2 isomer of the monovacant Wells-Dawson, $[P_2W_{17}O_{61}]^{10-}$, in aqueous solution. The crystals are grown by placing the reaction mixture in a chamber to facilitate slow ethanol vapor diffusion into the water. After several days a crystal suitable for X-ray diffraction was mounted and determined to be $K_7[Sn(C_6H_5)P_2W_{17}O_{61}]$ (**2**). The low yield from the diffusion method prompted us to design a synthesis by evaporation after the addition of DMA^+Cl^- to provide long, light blue needles of $((CH_3)_2NH_2)_7[Sn(C_6H_5)P_2W_{17}O_{61}]$ (**2'**) in higher yield. The identity and purity of these samples were confirmed by ^1H and ^{31}P NMR, and FT-IR spectroscopies. They were identical to those from the crystals used for single crystal X-ray diffraction studies. The ^{31}P NMR spectrum shows two singlets at -13.18 ppm and -9.47, a result consistent with the X-ray studies showing one proximal and one distal phosphorus atom in each polyanion unit.

The complex $((CH_3)_2NH_2)_6K[Sn(C_6H_5)(H_2O)P_2W_{20}O_{70}(H_2O)_2]$ (**3**) is synthesized by the addition of 1.1 eq. $(C_6H_5)SnCl_3$ to $[P_2W_{20}O_{70}(H_2O)_2]^{10-}$ and is isolated as colorless prisms after the addition of dimethylammonium chloride and evaporation of the reaction mixture at room temperature. The ^{31}P NMR spectrum of **3** shows one singlet at -13.40 which confirms its purity.

X-ray structure of 1

X-ray diffraction studies of **1** show that the Sn(IV) atom resides in a distorted C_{4v} local environment slightly different from the W(VI) centers in the polyanion unit (Figure 1.2). The four equatorial oxygens that define a square plane around the Sn atom have an average distance of 2.038 Å from the Sn center. This is about 0.14 Å longer than the average W-O_{eq} distance which is expected for a tetravalent (Sn^{4+}) metal ion rather than a hexavalent (W^{6+}) metal ion. The doming distance is the distance that a metal center is displaced out of the equatorial plane defined by the four equatorial oxygens toward the terminally bonded group, which is the phenyl group in this case. The doming distance of Sn in **1** is 0.49 Å, which is on average 0.09 Å longer than the W centers in this structure and in the parent Keggin complex.[85] The two axial ligands of tin are a carbon atom from the phenyl ring and an internal μ_4-oxo that is shared between the central phosphorus, two tungstens, and the tin atom. The C-Sn-O_{trans} bond angle (O_{trans} is the μ_4-oxo bound to Sn) is not linear (171.4(3)°), a structural feature shared in all three complexes (Table 1.1).

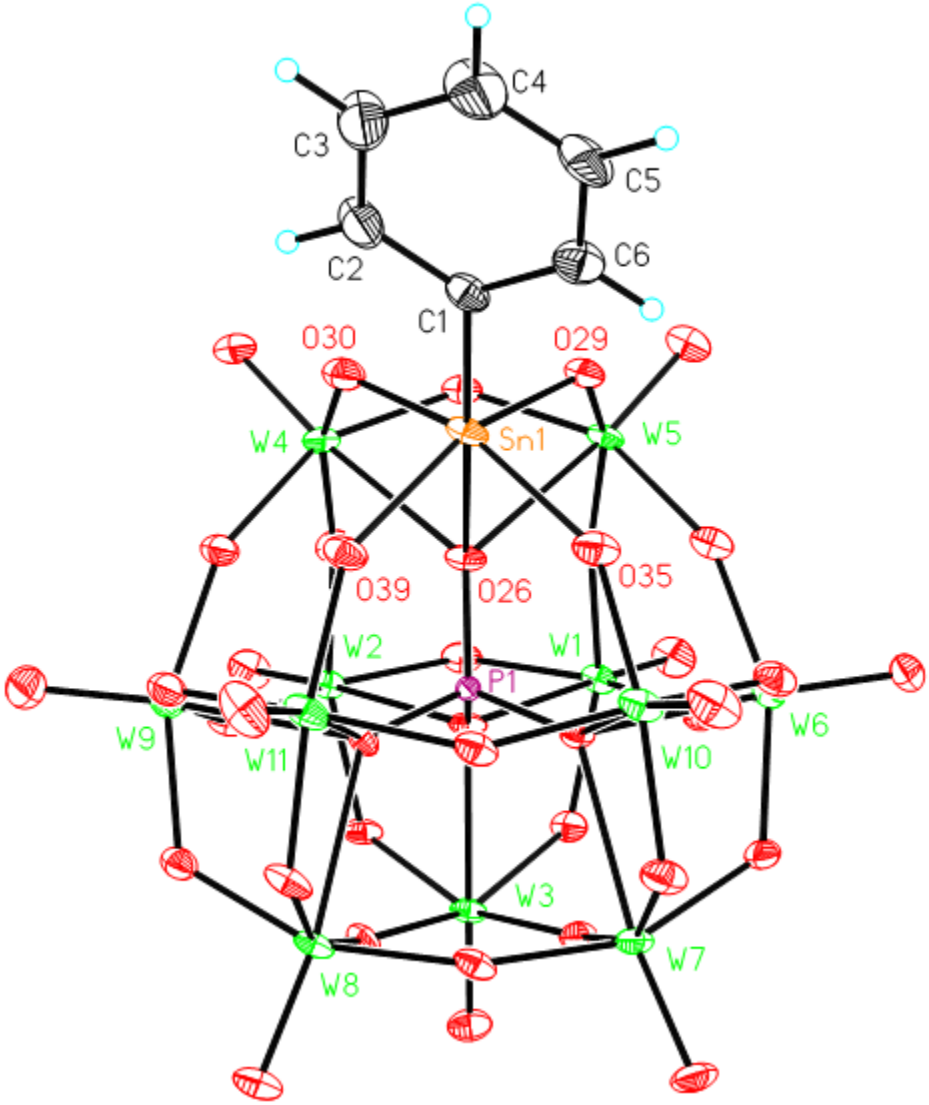

Figure 1.2. Thermal ellipsoid plot and numbering scheme for polyanion **1a** (plotted at 50% probability).

Table 1.1. Bond distances and angles of the Sn centers in complexes **1**, **2** and **3**.

	1	**2**	**3**
$Sn\text{-}O_{eq.}$ (Å)	2.041(6) 2.057(6) 2.037(6) 2.016(6)	2.073(6) 2.053(6) 2.049(6) 2.039(6)	2.090(10) 2.066(10) 2.083(10) 2.092(10)
Sn-C (Å)	2.097(8)	2.104(9)	2.017(14)
$Sn\text{-}O_{axial}$ (Å)	2.487(5)	2.308(6)	2.091(16)
$C\text{-}Sn\text{-}O_{trans}$ (°)	171.4(3)	165.5(3)	176.7(6)
Sn doming distance (Å)	0.49	0.35	0.30

The packing of **1** in the crystal lattice (Figure 1.3) shows alternating columns of phenyl rings and columns of polyanions, an interesting feature also present in the structure of $[\{(C_6H_5)Sn(OH)\}_3(A\text{-}\alpha\text{-}GeW_9O_{34})]^{4-}$ by Kortz and co-workers who describe this as a "sequence of hydrophobic and hydrophilic regions".[84] There is a weak contact between H4 (Sn-phenyl) of one polyanion to a terminal oxo, O17, of a neighboring polyanion. There are also strong hydrogen bonds between the DMA^+ molecules and the polyanion unit: the distance of N2S-O15 is 2.878(14) Å, and the angle of N-H-O is 139.6°; the distance of N1S-O36 is 2.778(11) Å, and the angle of N-H-O is 144.4°. These multiple, strong hydrogen bonding interactions between the DMA^+ counter cations, solvent water molecules and the polyanion unit very likely direct the orientation of the POM during crystal growth and afford a positionally disorder-free crystal structure.

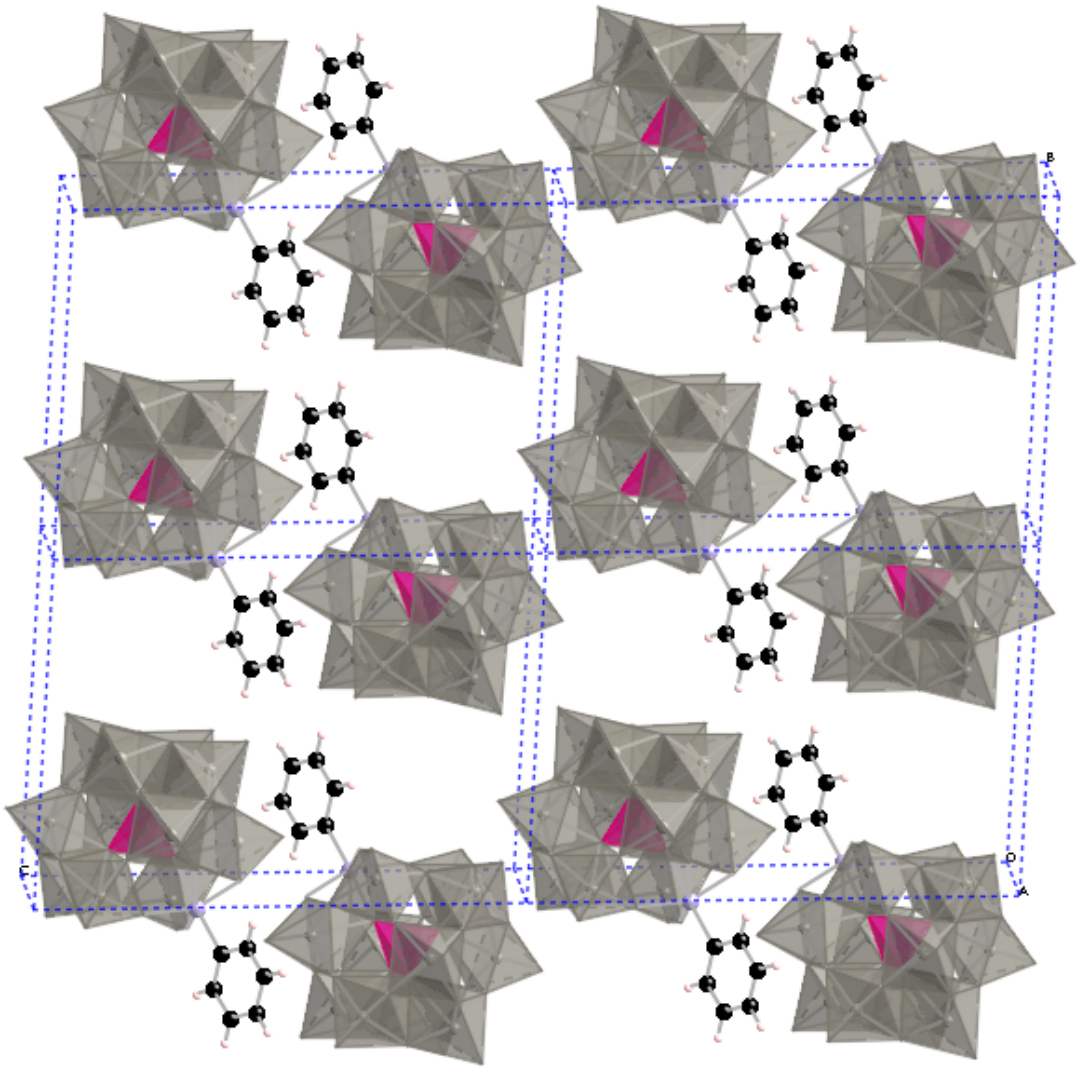

Figure 1.3. Packing of polyanion **1a** in the crystal lattice. Solvent molecules and counter cations omitted for clarity.

X-ray structure of 2

X-ray studies of **2** show that the Sn center has similar structural features to **1** (Figure 1.4). The four equatorial oxygen atoms around the Sn(IV) atom have an

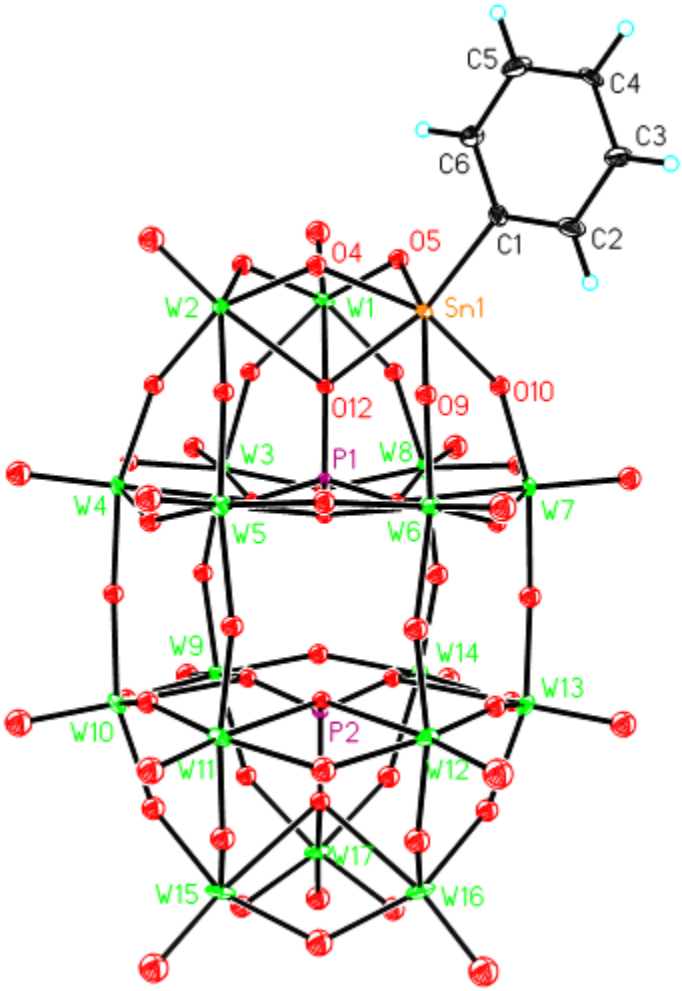

Figure 1.4. Thermal ellipsoid plot and numbering scheme for polyanion **2a** (plotted at 50% probability).

average distance of 2.053 Å to Sn, which is 0.12 Å longer than the W(VI)-$O_{eq.}$ distances in the same complex. The doming value for the Sn atom is 0.35 Å, which is on average 0.04 Å less than the other tungsten atoms in cap positions in the same structure and in the parent Wells-Dawson $[P_2W_{18}O_{62}]^{6-}$ structure.[86] This is in contrast to structure **1** and so the doming distance of Sn seems to be the result of the geometry

in the polyanion rather than a universal feature of Sn itself. The Sn atom is also coordinated to an internal μ_4-oxo as in **1**, and the C-Sn-O_{trans} bond angle is 165.5(3)°. Interestingly, the phenyl ring interacts with two potassium atoms in the crystal lattice (K6 and K2) through cation-π interactions. Cation-π interactions arise from an electrostatic force between a positive charge and the quadrupole moment of an aromatic.[87] A strong cation-π interaction is one where the distance between the cation and aromatic is the same as the sum of the ionic radius of the cation and the van der Waals radius of the atom in the aromatic.[88] In **1**, K6 and K2 are at a distance of 3.11 and 3.43 Å to the carbon of the ring, respectively (Figure 1.5). The sum of the ionic radius of K and the van der Waals radius of C is 3.30 Å, so K6 may be considered a strong cation-π interaction and K2 a weak interaction. These electronic interactions along with the rigidity and steric nature of the phenyl ring are responsible for the disorder-free polyanion in the unit cell of **2**.

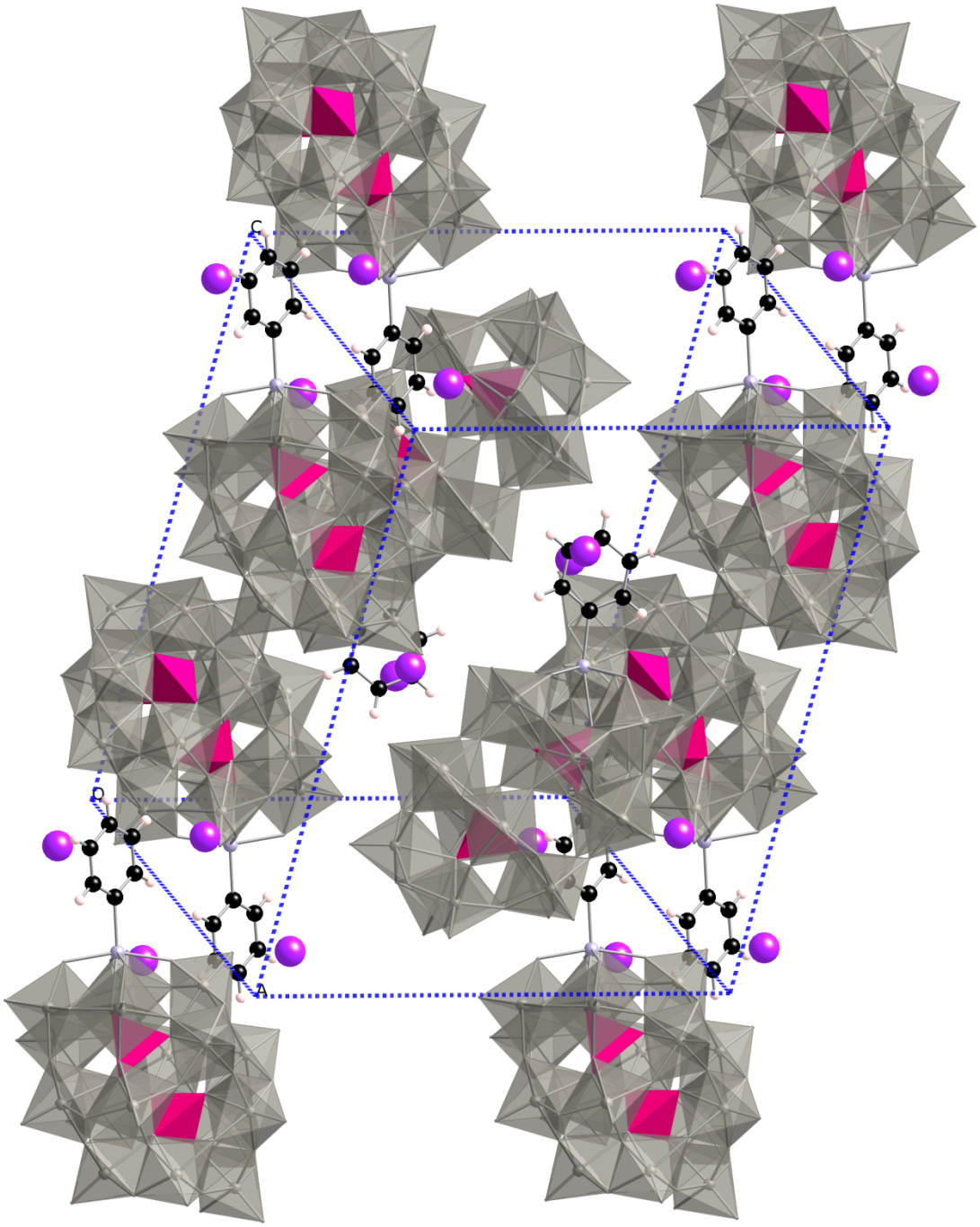

Figure 1.5. Packing diagram of $K_7[Sn(C_6H_5)P_2W_{17}O_{61}]$ (**2**). Solvent molecules and all potassium atoms except K2 and K6 have been omitted for clarity.

X-ray structure of 3

X-ray studies of **3** show that the Sn atom resides in a distorted, local C_{4v} environment (Figure 1.6). The Sn(IV) atom is coordinated to the polytungstate $[P_2W_{20}O_{70}(H_2O)_2]^{10-}$ ligand through four equitorial POM oxygens. These four oxygen atoms have an average distance of 2.083 Å to the Sn center, which is 0.19 Å longer than the W-$O_{eq.}$ distances of the other two W(VI)-$O_{eq.}$ in the central belt. The Sn atom is displaced out of the plane towards the outward-facing phenyl group by 0.30 Å, while the other two tungsten atoms in the central belt are doming inward toward the central cavity (terminal-tungsten-oxo groups pointing inward.) This feature is common in Knoth-type structures. In fact, the parent structure, $\{P_2W_{21}\}$, also has one of the three tungsten atoms in the central belt doming outward and the other two doming inward in the solid state.[74] The ligand *trans* to the phenyl group on the Sn in **3** is an aqua ligand rather than a μ_4-oxo as in **1** and **2**. The C-Sn-O_{trans} bond angle is 176.7(6)°. It is expected that strong hydrogen bonds between this *trans* aqua ligand and the two inward-pointing terminal W=O oxygens (O-O distances at 2.570(10) and 2.571(10) Å, respectively) stabilize this configuration. The packing of **3** in the crystal lattice (Figure 1.7) also shows alternating columns of phenyl rings and columns of polyanion units similar to that of **1**. There is a weak contact between H3 from the phenyl ring and a bridging oxygen atom (O66) in the cap of a neighboring polyanion. As in **1** and **2**, there is no positional disorder of the Sn center among different positions in the polyanion framework.

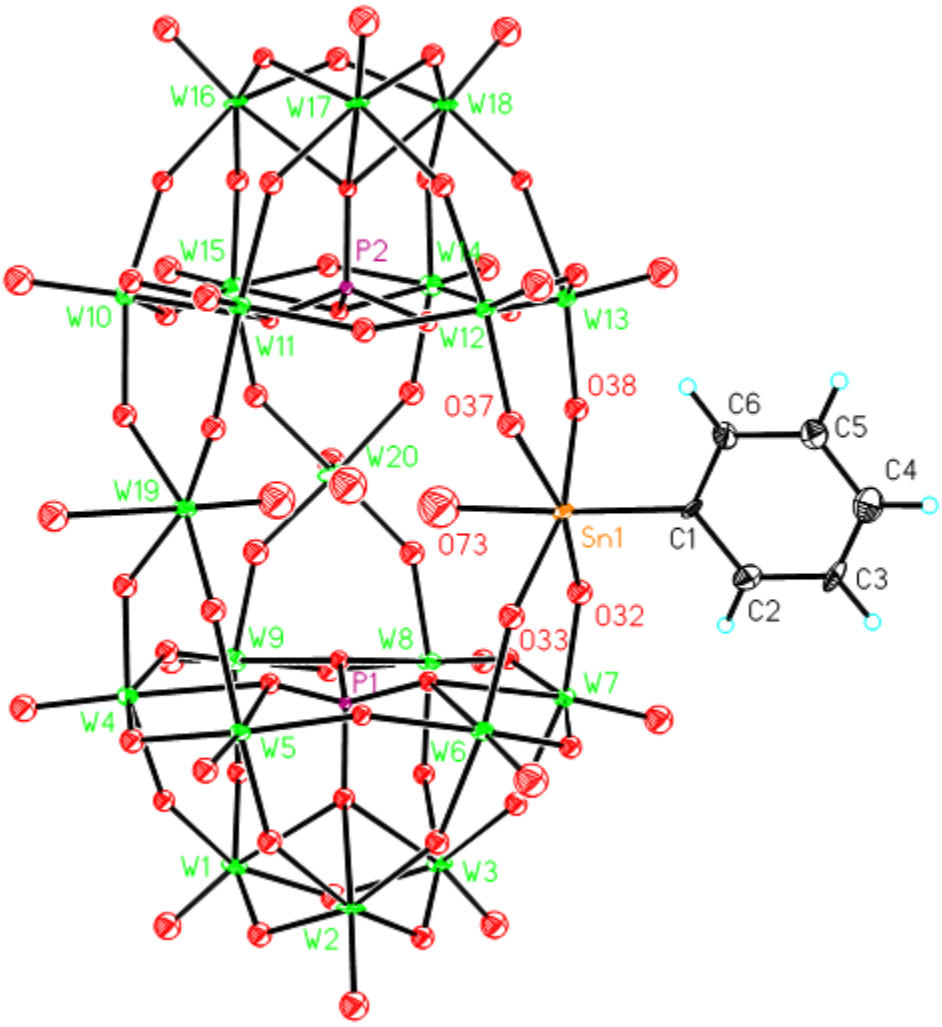

Figure 1.6. Thermal ellipsoid plot and numbering scheme for polyanion **3a** (plotted at 50% probability).

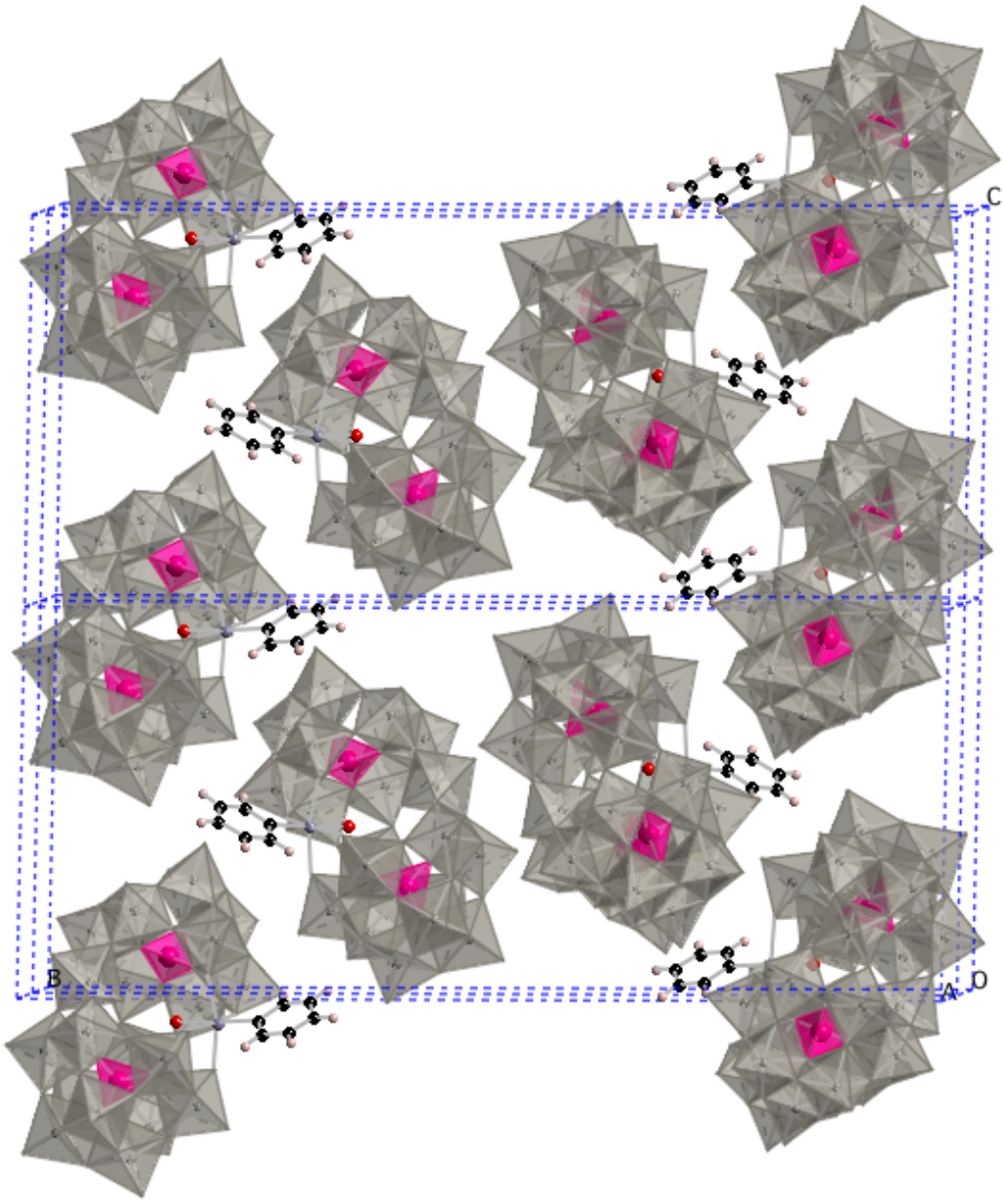

Figure 1.7. Packing of polyanion **3a** in the crystal lattice. Solvent molecules and counter cations are omitted for clarity.

1.4 Experimental

General methods and materials

The POM starting materials, $K_{10}[P_2W_{20}O_{70}(H_2O)_2]\bullet 22H_2O$ $\{P_2W_{20}\}$,[89] $K_7[PW_{11}O_{39}]\bullet 14H_2O$ $\{PW_{11}\}$,[89] and $K_{10}[\alpha_2\text{-}P_2W_{17}O_{61}]\bullet 20H_2O$ $\{P_2W_{17}\}$[90] were prepared according to the published procedures and their purities were checked by ^{31}P NMR and FT-IR spectroscopy. $(C_6H_5)SnCl_3$ was purchased from Alfa Aesar and used as received. NMR data (^{31}P and ^{1}H) were collected on a Varian INOVA 400 MHz instrument. NMR samples were made using D_2O, ^{31}P chemical shifts were referenced to 85% H_3PO_4 (0 ppm) as an external standard and ^{1}H chemical shifts were referenced to tetramethyl silane (0 ppm). FT-IR data (2% KBr pellet) was collected on a Thermo Nicolet 6700 instrument. For FT-IR data, s = strong, m = medium, w = weak. Elemental Analyses of W, Sn, P, and K were carried out by Columbia Analytical Services (Phoenix, AZ), and analyses of C and N were carried out by Atlantic Microlabs (Norcross, GA). Unless otherwise noted, solutions were filtered on a Corning PES filter (0.20 μm) attached to a disposable Luer-lock syringe.

Synthesis of $K_{10}[P_2W_{20}O_{70}(H_2O)_2]\bullet 22H_2O$

This procedure is an adaptation of the published procedure[89] with additional notes which improve the synthesis. A solution of 100 mL of water and 10 mL of 1.0 M phosphoric acid were placed in a 250 mL beaker and heated to 50 ^{o}C, then K_2WO_4 (32.60 g) was added. A slightly cloudy heterogeneous solution resulted (pH 8.49) and 49.0 mL of a solution of hydrochloric acid (3.0 M) was added dropwise (1 drop / 2 seconds) under vigorous stirring. The solution went homogeneous after a few drops

of acid were added, but became heterogeneous again after about 1/3 of the acid was added (pH 8.00). The solution was clear again after almost all of the acid is added (pH 3.85). After all 49.0 mL of acid was added the pH was 3.11 and the solution was homogeneous. If more acid is added then PW_{12} forms, thus care must be taken not to do so. A watch glass was placed over the solution, the solution was allowed to cool to room temperature, and then it was filtered on fine filter paper into a 300-mL beaker. Clusters of microcrystals begin to appear within an hour. The next day, the solution was homogeneous with several large clusters of colorless and white microcrystals. After a 2-4 days the crystals were collected on a coarse frit and a *clean* filter flask, washed with 5 mL of water at 5 ^{o}C, dried for 20 minutes with continued suction, and weighed. About 17 grams of product were collected and saved in a weigh boat. The filtrate in the filter flask was put in a beaker and placed the refrigerator at 5 ^{o}C overnight. After several days the solution in the refrigerator was removed and the microcrystals collected, placed in a coarse frit, washed with 1 mL of water at 5 ^{o}C, dried for 10 minutes, and then weighed. About 4 grams were collected. The two samples of crystals were combined and dissolved in 1.5 mL of water per gram of POM, heated until the solution went homogeneous (no higher than 60 ^{o}C). The solution was cooled to room temperature, and then filtered on fine filter paper into a 140-mL beaker. Large, colorless prisms appeared in 1-2 days and were collected when the solvent had reached the top of the crystals. Once dry, the crystals were ground into a powder. The crystals were P_2W_{20} by ^{31}P NMR (-12.3 ppm) with a small (2%) unidentified impurity peak (-9.9 ppm). Yield: 14.2 g.

Synthesis of $K_7[PW_{11}O_{39}]\bullet 14H_2O$

This procedure is an English translation of the published procedure[89] with additional notes which improve the synthesis. A solution of $Na_2WO_4\bullet 2H_2O$ (181.5 g) in 300 mL H_2O was prepared. To the homogeneous solution, 50 mL of 1.0 M H_3PO_4 were added over 1 minute. Then, 88 mL of glacial acetic acid were added dropwise. The solution was refluxed for at least an hour, and then cooled to approximately 80 ^oC and a sample of KCl (60 g) was added to the homogeneous solution and the solution stayed clear. The solution was allowed to come to room temperature, filtered, and left to crystallize. One day later several large colorless crystals appeared. After several days, the crystals were collected on a frit, washed with cold water, and dried under aspiration for 10 minutes. The crystals typically smell of acetic acid. The ^{31}P NMR showed one peak at -10.4 ppm. Yield: 63% in W.

Synthesis of $K_{10}[\alpha_2\text{-}P_2W_{17}O_{61}]\bullet 20H_2O$

This procedure is an adaptation of the published procedure.[90] In a 1-L beaker a sample of 80.0 g ($1.15 * 10^{-2}$ mol) of $K_6[P_2W_{18}O_{62}]$ was dissolved in 200 mL water, and a solution of 20.0 g (0.2 mol) of potassium hydrogen carbonate in 200 mL of water was added dropwise while stirring. Note: Either the alpha or beta isomer of $K_6[P_2W_{18}O_{62}]$ can be used, but the alpha isomer results in higher yield. After 1 hr, the reaction was complete, and the white precipitate was filtered on a coarse sintered glass frit, dried under vacuum for 10 minutes, and then redissolved in 500 mL of hot water (95 ^oC). The snow-like crystals that appeared on cooling to ambient temperature were filtered after 4 hr, dried under vacuum for 5 hr, and then air-dried

for 2 days. Yield: 57 g (70% in W.) The ^{31}P NMR spectrum in water shows peaks at -6.6 and -13.7 ppm. These values match other published values[91] for this complex, but differ from the Inorganic Syntheses procedure[90] because the Inorganic Syntheses NMR spectrum was done in one molar acetic acid/sodium acetate buffer. The IR spectrum shows peaks at 1084, 1050, 1012 cm^{-1}.

Synthesis of $((CH_3)_2NH_2)_4[Sn(C_6H_5)PW_{11}O_{39}]\cdot 5H_2O$ (1)

$\{PW_{11}\}$ (2.00 g, 0.611 mmol) was dissolved in 16.0 mL of water, and then $(C_6H_5)SnCl_3$ (0.111 mL, 0.672 mmol) was added *via* automatic pipettor quickly under vigorous stirring. The heterogeneous white solution that resulted was stirred for 30 minutes, and then filtered. To the filtrate, a solution of dimethylamine hydrochloride (4.0 M) was added dropwise under stirring (*ca.* 0.7 mL), followed by a solution of LiCl (1.0 M, *ca.* 0.6 mL), and the resulting solution was filtered on a fine filter paper into a 50-mL beaker. After 2 days, a mixture of colorless prisms suitable for X-ray diffraction and whitish gray semi-crystalline spheres appeared together and were harvested (^{31}P NMR confirms that these two materials are identical). Yield: 0.95 g (49% with respect to the polyanion) [MW = 3147 g/mol]. ^{31}P NMR: -11.53 ppm. ^{1}H NMR (aromatic region): 8.08 (d, 2H), 7.55 (m, 3H) ppm. FT-IR (2% KBr pellet): 1464 (s), 1434 (m), 1412 (m), 1066 (s), 967 (s), 887 (m), 793 (s), 703 (w), 659 (w), 591 (w), 508 (w) cm^{-1}. Elemental analysis, Calculated: C, 5.34%; N, 1.78%; W, 64.25%; Sn, 3.77%; P, 0.98%. Found: C, 5.32%; N, 1.76%; W, 63.51%; Sn, 3.55%; P, 1.02%.

Synthesis of $K_7[Sn(C_6H_5)P_2W_{17}O_{61}]$ (2)

$\{P_2W_{17}\}$ (1.00 g, 0.204 mmol) was dissolved in 20.0 mL of water, and then $(C_6H_5)SnCl_3$ (0.037 mL, 0.225 mmol) was added *via* automatic pipettor dropwise under vigorous stirring. The homogeneous white solution that resulted was stirred for 30 minutes, and then filtered to remove insoluble particles. The resulting solution was placed in a small vial which was then placed inside a larger container with ethanol and sealed to facilitate slow ethanol vapor diffusion into the crystallization solution. After several days a crystal suitable for X-ray diffraction was mounted and determined to be $K_7[Sn(C_6H_5)P_2W_{17}O_{61}]$ (**2**).

Synthesis of $((CH_3)_2NH_2)_7[Sn(C_6H_5)P_2W_{17}O_{61}]\bullet 20H_2O$ (2')

$\{P_2W_{17}\}$ (1.00 g, 0.204 mmol) was dissolved in 20.0 mL of water, and then $(C_6H_5)SnCl_3$ (0.037 mL, 0.225 mmol) was added *via* automatic pipettor dropwise under vigorous stirring. The resulting heterogeneous white solution was stirred for 30 minutes, and then filtered to remove insoluble particles. To the filtrate, a solution of dimethylamine hydrochloride (4.0 M, 2.0 mL) was added dropwise under stirring. The solution was filtered on a fine filter paper into a 50-mL beaker and allowed to evaporate. The solution gradually turned to light blue during crystal growth, and after 7 days light blue needles appeared. Yield: 0.509 g (49% with respect to the polyanion) [MW = 5042 g/mol]. ^{31}P NMR: -13.18 ppm, -9.47 ppm. ^{1}H NMR (aromatic region): 7.74 (q, 2H), 7.56 (m, 3H) ppm. FT-IR (2% KBr pellet): 1465 (s), 1437 (w), 1413 (w), 1384 (m), 1249 (w), 1230 (w), 1089 (s), 1018 (m), 967 (sh), 953 (m), 908 (m), 769 (m) cm^{-1}. Elemental analysis, Calculated: C, 4.76%; N, 1.95%; W,

61.99%; Sn, 2.35%; P, 1.23%. Found: C, 4.82%; N, 1.97%; W, 60.82%; Sn, 2.20%; P, 1.11%. The crystal suitable for single crystal X-ray diffraction, **2**, was grown from slow diffusion of ethanol into the potassium salt solution (no dimethylamine hydrochloride was added). The materials from both diffusion and evaporation (**2** and **2'**) are identical based on ^{1}H and ^{31}P NMR, and FT-IR spectroscopies.

Synthesis of $((CH_3)_2NH_2)_6K[Sn(C_6H_5)(H_2O)P_2W_{20}O_{70}(H_2O)_2]\bullet 11H_2O$ (3)

$\{P_2W_{20}\}$ (1.0 g, 0.176 mmol) was dissolved in 10.0 mL water, and then $(C_6H_5)SnCl_3$ (0.033 mL, 0.203 mmol) was added *via* automatic pipettor all in one portion under vigorous stirring. The resulting heterogeneous solution typically has a pH of approximately 2-3 and is stirred for 10 minutes. If the pH at this time was below 2.75, it was raised to pH 2.75 with the dropwise addition of 0.1 M KOH while stirring. The solution was then filtered through a fine filter paper to remove insoluble particles, and a solution of 5.0 M dimethylamine hydrochloride (*ca.* 0.44 mL) was added to the filtrate while stirring. The solution was left to evaporate in a partially covered 50-mL beaker. After 1 day, colorless prismatic crystals appeared. After 8 days when the solution had reached approximately 4 mL the crystals were harvested. Yield: 0.386 g (39% with respect to the polyanion). [MW = 5622 g/mol] ^{31}P NMR: -13.40 ppm. ^{1}H NMR (aromatic region): 7.96 (d, 2H), 7.61 (m, 3 H) ppm. FT-IR (2% KBr pellet): 1464 (m), 1435 (w), 1411 (w), 1093 (s), 1081 (s), 1026 (m), 960 (m), 932 (m), 763 (s), 628 (w), 523 (w), 445 (w) cm^{-1}. Elemental analysis, Calculated: C, 3.86%; N, 1.50%; W, 65.40%; Sn, 2.12%; P, 1.10%; K, 0.70%. Found: C, 4.02%; N, 1.54%; W, 65.07%; Sn, 1.94%; P, 1.02%; K 0.70%.

X-ray Crystallography

The complete datasets for complexes **1**, **2** and **3** were collected at Emory University. Single crystals of $((CH_3)_2NH_2)_4[Sn(C_6H_5)PW_{11}O_{39}]$ (**1**), $K_7[Sn(C_6H_5)P_2W_{17}O_{61}]$ (**2**) and $((CH_3)_2NH_2)_6K[Sn(C_6H_5)(H_2O)P_2W_{20}O_{70}(H_2O)_2]$ (**3**) suitable for X-ray analysis, were each coated with Paratone-N oil, suspended in a small fiber loop, and placed in a cooled gas stream on a Bruker D8 SMART APEX II CCD sealed tube diffractometer. Diffraction intensities were measured using graphite monochromated Mo Kα radiation (λ = 0.71073 Å) at 173(2) K and a combination of φ and ω scans with 10 s frames traversing at 0.5° increments. Data collection, indexing, and initial cell refinements were carried out using SMART;[92] frame integration and final cell refinements were done using SAINT.[93] The molecular structure of each complex was determined using Direct Methods and Fourier techniques and refined by full-matrix least squares. A multiple absorption correction, including face indexing, was applied using the program SADABS.[94] The structure of **1**, **2** and **3** were solved using Direct Methods and difference Fourier techniques. The largest residual electron density for each structure was located close to (less than 1.0 Å from) the W atoms and was most likely due to imperfect absorption corrections frequently encountered in heavy-metal atom structures. Scattering factors and anomalous dispersion corrections are taken from the *International Tables for X-ray Crystallography*. Structure solution, refinement, graphic and generation of publication materials were performed by using SHELXTL, V6.14 software. The crystal data and structure refinement parameters are summarized in Table 1.2 and 1.3.[95]

Table 1.2. Crystal data and structural refinement for the X-ray structures of **1** and **2**.

	1	**2**
molecular formula	$C_{14}H_{47}N_4O_{44}PSnW_{11}$	$C_6H_{45}K_7O_{75}P_2SnW_{17}$
formula wt. (g mol^{-1})	3147.45	4884.91
temperature (K)	173(2)	173(2)
radiation (λ, Å)	0.71073	0.71073
crystal system	triclinic	monoclinic
space group	$P\bar{1}$	$P2_1/c$
a (Å)	11.9176(9)	13.828(1)
b (Å)	12.9766(10)	20.9602(18)
c (Å)	18.0229(13)	24.2620(18)
α (°)	92.7080(1)	90
β (°)	98.4240(1)	93.6880(1)
γ (°)	106.9550(1)	90
Volume (Å^3)	2625.4(3)	7017.5(9)
Z	2	4
ρ_{calcd} (g cm^{-3})	3.969	4.608
μ (mm^{-1})	24.592	28.671
F(000)	2760	8472
crystal size (mm^3)	0.24 x 0.15 x 0.14	0.23 x 0.21 x 0.10
reflections collected	49450	129463
independent reflections	14919 [R(int) = 0.0509]	20657 [R(int) = 0.0657]
absorption correction	semi-empirical from equivalents	semi-empirical from equivalents
refinement method	full-matrix least squares on F^2	full-matrix least-squares on F^2
goodness-of-fit on F^2	1.048	1.057
final R indices [R > 2σ (I)]	R1[a] = 0.0370, wR2[b] = 0.0915	R1[a] = 0.0359, wR2[b] = 0.0876
largest diff. peak and hole (e Å^{-3})	4.325 and -2.229	4.350 and -3.967

[a] $R_1 = \Sigma||F_o| - |F_c|| / |F_o|$

[b] $wR_2 = \{\Sigma[w(F_o^2 - F_c^2)^2] / \Sigma[w(F_o^2)^2]\}^{0.5}$

Table 1.3. Crystal data and structural refinement for the X-ray structure of **3**.

	3
molecular formula	$C_{18}H_{75}KN_6O_{84}P_2SnW_{20}$
formula wt. (g mol^{-1})	5622.38
temperature (K)	173(2)
radiation (λ, Å)	0.71073
crystal system	monoclinic
space group	$P2_1/c$
a (Å)	13.0559(17)
b (Å)	40.252(5)
c (Å)	17.858(3)
α (°)	90
β (°)	108.789(2)
γ (°)	90
Volume ($Å^3$)	8885(2)
Z	4
ρ_{calcd} (g cm^{-3})	4.076
μ (mm^{-1})	26.239
F(000)	9516
crystal size (mm^3)	0.16 x 0.15 x 0.09
reflections collected	168521
independent reflections	26062 [R(int) = 0.0884]
absorption correction	semi-empirical from equivalents
refinement method	full-matrix least-squares on F^2
goodness-of-fit on F^2	1.120
final R indices [R > 2σ (I)]	$R1^a$ = 0.0557, $wR2^b$ = 0.1221
largest diff. peak and hole (e $Å^{-3}$)	7.044 and -4.450

$^aR_1 = \Sigma||F_o| - |F_c|| / |F_o|$

$^bwR_2 = \{\Sigma[w(F_o^2 - F_c^2)^2] / \Sigma[w(F_o^2)^2]\}^{0.5}$

1.5 Characterization data for complexes 1-3

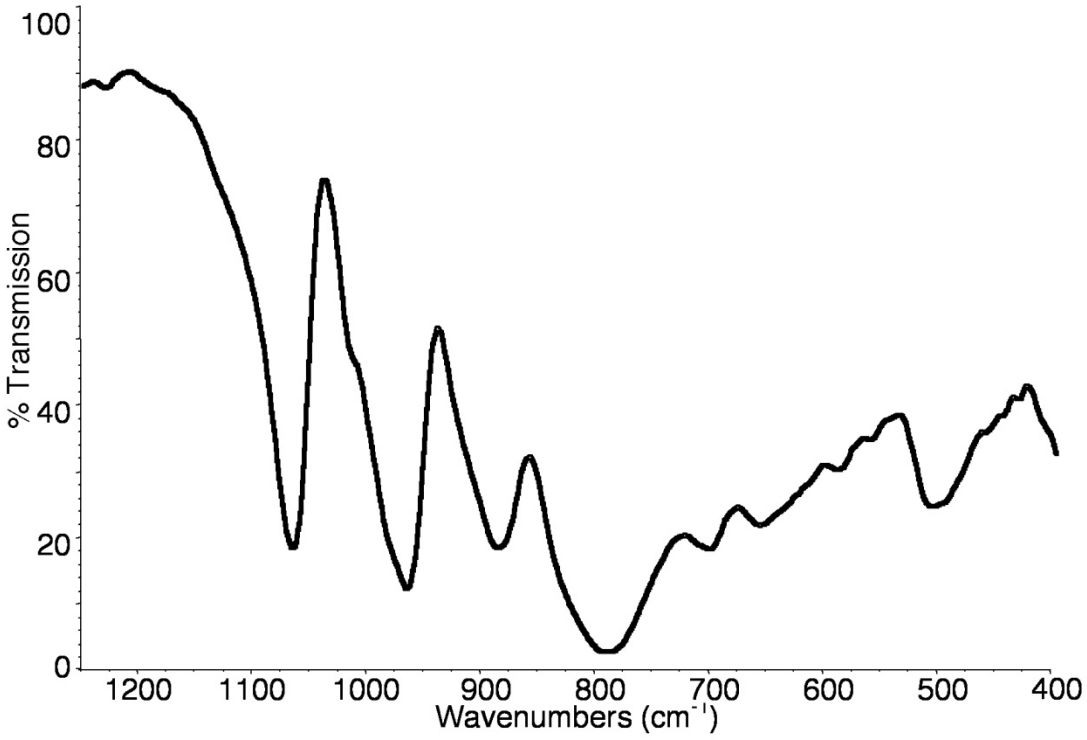

Figure 1.8. FT-IR spectrum of $((CH_3)_2NH_2)_4[Sn(C_6H_5)PW_{11}O_{39}]$ (**1**), 2% by weight in KBr.

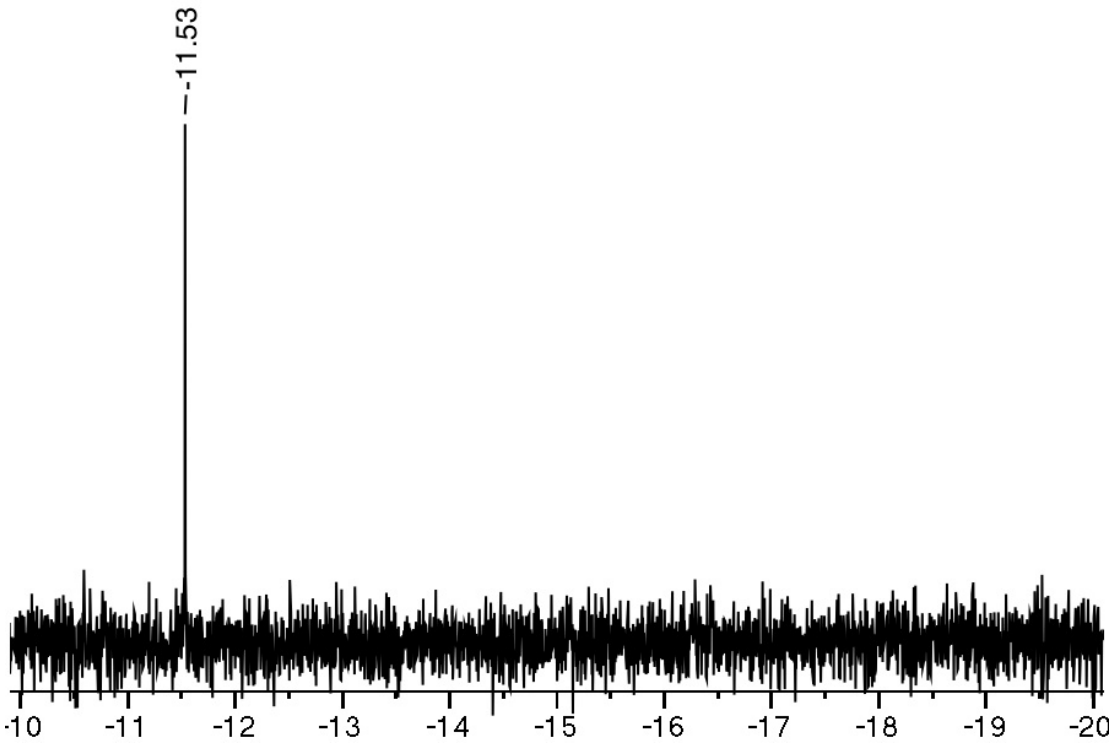

Figure 1.9. ^{31}P NMR spectrum of $((CH_3)_2NH_2)_4[Sn(C_6H_5)PW_{11}O_{39}]$ (**1**) in D_2O. Spectrum referenced to an external standard of 85% phosphoric acid (0 ppm).

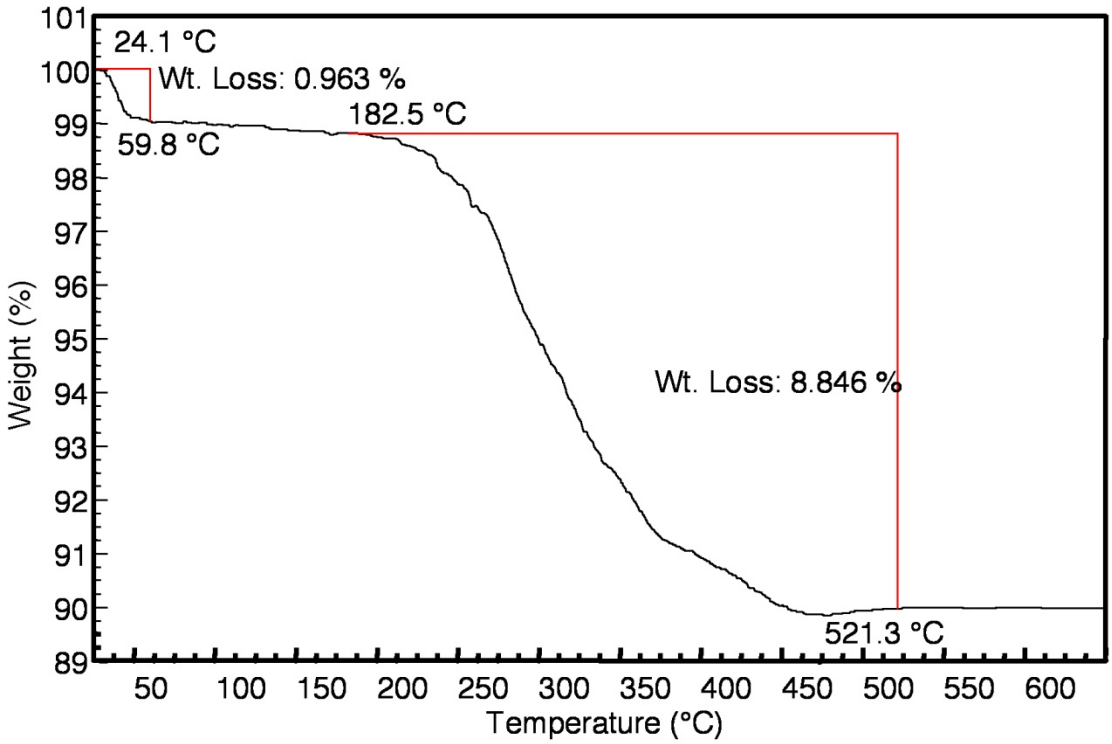

Figure 1.10. TGA weight loss curve of $((CH_3)_2NH_2)_4[Sn(C_6H_5)PW_{11}O_{39}]$ (**1**), 16.838 mg sample under inert atmosphere. The first weight loss event corresponds to the loss of 1 water molecule. The second weight loss event corresponds to the loss of the 4 DMA counterions and the phenyl ring. The dry sample used for elemental analysis and TGA contains approximately 1 water molecule per POM, whereas the wet crystal used for X-ray contains at least 5 waters of hydration (5 water molecules were located and included in the refinement).

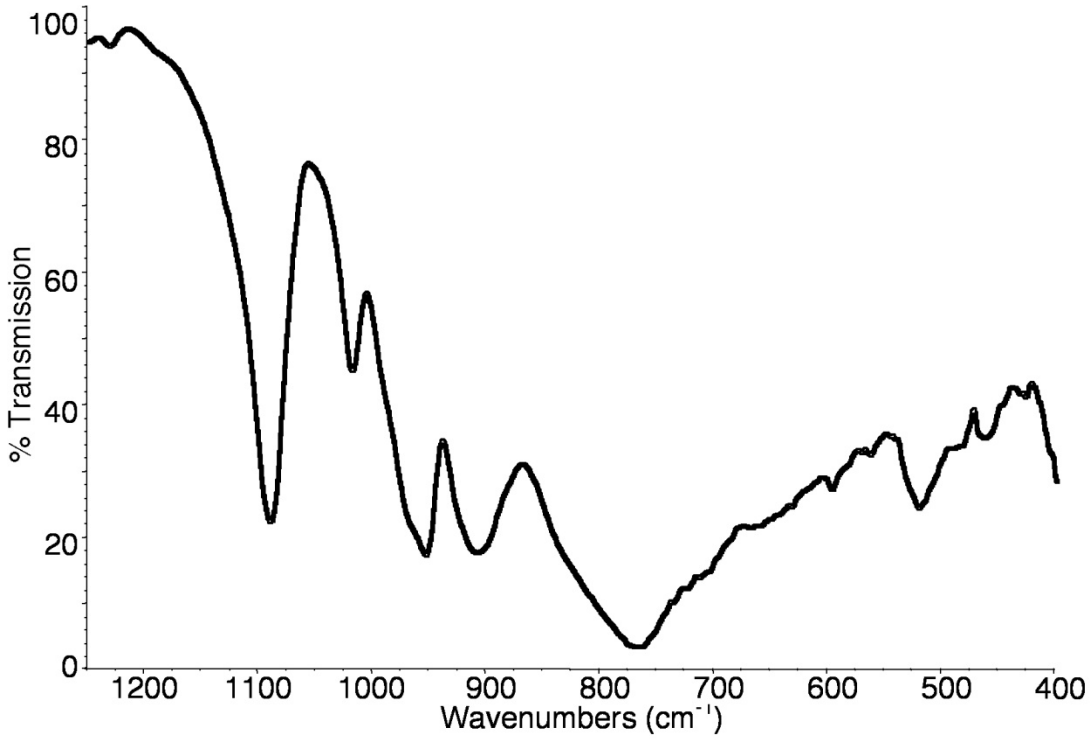

Figure 1.11. FT-IR spectrum of $((CH_3)_2NH_2)_7[Sn(C_6H_5)P_2W_{17}O_{61}]$ (**2'**), 2% by weight in KBr.

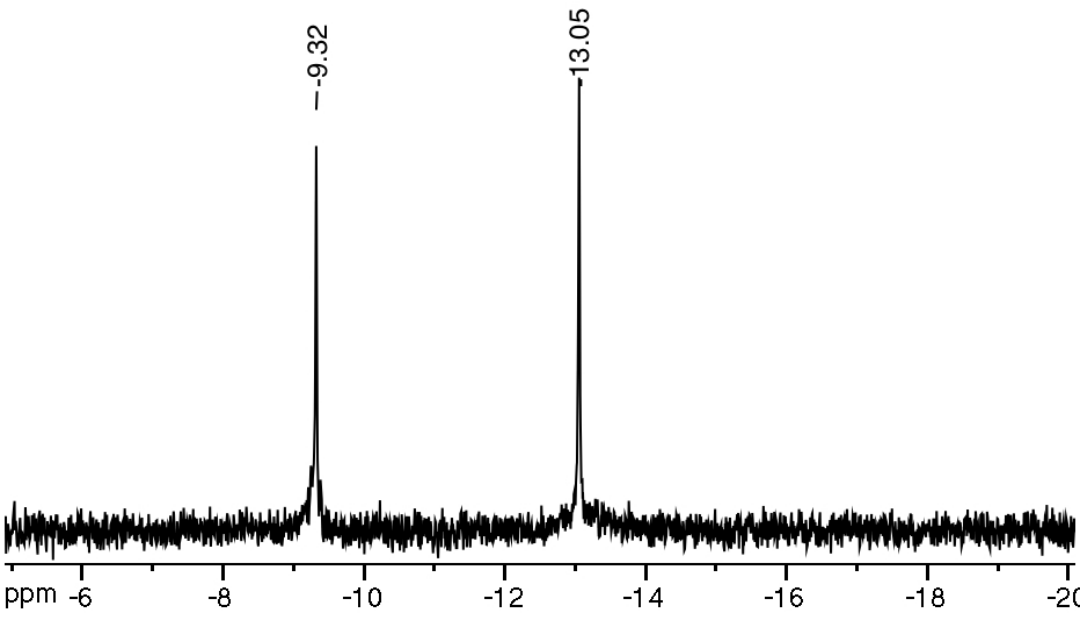

Figure 1.12. ^{31}P NMR spectrum of $((CH_3)_2NH_2)_7[Sn(C_6H_5)P_2W_{17}O_{61}]$ (**2'**) in D_2O. Spectrum referenced to an external standard of 85% phosphoric acid (0 ppm).

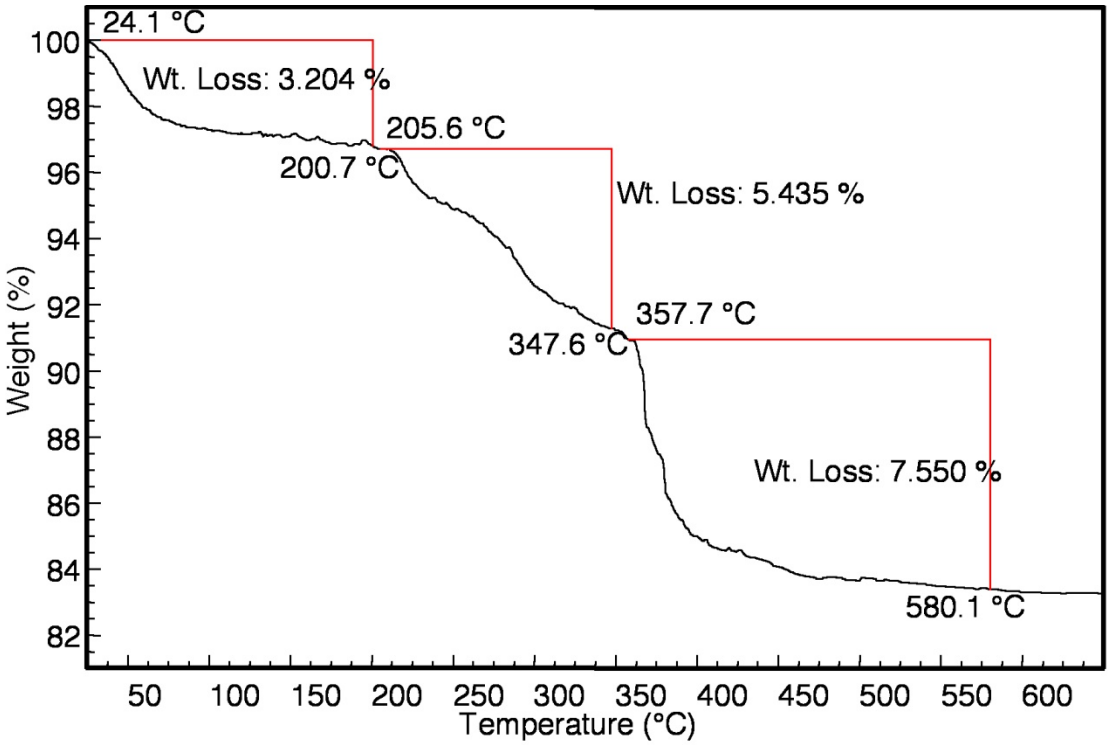

Figure 1.13. TGA weight loss curve of $((CH_3)_2NH_2)_7[Sn(C_6H_5)P_2W_{17}O_{61}]$ (**2'**), 16.8120 mg sample under inert atmosphere. The first weight loss event corresponds to approximately 9 loosely bound water molecules. The second weight loss event corresponds to the loss of 11 additional more tightly bound water molecules as well as the phenyl ring. The final weight loss event is accounted for the 7 DMA counter cations.

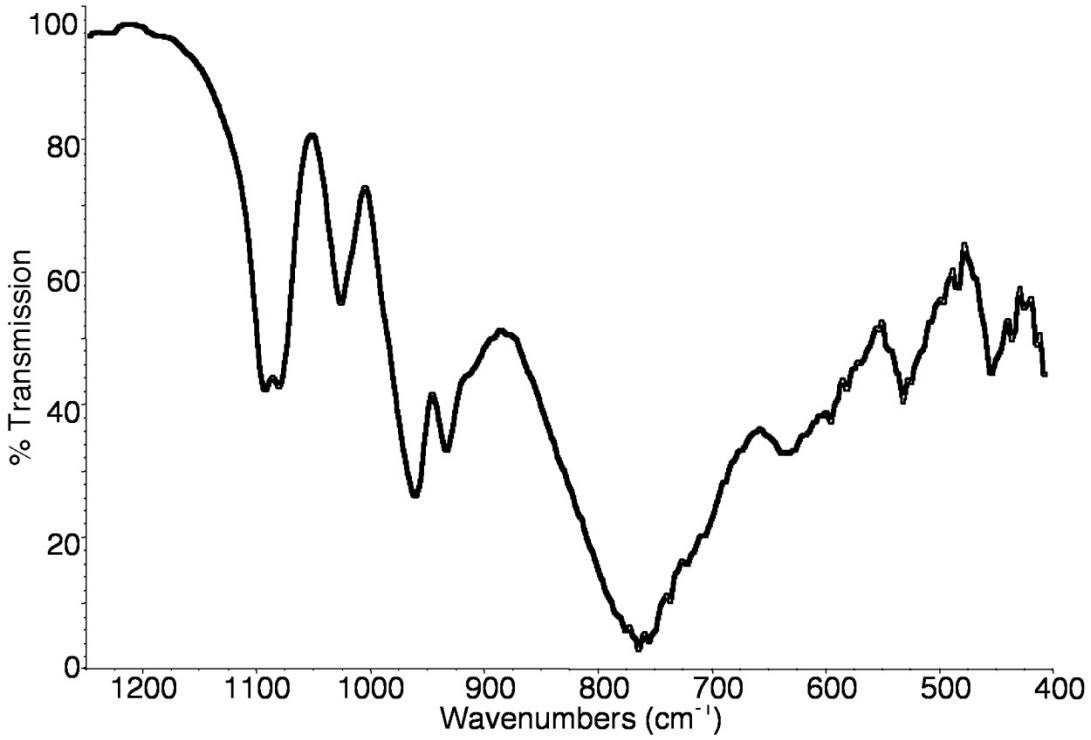

Figure 1.14. FT-IR spectrum of $((CH_3)_2NH_2)_6K[Sn(C_6H_5)(H_2O)P_2W_{20}O_{70}(H_2O)_2]$ (**3**), 2% by weight in KBr.

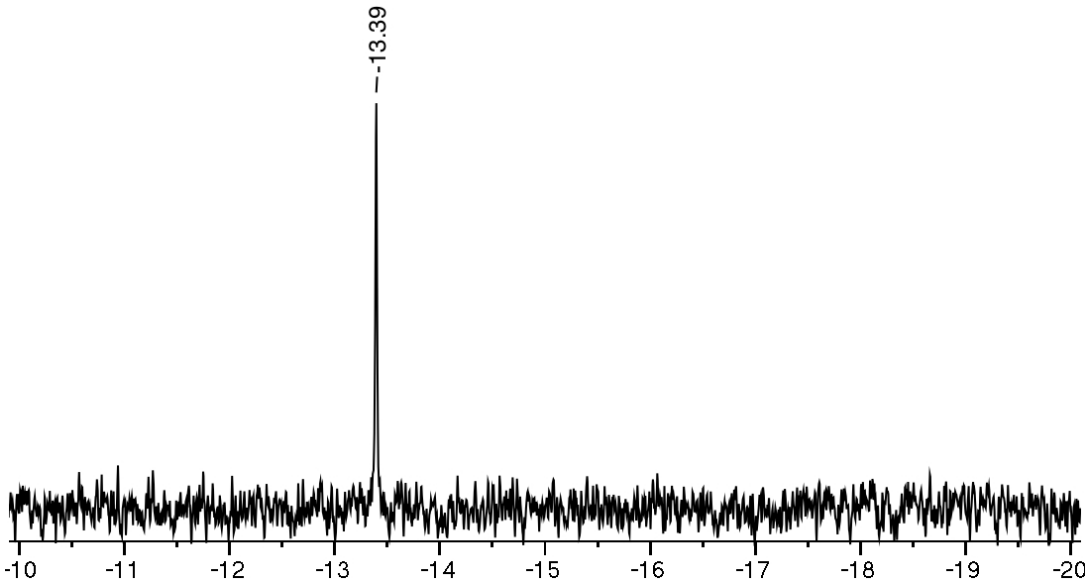

Figure 1.15. ^{31}P NMR of $((CH_3)_2NH_2)_6K[Sn(C_6H_5)(H_2O)P_2W_{20}O_{70}(H_2O)_2]$ (**3**) in D_2O. Spectrum referenced to an external standard of 85% phosphoric acid (0 ppm).

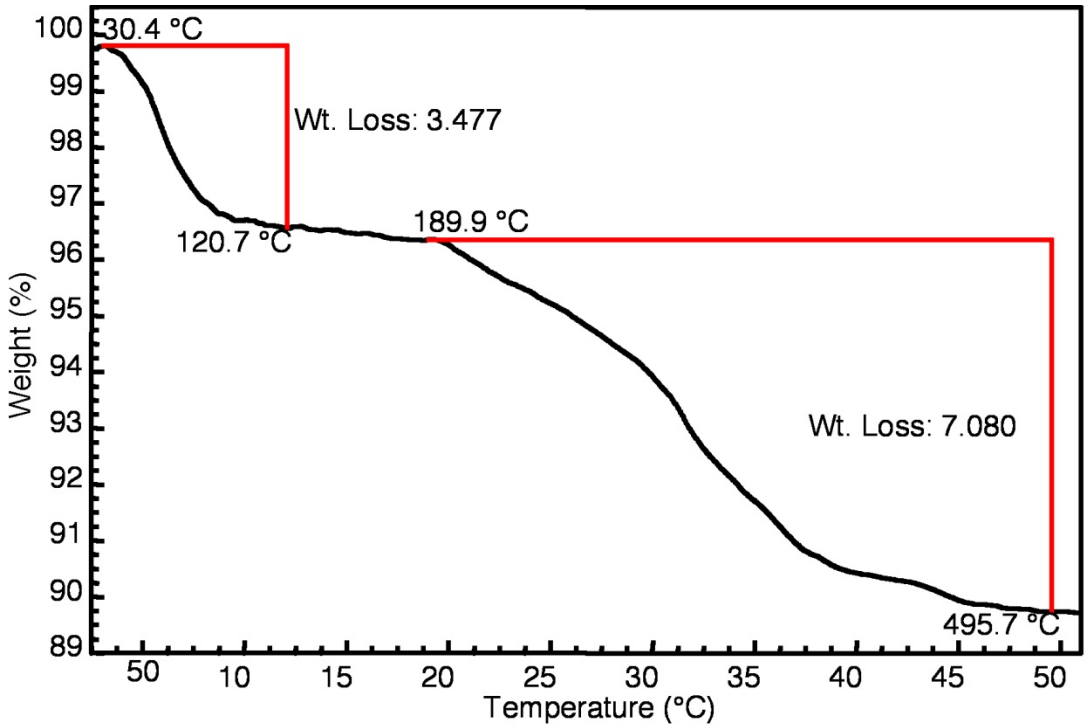

Figure 1.16. TGA weight loss curve of $((CH_3)_2NH_2)_6K[Sn(C_6H_5)(H_2O)P_2W_{20}O_{70}(H_2O)_2]$ (**3**), 12.2783 mg sample under inert atmosphere. The first weight loss event corresponds to 11 water molecules. The second weight loss event corresponds to the phenyl ring and 6 DMA molecules.

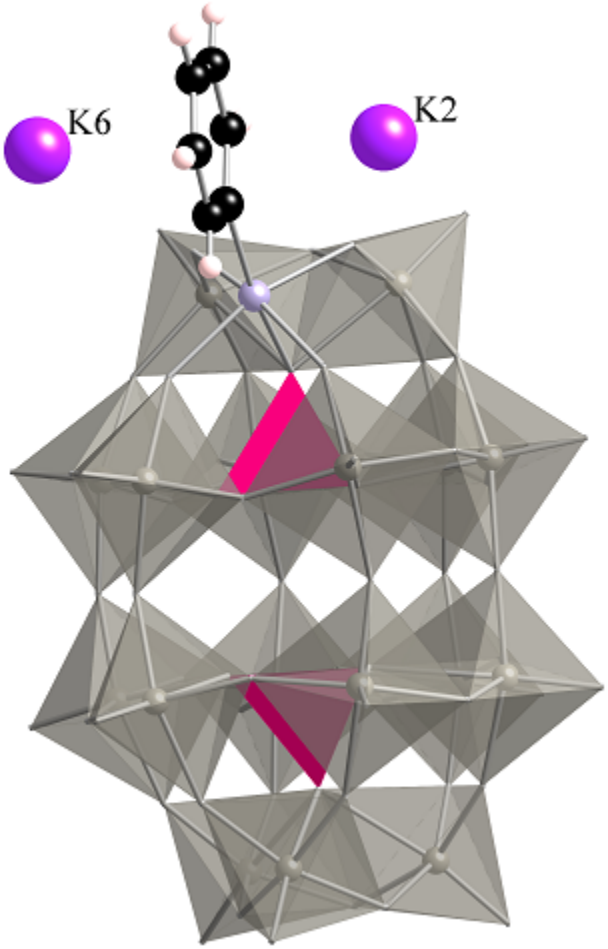

Figure 1.17. Combined polyhedral/ball-and-stick representation of **2a** showing the cation-π interaction of the phenyl ring with two potassium ions (K2 and K6).

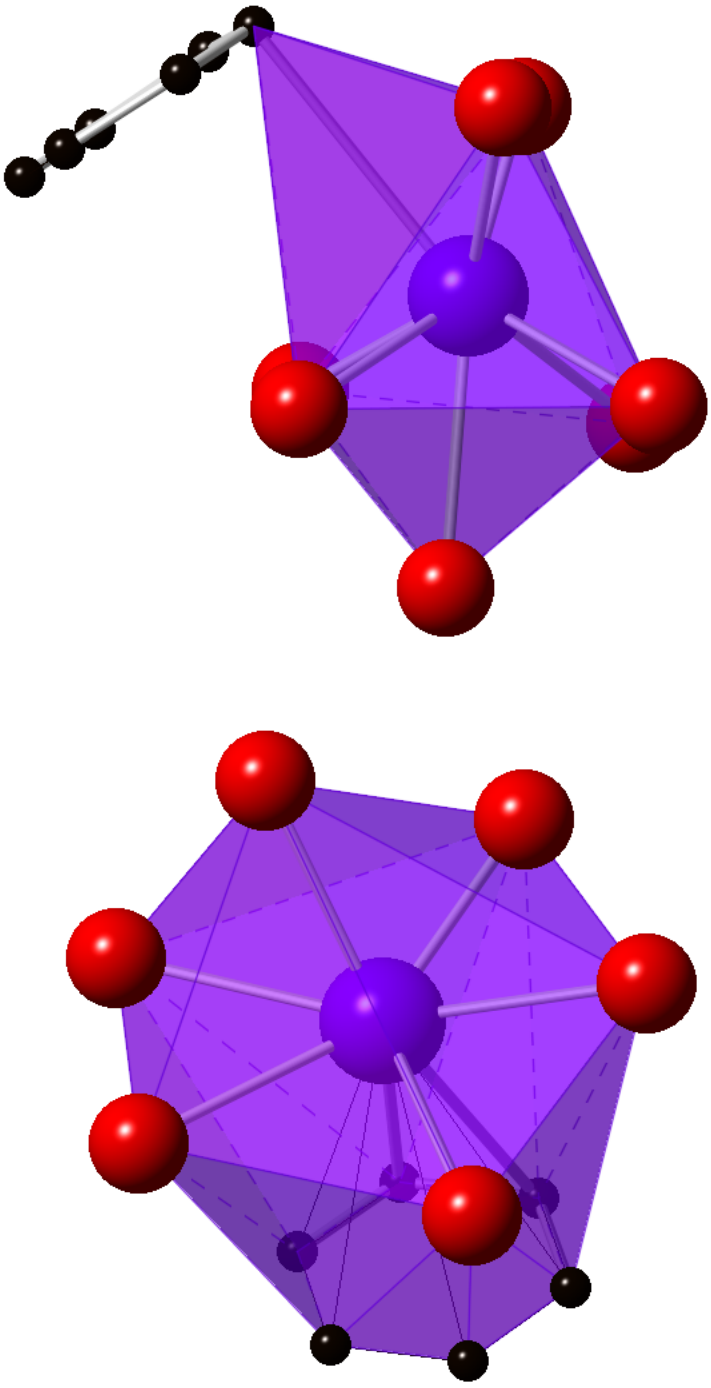

Figure 1.18. Cation-π interactions of K2 (top) and K6 (bottom) in **2**.

1.6 Conclusions

We have successfully removed the crystallographic positional disorder that is nearly always observed in mono-substituted Keggin, Wells-Dawson, and Knoth-type polytungstates by the incorporation of a rigid and bulky phenyltin group. Each complex (**1**, **2** and **3**) shows the $[(C_6H_5)Sn]^{3+}$ unit at one unique metal position of the polyanion while most mono-substituted POMs of these families show the metal center disordered over several positions as a consequence of crystallographically-imposed symmetry elements. In addition to the steric size of the phenyl group itself, hydrogen bonds and cation-π interactions in the crystal lattice also demonstrate the ability of a phenyl group to promote disorder-free packing during crystal growth. Furthermore, these are the first examples of a single phenyltin unit incorporated into a polyanion framework. These results suggest that the incorporation of phenyltin units into POMs may be useful in crystallographic studies, for example, to obtain disorder-free structures of transition metal-substituted POMs (as shown in chapter 2) or to direct crystal growth of POMs in organic solvents through π-π interactions.

CrystEngComm, **2010**, *12*, 1518-1525 – Portions of this document have been reproduced by permission of The Royal Society of Chemistry (RSC)
http://pubs.rsc.org/en/Content/ArticleLanding/2010/CE/B919934A

References

1. M. T. Pope and A. Müller, *Angew. Chem. Int. Ed.*, 1991, **30**, 34-48.

2. M. T. Pope and A. Müller, eds., *Polyoxometalates: From Platonic Solids to Anti-retroviral Activity*, Kluwer Academic Publishers, Dordrecht, Netherlands, 1993.

3. C. L. Hill, ed., *Special Thematic Issue on Polyoxometalates*, 1998.

4. J. J. Borrás-Almenar, E. Coronado, A. Müller and M. T. Pope, *Polyoxometalate Molecular Science*, Kluwer Academic Publishers, Dordrecht, 2003.

5. L. Cronin, in *Comprehensive Coordination Chemistry II: From the Molecular to the Nanoscale: Synthesis, Structure, and Properties*, eds. J. A. McCleverty and T. J. Meyer, Elsevier, Amsterdam, Editon edn., 2004, vol. 7, pp. 1-57.

6. M. T. Pope, in *Comprehensive Coordination Chemistry II: From Biology to Nanotechnology*, ed. A. G. Wedd, Elsevier Ltd., Oxford, UK, Editon edn., 2004, vol. 4, pp. 635-678.

7. C. L. Hill, in *Comprehensive Coordination Chemistry-II: From Biology to Nanotechnology*, ed. A. G. Wedd, Elsevier Ltd., Oxford, UK, Editon edn., 2004, vol. 4, pp. 679-759.

8. C. L. Hill and C. M. Prosser-McCartha, *Coord. Chem. Rev.*, 1995, **143**, 407-455.

9. T. Okuhara, N. Mizuno and M. Misono, *Advances in Catalysis*, 1996, **41**, 113-252.

10. R. Neumann, *Prog. Inorg. Chem.*, 1998, **47**, 317-370.

11. N. Mizuno and M. Misono, *Chem. Rev.*, 1998, **98**, 199-218.

12. J. B. Moffat, *Metal-Oxygen Clusters: The Surface and Catalytic Properties of Heteropoly Oxometalates.*, Kluwer Academic/Plenum Publishers, New York, 2001.

13. I. V. Kozhevnikov, *Catalysis by Polyoxometalates*, Wiley, Chichester, England, 2002.

14. R. Neumann, *Mod. Oxidation Methods*, 2004, 223-251.

15. Y. V. Geletii, B. Botar, P. Kögerler, D. A. Hillesheim, D. G. Musaev and C. L. Hill, *Angew. Chem. Int. Ed.*, 2008, **47**, 3896-3899.

16. A. Sartorel, M. Carraro, G. Scorrano, R. D. Zorzi, S. Geremia, N. D. McDaniel, S. Bernhard and M. Bonchio, *J. Am. Chem. Soc*, 2008, **130**, 5006–5007.

17. Y. V. Geletii, Z. Huang, Y. Hou, D. G. Musaev, T. Lian and C. L. Hill, *J. Am. Chem. Soc.*, 2009, **131**, 7522-7523.

18. R. Cao, H. Ma, Y. V. Geletii, K. I. Hardcastle and C. L. Hill, *Inorg. Chem.*, 2009, **48**, 5596-5598.

19. Q. Yin, J. M. Tan, C. Besson, Y. Geletii, D. G. Musaev,; A. E. Kuznetsov, Z. Luo, K. I. Hardcastle and C. L. Hill, *Science*, 2010, **328**, 342-345.

20. X. Fang, T. M. Anderson and C. L. Hill, *Angew. Chem. Int. Ed.* **2005**, *44*, 3540.

21. J. W. Han and C. L. Hill, *J. Am. Chem. Soc.*, 2007, **129**, 15094-15095.

22. B. S. Bassil, S. S. Mal, M. H. Dickman, U. Kortzhttp://pubs.acs.org/doi/abs/10.1021/ja801424q - ath4, H. Oelrich and L. Walder, *J. Am. Chem. Soc.,* 2008, **130**, 6696-6697.

23. A. E. Kuznetsov, Y. V. Geletii, C. L. Hill, K. Morokuma, D. G. Musaev, *Inorg. Chem.*, 2009, **48**, 1871-1878.

24. T. M. Anderson, W. A. Neiwert, M. L. Kirk, P. M. B. Piccoli, A. J. Schultz, T. Koetzle, F., D. G. Musaev, K. Morokuma, R. Cao and C. L. Hill, *Science*, 2004, **306**, 2074-2077.

25. D. Kumar, E. Derat, A. M. Khenkin, R. Neumann and S. Shaik, *J. Am. Chem. Soc.*, 2005, **127**, 17712-17718.

26. T. M. Anderson, R. Cao, E. Slonkina, B. Hedman, K. O. Hodgson, K. I. Hardcastle, W. A. Neiwert, S. Wu, M. L. Kirk, S. Knottenbelt, E. C. Depperman, B. Keita, L. Nadjo, D. G. Musaev, K. Morokuma and C. L. Hill, *J. Am. Chem. Soc.*, 2005, **127**, 11948-11949.

27. A. M. Khenkin, D. Kumar, S. Shaik and R. Neumann, *J. Am. Chem. Soc.*, 2006, **128**, 15451-15460.

28. R. Cao, T. M. Anderson, P. M. B. Piccoli, A. J. Schultz, T. F. Koetzle, Y. V. Geletii, E. Slonkina, B. Hedman, K. O. Hodgson, K. I. Hardcastle, X. Fang, M. L. Kirk, S. Knottenbelt, P. Kögerler, D. G. Musaev, K. Morokuma, M. Takahashi and C. L. Hill, *J. Am. Chem. Soc.*, 2007, **129**, 11118-11133.

29. C. L. Hill and R. B. Brown, Jr., *J. Am. Chem. Soc.*, 1986, **108**, 536-538.

30. D. Mansuy, J.-F. Bartoli, P. Battioni, D. K. Lyon and R. G. Finke, *J. Am. Chem. Soc.*, 1991, **113**, 7222-7226.

31. R. Neumann and C. Abu-Gnim, *J. Chem. Soc. Chem. Comm.*, 1989, 1324-1325.

32. O. A. Kholdeeva, *Topics in Catalysis*, 2006, **40**, 229-243.

33. J. Wang, L. Yan, G. Li, X. Wang, Y. Dinga and J. Suo, *Tetrahedron Letters*, 2005, **46**, 7023-7027.

34. I. V. Kozhevnikov and K. I. Matveev, *Russian Chem. Rev.*, 1982, **51**, 1075-1088.

35. I. V. Kozhevnikov and K. I. Matveev, *Appl. Catal.*, 1983, **5**, 135-150.

36. R. Neumann and M. Levin, *J. Am. Chem. Soc.*, 1992, **114**, 7278-7286.

37. N. M. Okun, J. C. Tarr, D. A. Hilleshiem, L. Zhang, K. I. Hardcastle and C. L. Hill, *J. Mol. Catal. A. Chem.*, 2006, **246**, 11-17.

38. C. L. Hill, *J. Mol. Catal. A: Chem*, 2007, **262**, 2–6.

39. O. A. Kholdeeva and R. I. Maksimovskaya, *J. Mol. Catal. A: Chem. Special Issue*, 2007, **262**, 7–24.

40. R. Acerete, S. Harmalker, C. F. Hammer, M. T. Pope and L. C. W. Baker, *J. Chem. Soc. Chem. Comm.*, 1979, 777-779.

41. X. Y. Zhang, M. T. Pope, M. R. Chance and G. B. Jameson, *Polyhedron*, 1995, **14**, 1381-1392.

42. M. S. S. Balula, I. C. M. S. Santos, J. A. F. Gamelas, A. M. V. Cavaleiro, N. Binsted and W. Schlindwein, *Eur. J. Inorg. Chem.*, 2007, 1027-1038.

43. T. L. Jorris, M. Kozik, N. Casañ-Pastor, P. J. Domaille, R. G. Finke, W. K. Miller and L. C. W. Baker, *J. Am. Chem. Soc.*, 1987, **109**, 7402-7408.

44. U. Kortz and S. Matta, *Inorg. Chem.*, 2001, **40**, 815-817.

45. C. N. Kato, A. Shinohara, K. Hayashi and K. Nomiya, *Inorg. Chem.*, 2006, **45**, 8108-8119.

46. O. A. Kholdeeva, G. M. Maksimov, R. I. Maksimovskaya, M. P. Vanina, T. A. Trubitsina, D. Y. Naumov, B. A. Kolesov, N. S. Antonova, J. J. Carbó and J. M. Poblet, *Inorg. Chem.*, 2006, **45**, 7224-7234.

47. O. A. Kholdeeva, M. N. Timofeeva, G. M. Maksimov, R. I. Maksimovskaya, W. A. Neiwert and C. L. Hill, *Inorg. Chem.*, 2005, **44**, 666-672.

48. S. Reinoso, P. Vitoria, L. S. Felices, L. Lezama and J. M. Gutiérrez-Zorrilla, *Inorg. Chem.*, 2006, **45**, 108-118.

49. S. Reinoso, P. Vitoria, J. M. Gutiérrez-Zorrilla, L. Lezama, J. M. Madariaga, L. S. Felices and A. Iturrospe, *Inorg. Chem.*, 2007, **46**, 4010-4021.

50. M. Sadakane, D. Tsukuma, M. H. Dickman, B. S. Bassil, U. Kortz, M. Capron and W. Ueda, *Dalton Trans.*, 2007, 2833-2838.

51. H. T. Evans, T. J. R. Weakley and G. B. Jameson, *J. Chem. Soc. Dalton Trans.*, 1996, 2537-2540.

52. B. Yan, Y. Xu, X. Bu, N. K. Goh, L. S. Chia and G. D. Stucky, *J. Chem. Soc. Dalton Trans.*, 2001, 2009-2014.

53. P. Mialane, L. Lisnard, A. Mallard, J. Marrot, E. Antic-Fidancev, P. Aschehoug, D. Vivien and F. Sécheresse, *Inorg. Chem.*, 2003, **42**, 2102-2108.

54. J.-Y. Niu, Z.-L. Wang and J.-P. Wang, *J. Solid State Chem.*, 2004, **177**, 3411-3417.

55. S. Reinoso, P. Vitoria, J. M. Gutiérrez-Zorrilla, L. Lezama, L. S. Felices and J. I. Beitia, *Inorg. Chem.*, 2005, **44**, 9731-9742.

56. L. S. Felices, P. Vitoria, J. M. Gutiérrez-Zorrilla, L. Lezama and S. Reinoso, *Inorg. Chem.*, 2006, **45**, 7748-7757.

57. R. d. P. F. Bonfim, L. C. d. Moura, H. Pizzala, S. Caldarelli, S. Paul, J. G. Eon, O. Mentré, M. Capron, L. Delevoye and E. Payen, *Inorg. Chem.*, 2007, **46**, 7371-7377.

58. E. Coronado, J. R. Galan-Mascaros, C. Gimenez-Saiz, C. J. Gomez-Garcia and S. Triki, *J. Am. Chem. Soc.*, 1998, **120**, 4671-4681.

59. H. Liu, C. J. Gómez-García, J. Peng, J. Sha, Y. Lia and Y. Yana, *Dalton Trans.*, 2008, 6211-6218.

60. L.-H. Bi, U. Kortz, B. Keita and L. Nadjo, *Dalton Trans.*, 2004, 3184-3190.

61. H. Liu, C. J. Gómez-García, J. Peng, J. Sha, L. Wang and Y. Yan, *Inorganica Chimica Acta*, 2009, **362**, 1957-1962.

62. Z. Han, Y. Zhao, J. Peng, H. Ma and E. W. Qun Liu, *J. Mol. Struct.*, 2005, **738**, 1-7.

63. V. Artero, D. Laurencin, R. Villanneau, R. Thouvenot, P. Herson, P. Gouzerh and A. Proust, *Inorg. Chem.*, 2005, **44**, 2826-2835.

64. A. Falber, B. P. Burton-Pye, I. Radivojevic, L. Todaro, R. Saleh, L. C. Francesconi and C. M. Drain, *Eur. J. Inorg. Chem.*, 2009, 2459-2466.

65. Q.-H. Luo, R. C. Howell, M. Dankova, J. Bartis, C. W. Williams, J. William DeW. Horrocks, J. Victor G. Young, A. L. Rheingold, L. C. Francesconi and M. R. Antonio, *Inorg. Chem.*, 2001, **40**, 1894-1901.

66. M. Sadakane, M. H. Dickman and M. T. Pope, *Inorg. Chem.*, 2001, **40**, 2715-2719.

67. C. Zhang, R. C. Howell, Q.-H. Luo, H. L. Fieselmann, L. J. Todaro and L. C. Francesconi, *Inorg. Chem.*, 2005, **44**, 3569-3578.

68. C. Boglio, G. Lenoble, C. Duhayon, B. Hasenknopf, R. Thouvenot, C. Zhang, R. C. Howell, B. P. Burton-Pye, L. C. Francesconi, E. Lacôte, S. Thorimbert, M. Malacria, C. Afonso and J.-C. Tabet, *Inorg. Chem.*, 2006, **45**, 1389-1398.

69. T. J. R. Weakly, *Polyhedron*, 1987, **6**, 931-937.

70. W. J. Randall, T. J. R. Weakley and R. G. Finke, *Inorg. Chem.*, 1993, **32**, 1068-1071.

71. M. Sadakane, A. Ostuni and M. T. Pope, *J. Chem. Soc. Dalton Trans.*, 2002, 63-67.

72. C. N. Kato, Y. Kasahara, K. Hayashi, A. Yamaguchi, T. Hasegawa and K. Nomiya, *Eur. J. Chem.*, 2006, 4834-4842.

73. T. Hasegawa, H. Murakami, K. Shimizu, Y. Kasahara, S. Yoshida, T. Kurashina, H. Seki and K. Nomiya, *Inorganica Chimica Acta*, 2008, **361**, 1385-1394.

74. C. M. Tourné, G. F. Tourné and T. J. R. Weakley, *J. Chem. Soc. Dalton Trans.*, 1986, 2237-2242.

75. R. I. Maksimovskaya and G. M. Maksimov, *Inorg. Chem.*, 2001, **40**, 1284-1290.

76. W. H. Knoth, P. J. Domaille and R. D. Farlee, *Organometallics*, 1985, **4**, 62-68.

77. F. Xin, M. T. Pope, G. J. Long and U. Russo, *Inorg. Chem.*, 1996, **35**, 1207-1213.

78. G. S. Kim, K. S. Hagen and C. L. Hill, *Inorg. Chem.*, 1992, **31**, 5316-5324.

79. G. Sazani, M. H. Dickman and M. T. Pope, *Inorg. Chem.*, 2000, **39**, 939-943.

80. F. Hussain and U. Kortz, *Chem Comm*, 2005, 1191-1193.

81. F. Hussain, M. Reicke and U. Kortz, *Eur. J. Inorg. Chem.*, 2004, 2733-2738.

82. F. Xin and M. T. Pope, *Organometallics*, 1994, **13**, 4881-4886.

83. L. F. Piedra-Garza, M. H. Dickman, O. Moldovan, H. J. Breunig and U. Kortz, *Inorg. Chem.*, 2009, **48**, 411-413.

84. S. Reinoso, M. H. Dickman, A. Praetorius, L. F. Piedra-Garza and U. Kortz, *Inorg. Chem.*, 2008, **47**, 8798-8806.

85. G. M. Brown, M. R. Noe-Spirlet, W. R. Busing and H. A. Levy, *Acta Cryst. B*, 1977, **B33**, 1038-1046.

86. B. Dawson, *Acta Cryst. B*, 1953, **6**, 113.

87. D. A. Dougherty, *Science*, 1996, **271**, 163-168.

88. J. C. Ma and D. A. Dougherty, *Chem. Rev.* 1997, **97**, 1303.

89. R. Contant, *Can. J. Chem.*, 1987, **65**, 568-573.

90. R. Contant, in *Inorganic Syntheses*, ed. A. P. Ginsberg, John Wiley and Sons, New York, Edition edn., 1990, vol. 27, pp. 104-111.

91. R. Contant and G. Herve, *Rev. Inorg. Chem.*, 2002, **22**, 63.

92. I. Bruker AXS, Analytical X-ray Sysems, Madison, WI, Edition edn., 2003.

93. I. Bruker AXS, Analytical X-Ray Sytems, Madison, WI, Edition edn., 2003.

94. G. Sheldrick, Edition edn., 2007.

95. I. Bruker AXS, Madison, WI, Edition edn., 2003.

Chapter 2: Controlled Synthesis of a Unique $M_aM_bM_c(PW_9)_2$ Sandwich-Type Complex *Via* an Unprecedented Synthetic Route

2.1 Abstract

The synthesis of a new and useful vacant polytungstate ligand and its use to obtain a crystallographically characterized $\{M_aM_bM_c(PW_9)_2\}$ sandwich-type complex, the first example of the purposeful and controlled metal incorporation into a derivatized POM, is reported. The aim of this study is to bring the functionality of a d-electron transition metal, the disorder-free properties of the phenyltin unit, and the stability of a W-center all together in one polyoxometalate. The covalent incorporation of a phenyltin unit into the polyanion effectively removes crystallographically-imposed symmetry elements typically seen in such species. To generate this complex, an unprecedented synthetic route is presented where a single tungsten unit is controllably removed from the polyanion by carefully increasing the solution pH value. This is the first example of the selective removal of a tungsten unit from a polyoxometalate. The addition of Cu(II) generates a sandwich-type polyoxometalate with three different units in the belt which each serve a unique purpose (stability, functionalization, and reactivity). Alternatively, the addition of another phenyltin unit produces a diphenyltin-substituted polyoxometalate which, like all the other crystal structures, is positionally disorder-free in the unit cell.

2.2 Introduction

Polyoxometalates (POMs) have attracted considerable recent attention because of their unique ensemble of alterable molecular properties and their consequent diverse applications in oxygen activation and catalysis, magnetism, luminescence, photochromism and nano-technology.[1-6] Defect or "lacunary" polytungstates have been particularly well-scrutinized because they can function as inorganic ligands for other transition metals, making them useful in studies ranging from fundamental coordination chemistry, chirality, peroxo binding, catalysis, ion pairing, surface reactions of minerals and supramolecular self-assembly.[7-14] Despite all of this vibrant research activity, several challenges involving lacunary polytungstates remain and efforts are focused on (1) controlling speciation during synthesis, (2) making functionalized polytungstate ligands, and (3) obtaining transition-metal-substituted derivatives whose structures can be unambiguously determined from single crystal X-ray diffraction.[15-17] The results presented herein address these three critical issues in polyoxometalate chemistry.

A central problem with many metal-substituted POMs that are derived from lacunary polytungstates is that the resulting complexes are frequently just as difficult to characterize structurally as they are experimentally valuable because of crystallographic disorder. For instance, the very active polyoxometalate-based catalyst reported by Hill and co-workers[18,19] termed the "hot catalyst" is a mono-iron-substituted Keggin species. Due to the high symmetry of the resulting crystals, researchers have been unable to locate the terminal ligand on the Fe center. From an intellectual vantage point, many of the ruthenium-nitrido- and manganese-nitrido-

substituted-POMs developed by Proust and co-workers[20-23] have note been able to be characterized by X-ray crystallography for the same reason. In these cases the nitrido assignment was made on non-crystallographic forms of characterization. Thus, this presents a significant problem in both fundamental and applied areas of polyoxometalate chemistry.

Recently we reported that the introduction of a rigid and bulky phenyltin group yields disorder-free crystals of mono-substituted Keggin, α-Wells-Dawson and Knoth-type derivatives, thus facilitating unequivocal location of the metal and quantification of bond distances and angles associated with these key centers.[24] We rationalized that one-W-unit-defect derivatives of the plenary compound from that study, $((CH_3)_2NH_2)_6K[Sn(C_6H_5)(H_2O)P_2W_{20}O_{70}(H_2O)_2]$ (**3**), might afford disorder-free transition metal-substituted sandwich type POMs of both fundamental and applied interest. We herein report here a set of new POMs that address all of the above issues.

The mono-organometal-substituted polytungstate,[25,26] $Rb_6K_5[Sn(C_6H_5)(H_2O)P_2W_{19}O_{69}(H_2O)]$ (**4**) derived from **3** is presented herein. This is the first functionalized polytungstate with a vacant site and is disorder-free in the unit cell. In addition, **4** reacts with a third transition metal to form unique sandwich-type structures, including a $\{M_aM_bM_c(PW_9)_2\}$ complex where M_a, M_b, and M_c are three different metal units in the central belt. Those structures generated from **4** are $Rb_2K_6[(Sn(C_6H_5)(H_2O))_2P_2W_{19}O_{69}(H_2O)]$ (**5**) and $((CH_3)_2NH_2)Rb_4K_4[Cu(H_2O)Sn(C_6H_5)(H_2O)P_2W_{19}O_{69}(H_2O)]$ (**6**). The polyanions of all of these complexes are rationally synthesized and their crystal structures are also

disorder-free. The originality of this report lies in the unprecedented synthetic route of controlled synthesis to remove a single $[O=W(OH_2)]^{4+}$ unit followed by functionalization with the addition of a new transition metal. This direct synthesis maintains both the crystal-directing phenyl group and the stabilizing tungsten unit in the belt. To the best of our knowledge this is the first time that a derivatized POM has undergone subsequent reactions of the POM framework and it represents a general strategy that could possibly be used for a wide range of POM systems.

2.3 Results and Discussion

The polytungstate of **3** selectively loses one of the two symmetric $[O=W(OH_2)]^{4+}$ units in the central belt position at pH 4.8 to form the monovacant polytungstate **4**. ^{31}P NMR studies confirm that **3** is stable in a pH 3.0 aqueous solution but starts to degrade at pH 4.5 to yield **4**. As a consequence, we directly synthesized **4** by reacting $[P_2W_{20}O_{70}(H_2O)_2]^{10-}$ (the well known polytungstate that is stable in solution from pH 2.0 to 8.0) with one equivalent of $(C_6H_5)SnCl_3$, and then adjusting the pH to 4.8 by the addition of 0.33 M KOH. The W atoms in the central belt position of polyanion **3** are more easily removed hydrolytically than those in the $[A\text{-}\alpha\text{-}PW_9O_{34}]^{9-}$ units because the resulting POM can more readily accommodate structural changes after the replacement of the $[O=W(OH_2)]^{4+}$ unit by an alkali metal counter cation (i.e. K1, Figure 2.1).

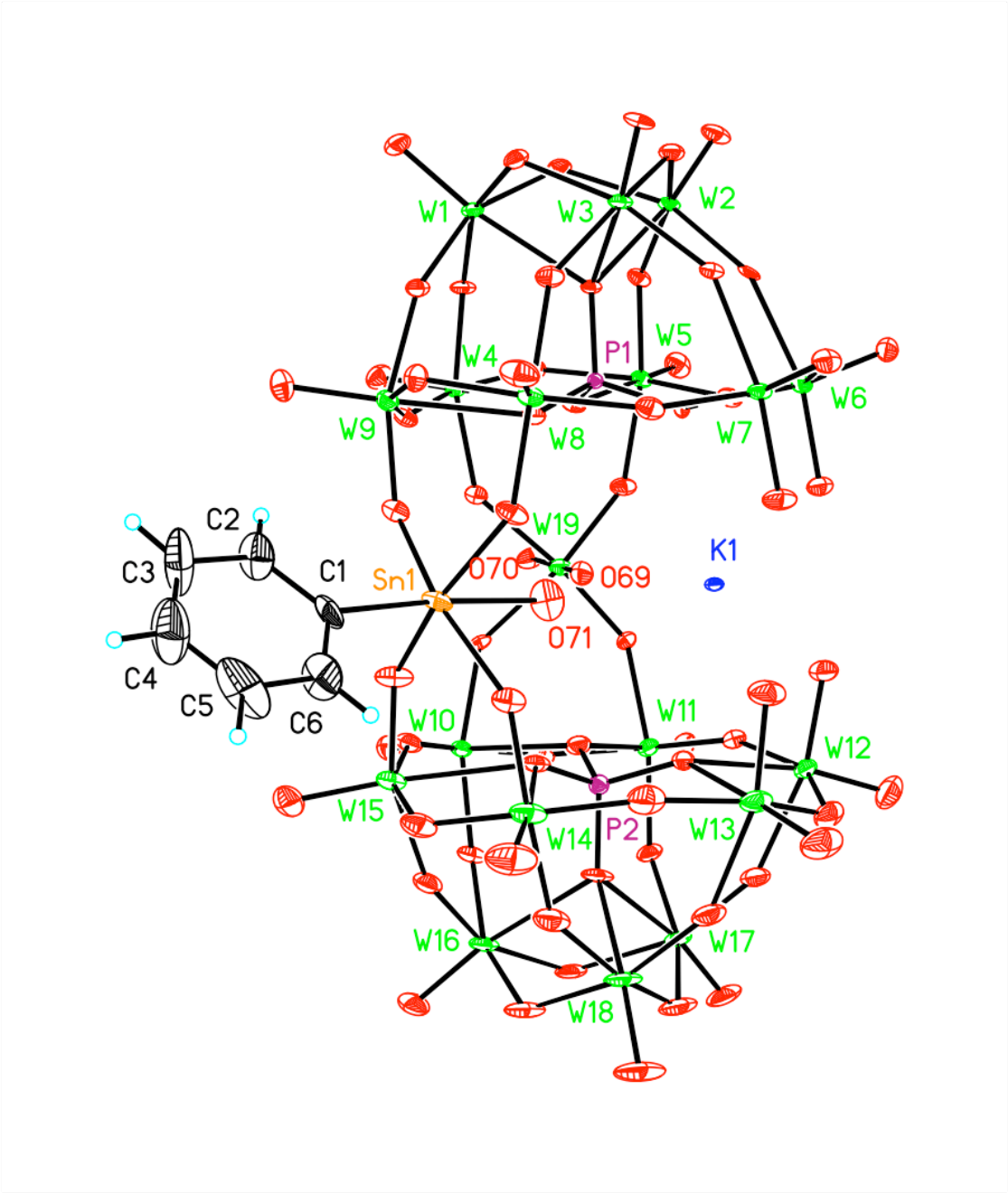

Figure 2.1. Thermal ellipsoid plot and numbering scheme of the polyanion of **4** (plotted at 50% probability). The vacant site is filled by the K1 cation in the solid state.

The structure of **4** is determined by using crystals obtained from both evaporation ($K_{11}[Sn(C_6H_5)(H_2O)P_2W_{19}O_{69}(H_2O)]\bullet 22H_2O$, **4a**) and diffusion ($K_{11}[Sn(C_6H_5)(H_2O)P_2W_{19}O_{69}(H_2O)]\bullet 15H_2O$, **4b**) methods. Complex **4a** crystallizes (triclinic $P\bar{1}$, V = 9373(9) Å^3, Z = 4) with two independent but isostructural polyanions in each asymmetric unit. These two polyanions are centrosymmetric with respect to each other (there is an inversion center for W, Sn, P, O, and C between the two polyanions in space). Each polyanion has one $[(C_6H_5)Sn(H_2O)]^{3+}$ unit and one $[O=W(H_2O)]^{4+}$ unit (W19) bridging two $[A\text{-}PW_9O_{34}]^{9-}$ units with the third position in the central belt occupied by a potassium atom (K1) in the solid state. Both the *trans* aqua ligand on Sn and the terminal W=O oxygen atom are directed inward toward the cavity. Slow diffusion of acetone into the same reaction solution affords colorless plates of **4b**, which crystallizes in the triclinic $P\bar{1}$ space group with V = 4650(3) Å^3 and Z = 2. The polyanions of **4a** and **4b** are structurally identical and the identity and purity of their bulk samples were confirmed by infrared and NMR (both ^{1}H and ^{31}P) spectroscopies. The bulk sample of **4** used for the following studies is obtained by adding an appropriate amount of RbCl to the reaction solution, which not only accelerates the crystal growth of **4** but also increases its yield.

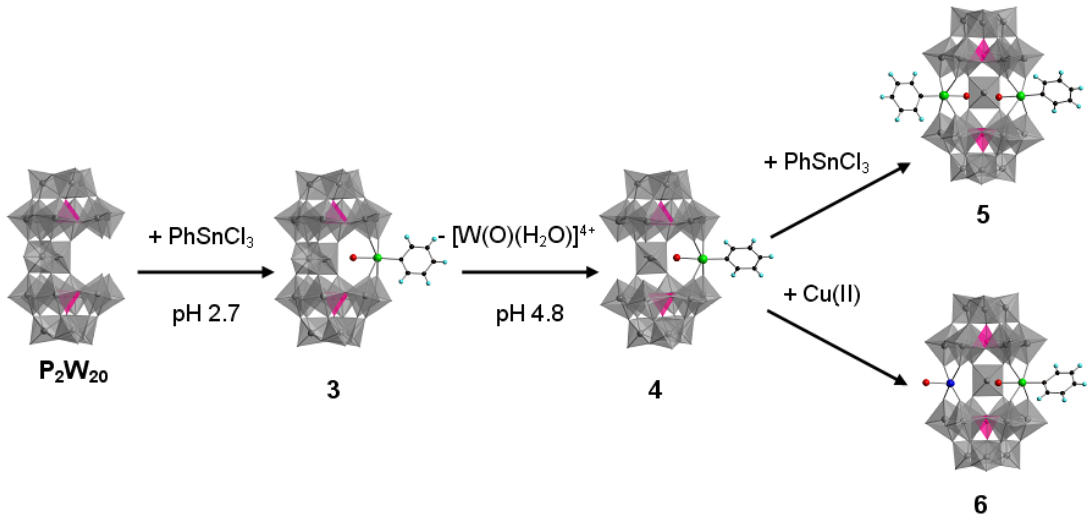

Scheme 1. Synthesis of the monovacant polytungstate ligand **4** and its use to form the diphenyltin polytungstate, **5**, and the $\{M_aM_bM_c(PW_9)_2\}$ type sandwich polytungstate, **6**. The WO_6 and PO_4 polyhedra are in gray and pink, respectively. The Sn (green), Cu (dark blue), O (red), C (black), and H (light blue) are in ball-and-stick notation.

Scheme 1 summarizes the controlled synthesis of the polyanion of **4** and the two polytungstates derived from it: the diphenyltin complex, $Rb_2K_6[(Sn(C_6H_5)(H_2O))_2P_2W_{19}O_{69}(H_2O)]$ (**5**), and the Cu adduct, $((CH_3)_2NH_2)Rb_4K_4[Cu(H_2O)Sn(C_6H_5)(H_2O)P_2W_{19}O_{69}(H_2O)]$ (**6**), a POM uniquely containing three different metals in the central belt. All of these complexes form crystals with fully occupied and crystallographically disorder-free metal centers. Attempts to synthesize **4** starting from $[P_2W_{19}O_{69}(H_2O)]^{14-}$, $\{P_2W_{19}\}$, and one equivalent of $(C_6H_5)SnCl_3$ were unsuccessful because of the instability of $\{P_2W_{19}\}$ in the very acidic solution caused by hydrolysis of the tin complex and also because the two vacant sites in the central belt of $\{P_2W_{19}\}$ can lead to incorporation of two phenyltin units. The synthetic route in Scheme 1 avoids these problems. Although

$[P_2W_{20}O_{70}(H_2O)_2]^{10-}$ is stable over a wide pH range, the polyanion of **3** selectively loses one $[O=W(OH_2)]^{4+}$ unit in the central belt position with an increase of pH.

The addition of one more equivalent of $(C_6H_5)SnCl_3$ to the aqueous solution of **4** affords the diphenyltin complex, **5**, which crystallizes in the monoclinic *C2/c* space group (V = 18297(4) Å^3, Z = 8). In this polyanion, two $[(C_6H_5)Sn(H_2O)]^{3+}$ units and one $[O=W(H_2O)]^{4+}$ unit (W19) are flanked by two $[A\text{-}PW_9O_{34}]^{9-}$ groups with the two *trans* aqua ligands on Sn1 and Sn2 and the terminal W=O oxygen pointing into the central cavity (Figure 2.2). This complex is structurally similar to an arsenic analogue $[((C_6H_5)Sn)_2As_2W_{19}O_{67}(H_2O)]^{8-}$ reported by Kortz,[27] but the Sn atoms in latter structure are five-coordinated without the inward-pointing aqua ligands present in the polyanion of **5**. At least three factors explain this difference in ligation: (1) the two As atoms in the Kortz compound have lone pairs pointing into the central cavity that sterically preclude the aqua ligands, (2) the As-As distance (5.464 Å) is much shorter than the P-P distance (6.706 Å) in **5**, and (3) the average M-M (M = W and Sn) distance in the central belt of $[((C_6H_5)Sn)_2As_2W_{19}O_{67}(H_2O)]^{8-}$ is 5.059 Å, while it is 6.129 Å in **5**. The Sn-C distances in **5** (2.126(12) Å and 2.106(13) Å, respectively) are very close to those in **4** (2.121(13) Å. The ^{31}P NMR spectrum of an aqueous solution of **5** (one singlet at -11.01 ppm) indicates that the C_{2v} solid state structure is maintained in solution.

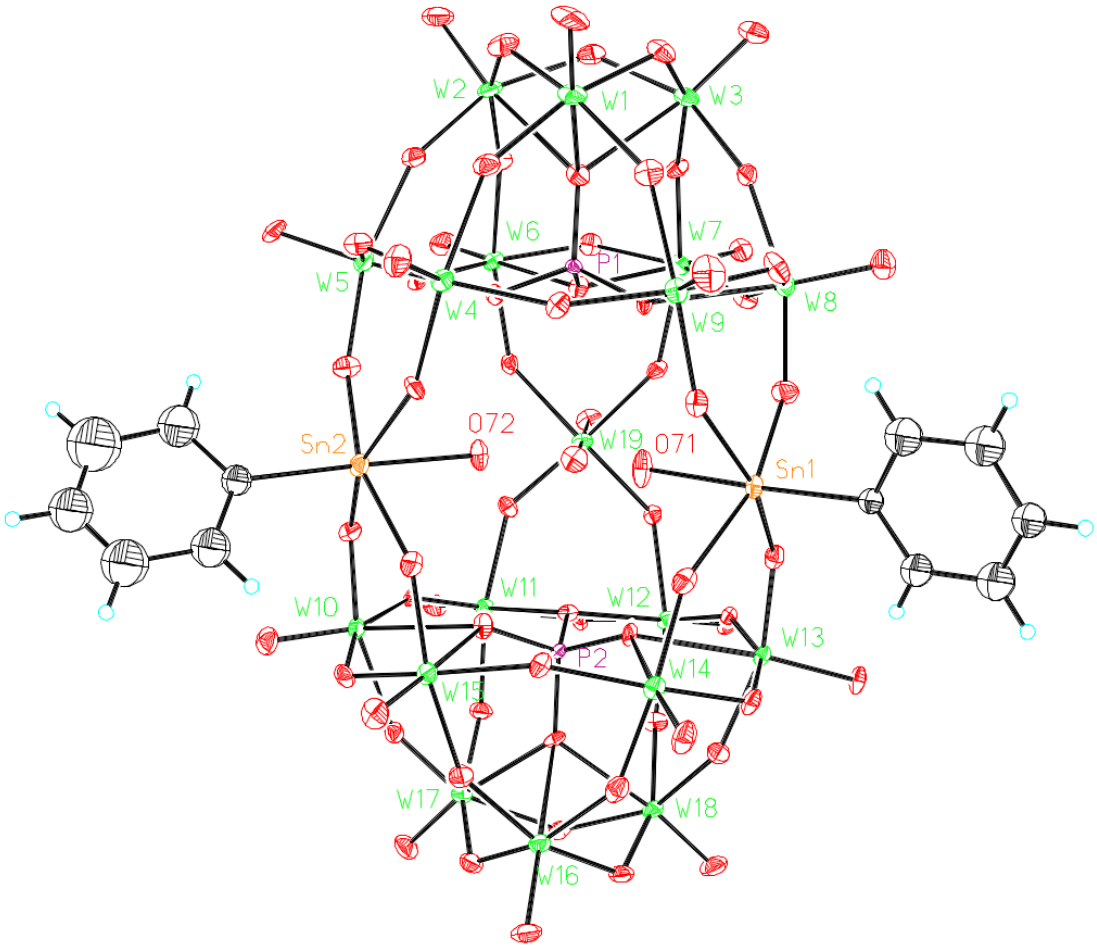

Figure 2.2. Thermal ellipsoid plot and numbering scheme of the polyanion of **5** (plotted at 50% probability). Both aqua oxygens on Sn1 and Sn2 and the terminal oxo oxygen on W19 point into the central cavity.

Reaction of a solution of **4** with Cu(II) gives the unique central tri-metal POM, **6**, whose structure is shown in Figure 2.3 (triclinic $P\bar{1}$, V = 4669(4) Å^3, Z = 2). The five-coordinated Cu atom is located in the center of an equatorial plane defined by the four oxygens from the polytungstate ligand with the fifth axial ligand pointing outward. The Cu-O(W) distances (1.914(8) - 1.961(8) Å, 1.946 Å on average) are typical of Cu-O single bonds and the longer Cu1-O72 bond (2.261(12) Å) is

consistent with a datively bonded aqua ligand. The bond valance sum (2.15) argues strongly for the Cu(II) oxidation state. The purity of bulk sample of **6** was confirmed by infrared and NMR (^{31}P and ^{1}H) spectroscopies with a single broad ^{31}P NMR peak at -22.06 ppm.

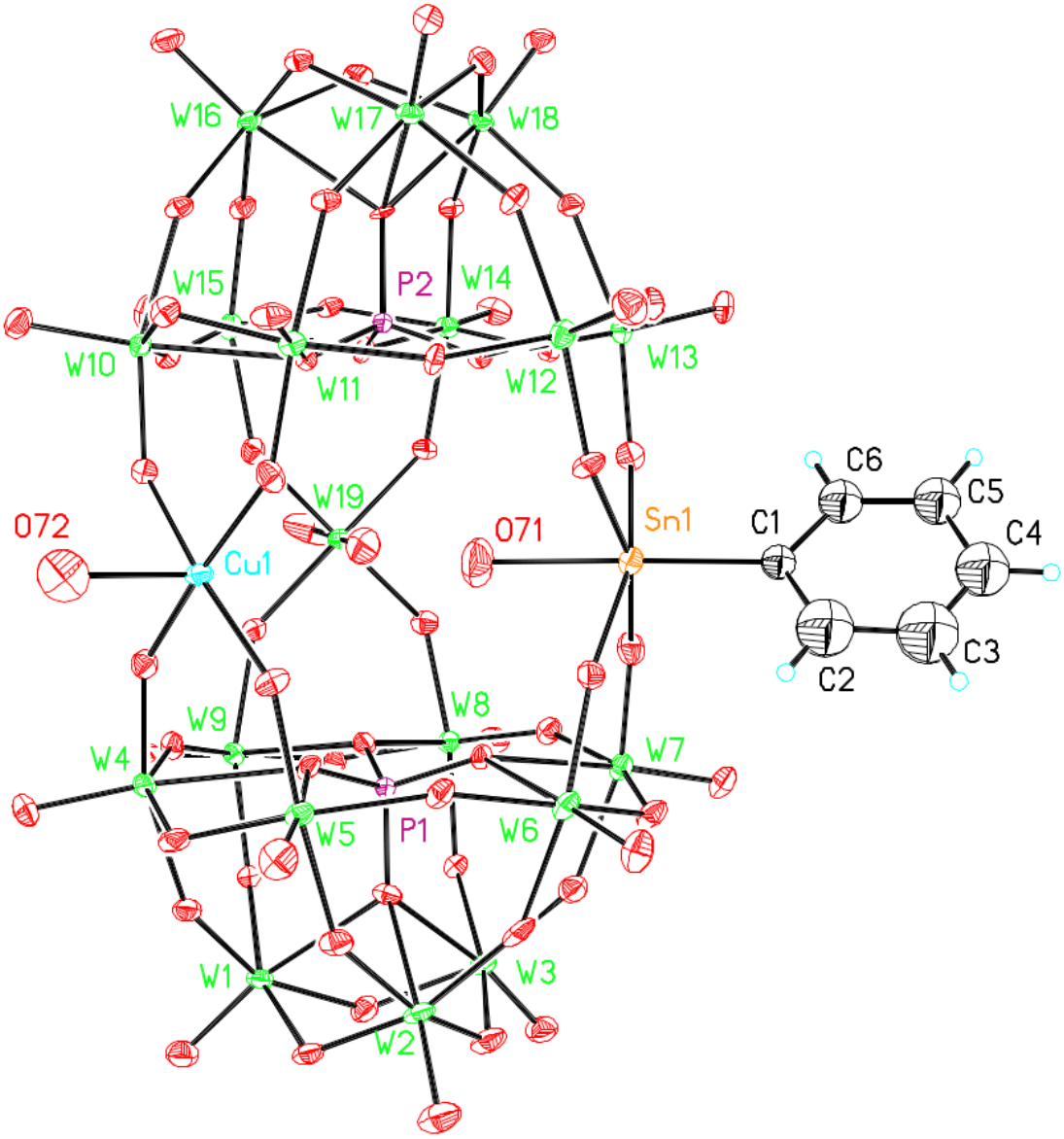

Figure 2.3. Thermal ellipsoid plot and numbering scheme for the polyanion of **6** (plotted at 50% probability). The Cu atom is five coordinate, and its aqua ligand points out from the central cavity.

The polyanion of **6** is noteworthy in several aspects. First, it represents a rare example where three different metal centers (W, Sn and Cu) are flanked by two polytungstate ligands ($[A\text{-}PW_9O_{34}]^{9-}$ in this study) to form a $\{M_aM_bM_c(A\text{-}PW_9O_{34})_2\}$ sandwich-type structure (Figure 2.4). Although such a complex was reported before, no crystallographic results were provided[28] most likely due to the three-fold disorder in structurally analogous systems without the externally directed phenyl group. Also noteworthy are the polyoxometalate structures have previously characterized where two different metals were incorporated into the belt.[29] The structures presented herein surpass these by adding more complexity to the system with three different units in the belt. Secondly, our ligand system facilitates binding of different metals proximal to one another, a property important in catalytic, electron transfer, and ion pairing studies.[30,33] Finally, the polyanion of **6** exhibits d-block (Cu), p-block (Sn) and d^0-metal (W) elements together in one polyanion unit, a remarkable compositional situation. In addition to the unique features regarding the polyanion moiety, the organotin group can possibly be functionalized to (1) tune the electronic properties of the organic ligand which would affect the reduction potential of the third transition metal center,[34] (2) ligate other metals or metal clusters, (3) undergo subsequent reactions through the functionalized group,[35] or (4) immobilize the polyanion unit on nanoparticles or surfaces, which has been a challenge to date using physical absorption or electrostatic interaction.[36] The results presented herein open the door to these strategies.

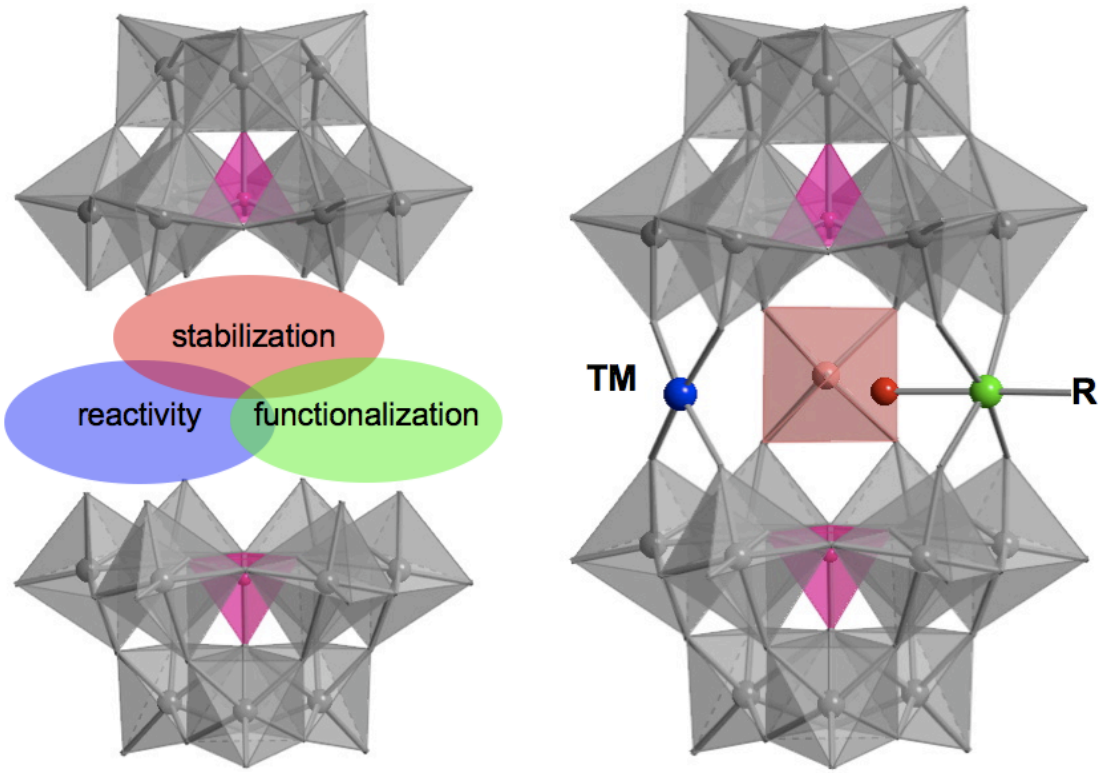

Figure 2.4. Schematic illustration of the $\{M_aM_bM_c(A\text{-}PW_9O_{34})_2\}$ sandwich-type structure. The $[A\text{-}PW_9O_{34}]^{9-}$ ligands are shown as translucent ball-and-stick polyhedra with WO_6 in grey and PO_4 in pink. The three bridging units in the central belt, $[O{=}W(H_2O)]^{4+}$, $[R\text{-}Sn(H_2O)]^{3+}$, and the third transition metal (TM), are shown in light red, green, and blue, respectively.

2.4 Experimental

General methods and materials

Polytungstates $K_{10}[P_2W_{20}O_{70}(H_2O)_2]\bullet 22H_2O$[37] and $((CH_3)_2NH_2)_6K[Sn(C_6H_5)(H_2O)P_2W_{20}O_{70}(H_2O)_2]\bullet 11H_2O$ (**3**)[24] were synthesized according to published procedures and their purities were checked by ^{31}P NMR and FT-IR spectroscopies. The compounds $(C_6H_5)SnCl_3$, $Cu(NO_3)_2\bullet 3H_2O$, and $(CH_3)_2NH\bullet HCl$ were purchased from Alfa Aesar and used as received. Elemental analyses of C, H and N were performed by Atlantic Microlab (Norcross, Georgia), and heavy atoms (K, Rb, Cu, Sn, P, and W) were performed by Columbia Laboratory (Tucson, Arizona). Infrared spectra (2% sample in KBr) were recorded on a Thermo Nicolet 6700 instrument. ^{31}P NMR measurements were made in 100% D_2O on a Varian INOVA 400 MHz spectrometer, and peaks were referenced to external 85% H_3PO_4. Thermogravimetric data were collected on a TGA 1000 instrument.

Synthesis of $((CH_3)_2NH_2)_6K[Sn(C_6H_5)(H_2O)P_2W_{20}O_{70}(H_2O)_2]\bullet 11H_2O$ (3)

$\{P_2W_{20}\}$ (1.0 g, 0.176 mmol) was dissolved in 10.0 mL water, and then $(C_6H_5)SnCl_3$ (0.033 mL, 0.203 mmol) was added *via* automatic pipettor all in one portion under vigorous stirring. The resulting cloudy solution typically has a pH of approximately 2-3 and was stirred for 10 minutes. If the pH at this time was below 2.75, it was raised to pH 2.75 with the dropwise addition of 0.1 M KOH while stirring. The solution was then filtered through a fine filter paper, and a solution of 5.0 M dimethylamine hydrochloride (*ca.* 0.44 mL) was added while stirring. The solution was left to evaporate in a partially covered 50-mL beaker. After 1 day,

colorless prismatic crystals appeared. After 8 days when the solution had reached approximately 4 mL the crystals were harvested. Yield: 0.386 g (39% with respect to the polyanion). [MW = 5622 g/mol] ^{31}P NMR: -13.40 ppm. ^{1}H NMR (aromatic region): 7.96 (d, 2H), 7.61 (m, 3 H) ppm. FT-IR (2% KBr pellet): 1464 (m), 1435 (w), 1411 (w), 1093 (s), 1081 (s), 1026 (m), 960 (m), 932 (m), 763 (s), 628 (w), 523 (w), 445 (w) cm^{-1}. Elemental analysis, Calculated: C, 3.86%; N, 1.50%; W, 65.40%; Sn, 2.12%; P, 1.10%; K, 0.70%. Found: C, 4.02%; N, 1.54%; W, 65.07%; Sn, 1.94%; P, 1.02%; K 0.70%.

Synthesis of $Rb_6K_5[Sn(C_6H_5)(H_2O)P_2W_{19}O_{69}(H_2O)]$ (4)

$K_{10}[P_2W_{20}O_{70}(H_2O)_2]$•$22H_2O$ (3.00 g, 0.528 mmol) was dissolved in 18 mL of water and $(C_6H_5)SnCl_3$ (0.095 mL, 0.578 mmol) was added dropwise. The resulting solution was stirred for 2 h at room temperature and then the white particles that formed were filtered. The pH of the resulting clear filtrate was increased from 2.4 to 4.8 by the dropwise addition of 0.33 M KOH (approximately 8-9 mL base was used until the pH was stabilized for 5 minutes). After the successful adjustment of pH, a solution of 5.0 M RbCl (0.633 mL) was added and the solution was filtered. Evaporation of the clear filtrate gave colorless, diamond-shaped prisms of **4** after 3 d at room temperature (1.35 g, yield 45%). FT-IR (2% KBr pellet): 1083(s), 1023(m), 949(s), 930(sh), 890(w), 849(m), 786(m), 746(w), 708(m), 593(m), 517(m), 443(m), 418(m) cm^{-1}. ^{31}P NMR (D_2O): -10.30 ppm. ^{1}H NMR (D_2O): 8.05 (d, 2H), 7.57 (m, 3 H) ppm. Anal. Calcd. for $Rb_6K_5[Sn(C_6H_5)(H_2O)P_2W_{19}O_{69}(H_2O)]$•$22H_2O$: C, 1.20%; W, 58.26%; Sn, 1.98%; P, 1.03%; Rb, 8.55%; K 3.26%. Found: C, 1.22%; W,

57.93%; Sn, 1.87%; P, 0.94%; Rb, 8.86%; K 3.24%. [MW = 5995 g/mol] Crystals **4a** and **4b** suitable for single crystal X-ray diffraction were obtained by the above procedure but without the addition of RbCl. Evaporation at room temperature for a week gave colorless blocks of **4a**, while diffusion of acetone to the aqueous reaction solution gave colorless prisms of **4b** after 3 d.

Synthesis of $Rb_2K_6[(Sn(C_6H_5)(H_2O))_2P_2W_{19}O_{69}(H_2O)]$ (5)

A sample of $(C_6H_5)SnCl_3$ (0.030 mL, 0.183 mmol) was added dropwise to a stirred solution of 9.0 mL water. A ground solid sample of **4** (1.00 g, 0.169 mmol) was added all at once producing a cloudy solution that became clear over a period of 1 min. After 2 h, 0.400 mL of a saturated KCl solution and 0.113 mL of a 3.0 M RbCl solution were added *via* a micropipettor and the solution was filtered. Evaporation of the clear filtrate gave colorless prisms in 3 d (0.505 g) which were recrystallized in a solution of 5 mL of water with 10 drops of 0.1 M HCl, 0.230 mL saturated KCl solution and 0.058 mL 3.0 M RbCl solution (pH = 2.60). Evaporation of the clear solution gave colorless prisms of **5** in 4 d (0.328 g, yield 33%). FT-IR (2% KBr pellet): 1090(s), 1073(m), 1032(m), 959(s), 942(sh), 903(m), 762(s), 700(m), 583(m), 519(m). ^{31}P NMR (D_2O): -11.01 ppm. ^{1}H NMR (D_2O): 7.99 (d, 2H), 7.60 (m, 3 H) ppm. Anal. Calcd. for $Rb_2K_6[(Sn(C_6H_5)(H_2O))_2P_2W_{19}O_{69}(H_2O)]\bullet 22H_2O$: C, 2.44 %; W, 59.1%; Sn, 4.02 %; P, 1.05 %; Rb, 2.89 %; K, 3.97 %. Found: C, 2.47 %; W, 58.5 %; Sn, 3.80 %; P, 0.97 %; Rb, 2.71 %; K, 3.91 %. [MW = 5906 g/mol]

Synthesis of $((CH_3)_2NH_2)Rb_4K_4[Cu(H_2O)Sn(C_6H_5)(H_2O)\text{-}P_2W_{19}O_{69}(H_2O)]$ (6)

To a stirred solution of **4** (0.50 g, 0.095 mmol) in 17 mL of water, $Cu(NO_3)_2 \bullet 3H_2O$ (0.0270 g, 0.112 mmol) was added. The solution was stirred for 1 h and then a solution of 5.0 M $(CH_3)_2NH \bullet HCl$ (0.33 mL) was added under stirring and the solution was filtered. Evaporation of the homogeneous blue filtrate gave light blue crystals of **6** after 9 d (0.160 g, yield 32%). FT-IR (2% KBr pellet): 1094 (s), 1085 (sh), 1026 (s), 954 (s), 931 (s), 896 (w), 779 (s), 737 (w), 697 (w), 583 (m), 522 (m) cm^{-1}. ^{31}P NMR (D_2O): broad peak -22 ppm. ^{1}H NMR (aromatic, D_2O): 8.42 (broad), 7.70 (broad), and 7.64 (broad) ppm. Anal. Calcd. for $((CH_3)_2NH_2)Rb_4K_4[Cu(H_2O)Sn(C_6H_5)(H_2O)P_2W_{19}O_{69}(H_2O)] \bullet 16H_2O$: C, 1.66%; N, 0.24%; W, 60.17%; Sn, 2.05%; P, 1.07%; Cu, 1.09%; Rb, 5.89%; K, 2.69%. Found: C, 1.70%; N, 0.25%; W, 59.54%; Sn, 1.91%; P, 0.96%; Cu, 1.13%; Rb, 5.67%; K, 2.51%. [MW = 5805 g/mol]

X-ray crystallography

(a) Instrumentation and methods. The complete datasets for complexes **4a**, **4b**, **5** and **6** were collected at Emory University. Single crystals suitable for X-ray analysis, were each coated with Paratone-N oil, suspended in a small fiber loop, and placed in a cooled gas stream on a Brüker D8 SMART APEX CCD sealed tube diffractometer. Diffraction intensities were measured using graphite monochromated Mo Kα radiation (λ = 0.71073 Å) at 173(2) K and a combination of φ and ω scans with 10 s frames traversing about ω at 0.5° increments. Data collection, indexing, and initial cell refinements were carried out using SMART;[38] frame integration and final cell refinements were done using SAINT.[39] The molecular structure of each complex was determined using Direct Methods and Fourier techniques and refined by full-matrix least squares. A multiple absorption correction, including face index, for each dataset at 173(2) K was applied using the program SADABS.[40] The largest residual electron density for each structure was located close to (less than 1.0 Å from) W atoms and was most likely due to imperfect absorption corrections frequently encountered in heavy-metal atom structures.

(b) Refinement details. The structures of **4a**, **4b**, **5** and **6** were solved using Direct Methods and difference Fourier techniques. All the heavy atoms were refined anisotropically. Some of the potassium ions and solvent water molecules were refined with partial occupancies; not all the countercations and solvent water molecules could be located in difference Fourier maps because of disorder. Scattering factors and anomalous dispersion corrections are taken from the *International Tables for X-ray Crystallography*. Structure solution, refinement,

graphic and generation of publication materials were performed by using SHELXTL, V6.14 software.[41]

Table 2.1. Crystal data and structural refinement for **4a** and **4b**.

complex	**4a**	**4b**
molecular formula	$C_6H_{53}K_{11}O_{93}P_2SnW_{19}$	$C_6H_{39}K_{11}O_{86}P_2SnW_{19}$
formula wt. (g mol^{-1})	5717.13	5591.02
temperature (K)	173(2)	173(2)
radiation (λ, Å)	0.71073	0.71073
crystal system	triclinic	triclinic
space group	$P\bar{1}$	$P\bar{1}$
a (Å)	11.809(7)	11.914(5)
b (Å)	24.155(13)	18.028(7)
c (Å)	35.310(19)	24.593(13)
α (°)	109.785(8)	109.060(8)
β (°)	95.200(8)	92.994(8)
γ (°)	94.589(9)	108.872(5)
Volume (Å^3)	9373(9)	4650(3)
Z	4	2
ρ_{calcd} (g cm^{-3})	3.920	3.913
μ (mm^{-1})	24.048	24.200
F(000)	9649	4772
crystal size (mm^3)	0.35 × 0.16 × 0.09	0.19 × 0.11 × 0.06
θ range	1.24 to 30.37º	0.89 to 30.32º
reflections collected	170688	83570
independent reflections	52507 [R(int) = 0.0668]	25921 [R(int) = 0.0560]
max./min. transmission	0.2208 and 0.0434	0.3246 and 0.0911
refinement method	full-matrix least-squares on F^2	full-matrix least-squares on F^2
data/restraints/param.	52507/0/1345	25921/0/1049
goodness-of-fit on F^2	1.039	1.034
final R indices [R > 2σ (I)]	R1[a] = 0.0486 wR2[b] = 0.1193	R1[a] = 0.0428 wR2[b] = 0.1103
R indices (all data)	R1[a] = 0.0636 wR2[b] = 0.1265	R1[a] = 0.0581 wR2[b] = 0.1194
largest diff. peak and hole (e Å^{-3})	6.183 and -3.333	4.893 and -3.208

[a] $R_1 = \Sigma||F_o| - |F_c|| / |F_o|$

[b] $wR_2 = \{\Sigma[w(F_o^2 - F_c^2)^2] / \Sigma[w(F_o^2)^2]\}^{0.5}$

Table 2.2. Crystal data and structural refinement for **5**.

complex	**5**
molecular formula	$C_{12}H_{60}K_6O_{94}P_2Rb_2Sn_2W_{19}$
formula wt. (g mol^{-1})	5906.40
temperature (K)	173(2)
radiation (λ, Å)	0.71073
crystal system	monoclinic
space group	*C2/c*
a (Å)	32.678(4)
b (Å)	14.1708(19)
c (Å)	39.662(5)
α (°)	90
β (°)	94.992(2)
γ (°)	90
Volume (Å^3)	18297(4)
Z	8
ρ_{calcd} (g cm^{-3})	4.124
μ (mm^{-1})	25.787
F(000)	19759
crystal size (mm^3)	0.45 × 0.15 × 0.11
θ range	1.63 to 32.59º
reflections collected	194610
independent reflections	31826 [R(int) = 0.0758]
max./min. transmission	0.1672 and 0.0304
refinement method	full-matrix least-squares on F^2
data/restraints/param.	31826/0/1067
goodness-of-fit on F^2	1.047
final R indices [R > 2σ (I)]	R1[a] = 0.0458 wR2[b] = 0.1331
R indices (all data)	R1[a] = 0.0747 wR2[b] = 0.1508
largest diff. peak and hole (e Å^{-3})	2.995 and -6.613

[a] $R_1 = \Sigma||F_o| - |F_c|| / |F_o|$

[b] $wR_2 = \{\Sigma[w(F_o^2 - F_c^2)^2] / \Sigma[w(F_o^2)^2]\}^{0.5}$

Table 2.3. Crystal data and structural refinement for **6**.

complex	**6**
molecular formula	$C_8H_{51}CuK_4NO_{88}P_2Rb_4SnW_{19}$
formula wt. (g mol^{-1})	5804.87
temperature (K)	173(2)
radiation (λ, Å)	0.71073
crystal system	triclinic
space group	$P\bar{1}$
a (Å)	12.071(7)
b (Å)	17.845(10)
c (Å)	24.577(13)
α (^{o})	69.222(7)
β (^{o})	80.827(8)
γ (^{o})	70.812(8)
Volume (Å^3)	4669(4)
Z	2
ρ_{calcd} (g cm^{-3})	4.051
μ (mm^{-1})	26.170
F(000)	4942
crystal size (mm^3)	0.25 × 0.12 × 0.08
θ range	0.89 to 30.39º
reflections collected	87288
independent reflections	26442 [R(int) = 0.0594]
max./min. transmission	0.2286 and 0.0588
refinement method	full-matrix least-squares on F^2
data/restraints/param.	26442/0/1028
goodness-of-fit on F^2	1.034
final R indices [R > 2σ (I)]	R1^a = 0.0432 wR2^b = 0.1081
R indices (all data)	R1^a = 0.0596 wR2^b = 0.1155
largest diff. peak and hole (e Å^{-3})	4.364 and -4.082

$^a R_1 = \Sigma||F_o| - |F_c|| / |F_o|$

$^b wR_2 = \{\Sigma[w(F_o^2 - F_c^2)^2] / \Sigma[w(F_o^2)^2]\}^{0.5}$

2.5 Characterization data for complexes 4-6

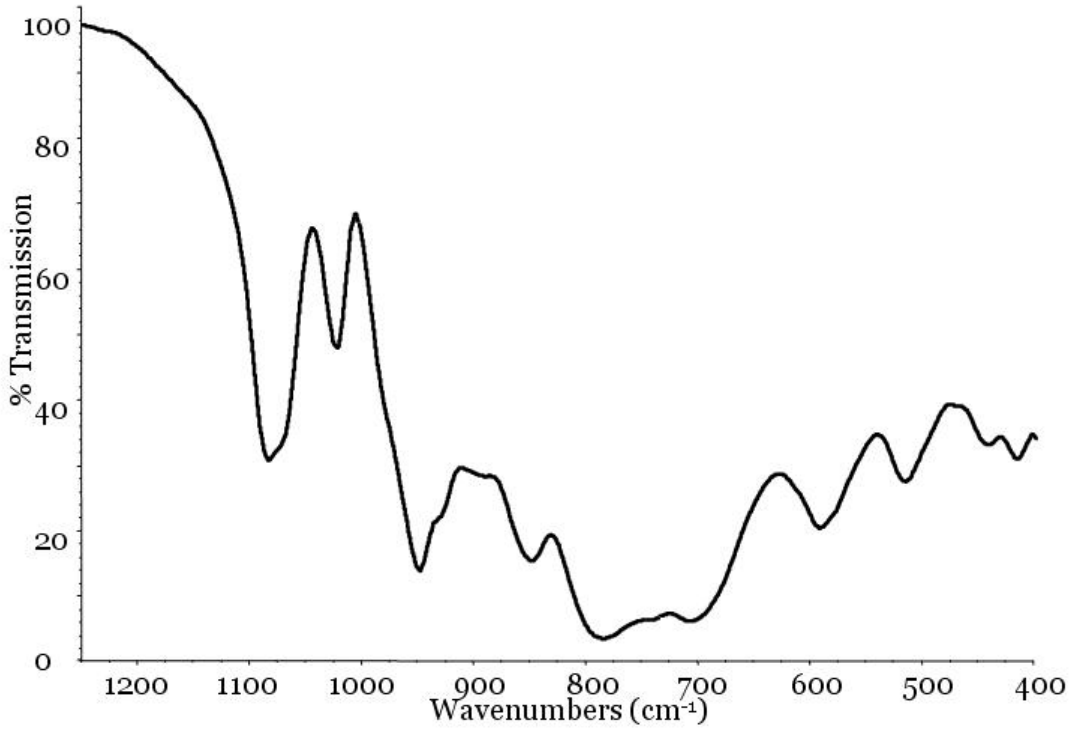

Figure 2.5. FT-IR spectrum of $Rb_6K_5[Sn(C_6H_5)(H_2O)P_2W_{19}O_{69}(H_2O)]\bullet 22H_2O$ (**4**).

Full spectrum

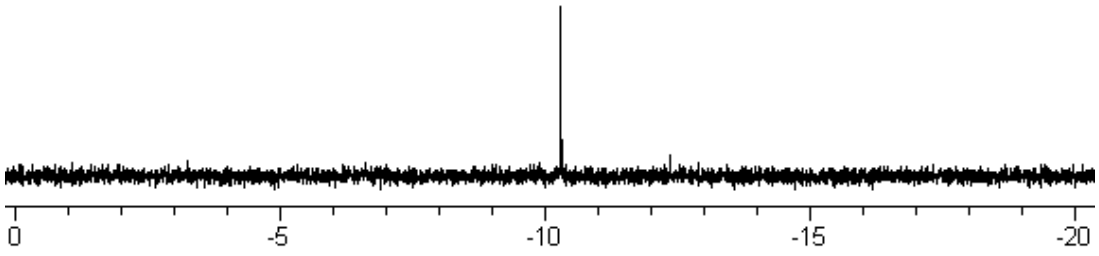

Expanded spectrum

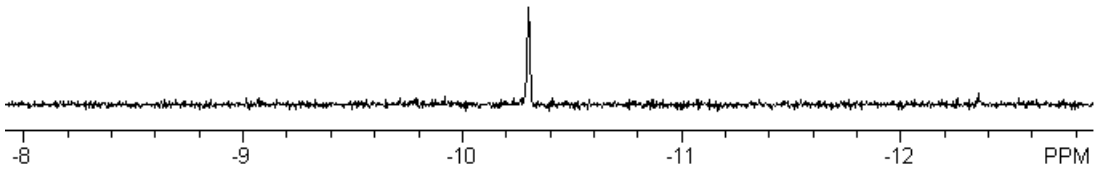

Figure 2.6. ^{31}P NMR of $Rb_6K_5[Sn(C_6H_5)(H_2O)P_2W_{19}O_{69}(H_2O)]$ (**4**) in D_2O.

Spectrum referenced to 85% H_3PO_4 (0.0 ppm) as an external reference.

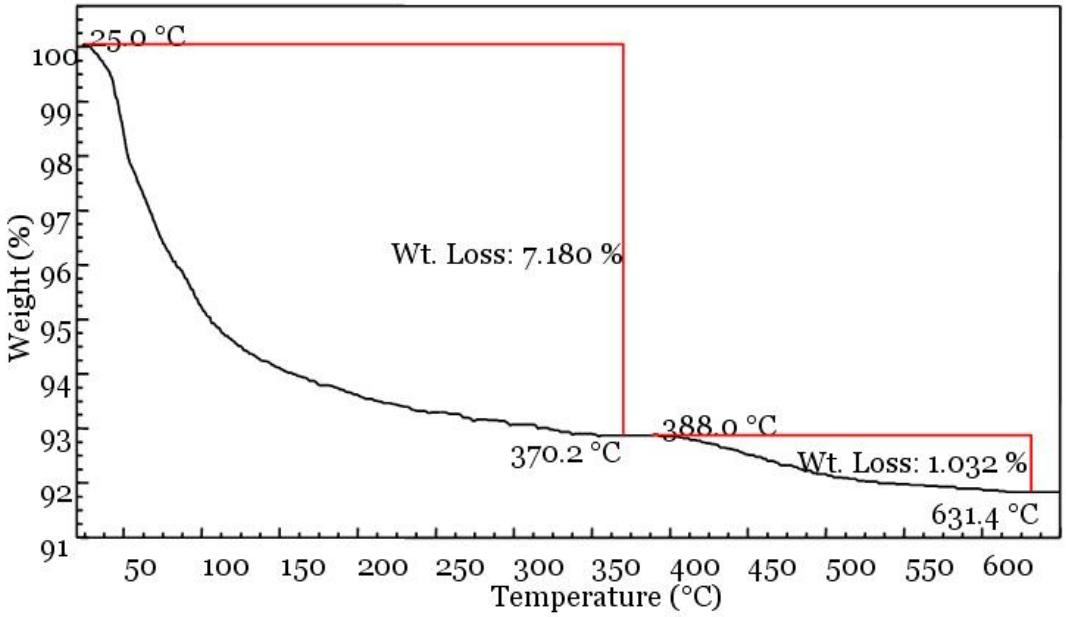

Figure 2.7. TGA weight loss curve of $Rb_6K_5[Sn(C_6H_5)(H_2O)P_2W_{19}O_{69}(H_2O)]\bullet 22H_2O$ (**4**). A 15.5772 mg sample is analyzed under inert atmosphere. The first weight loss event corresponds to the loss of 22 waters of hydration and the 2 metal-coordinated water molecules. The second weight loss event corresponds to the loss of 1.0 equivalent of phenyl.

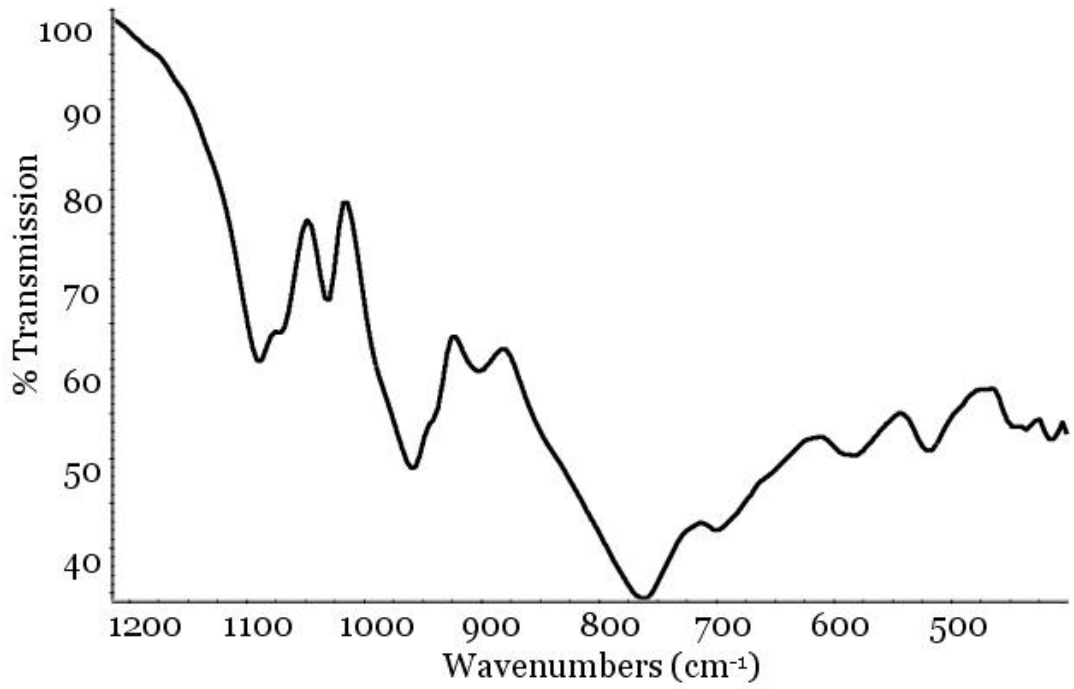

Figure 2.8. FT-IR spectrum of $Rb_2K_6[(Sn(C_6H_5)(H_2O))_2P_2W_{19}O_{69}(H_2O)]\bullet 22H_2O$ (**5**).

Full spectrum

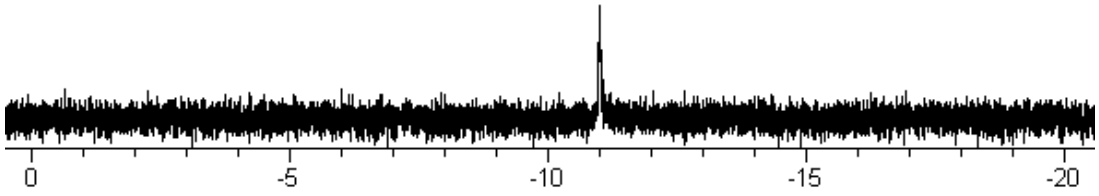

Expanded spectrum

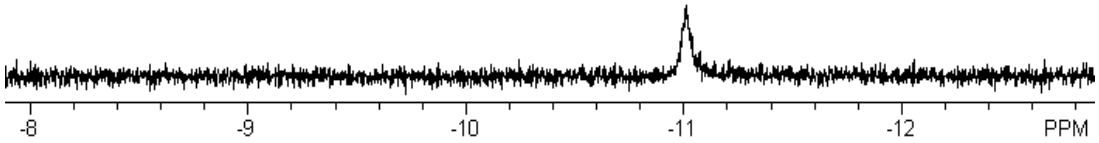

Figure 2.9. ^{31}P NMR of $Rb_2K_6[(Sn(C_6H_5)(H_2O))_2P_2W_{19}O_{69}(H_2O)]\bullet 22H_2O$ (**5**) in D_2O. Spectrum referenced to 85% H_3PO_4 (0.0 ppm) as an external reference.

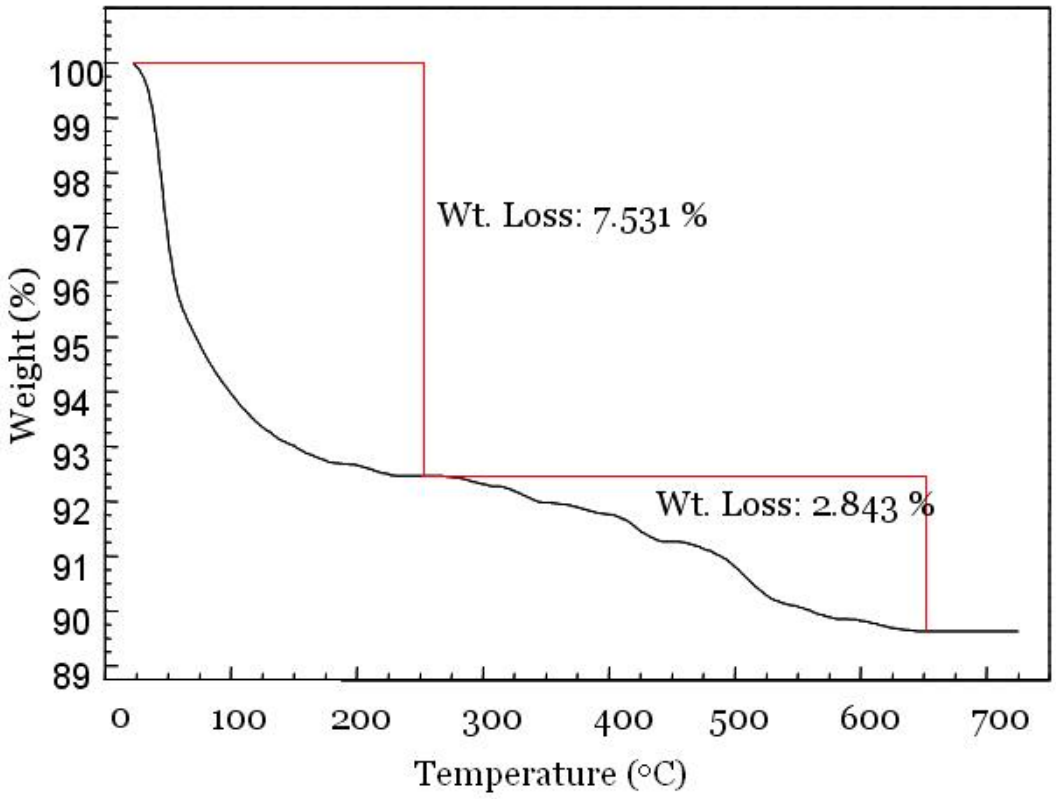

Figure 2.10. TGA weight loss curve of $Rb_2K_6[(Sn(C_6H_5)(H_2O))_2P_2W_{19}O_{69}(H_2O)]\bullet 22H_2O$ (**5**). A 14.032 mg sample is analyzed under inert atmosphere. The first weight loss event accounts for 22 waters of hydration and 3 metal-coordinated water molecules. The second weight loss event accounts for 2.0 equivalents of phenyl.

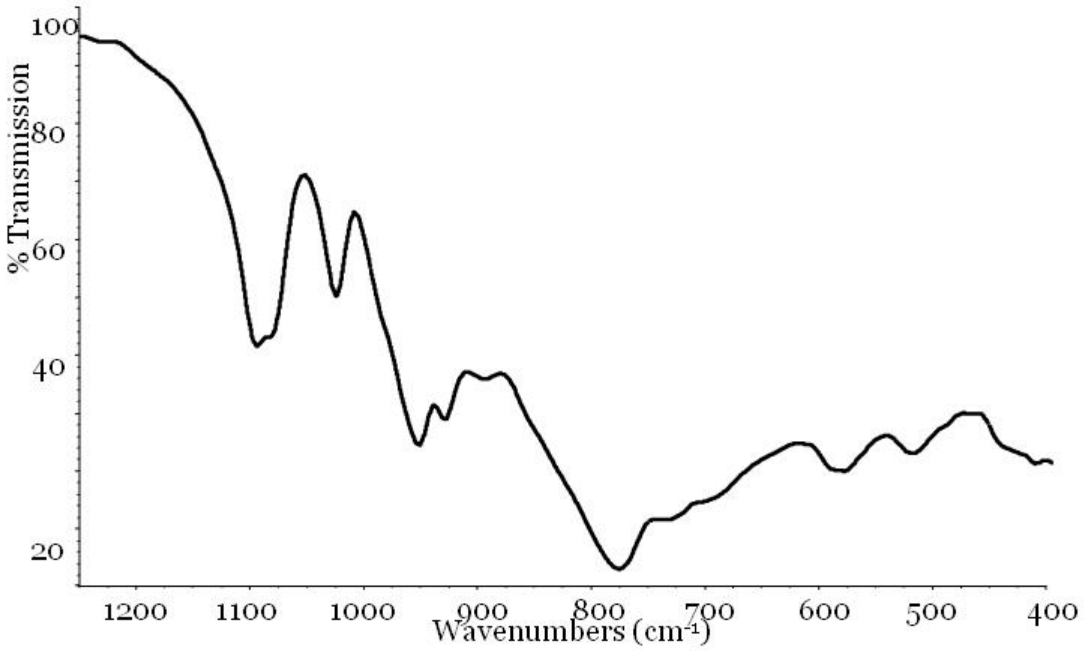

Figure 2.11. FT-IR spectrum of $((CH_3)_2NH_2)Rb_4K_4[Cu(H_2O)Sn(C_6H_5)(H_2O)$-$P_2W_{19}O_{69}(H_2O)]$ (**6**).

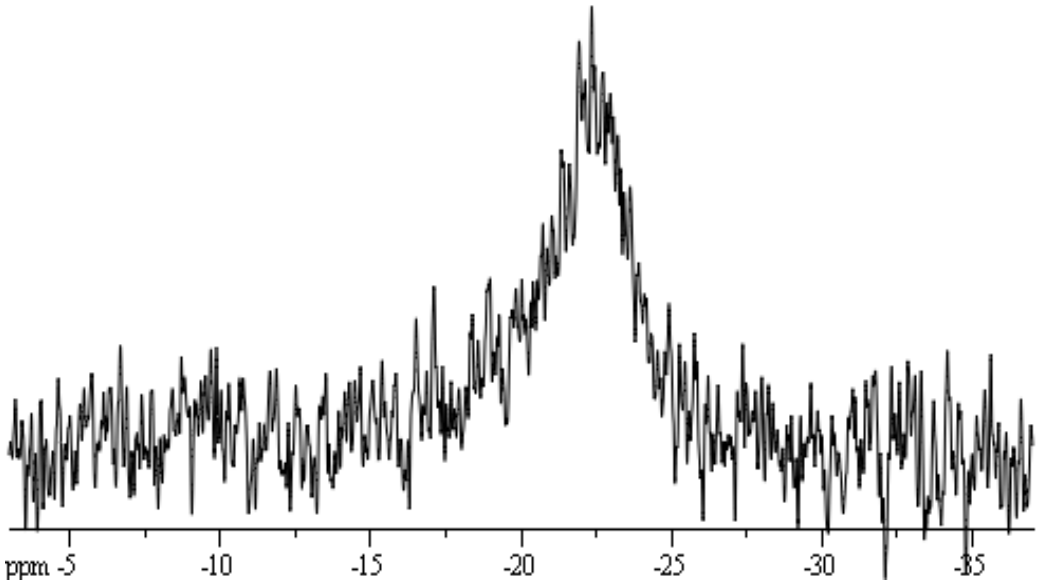

Figure 2.12. ^{31}P NMR of $((CH_3)_2NH_2)Rb_4K_4[Cu(H_2O)Sn(C_6H_5)(H_2O)P_2W_{19}O_{69}(H_2O)]$ (**6**) in D_2O. Spectrum referenced to 85% H_3PO_4 (0.0 ppm) as an external reference.

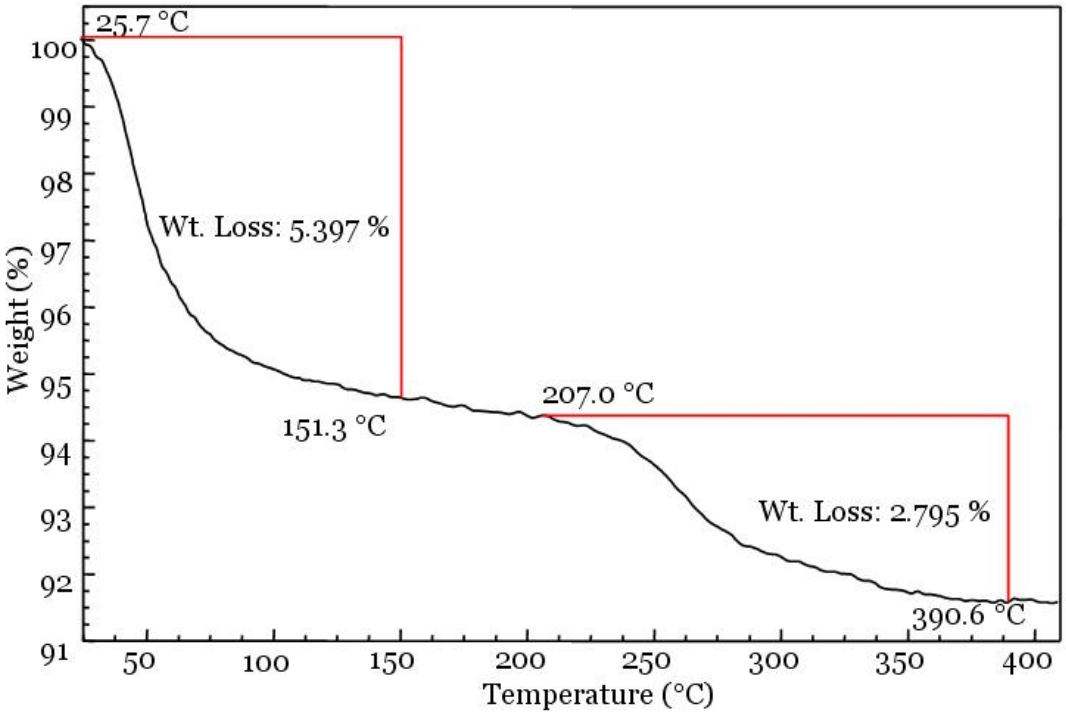

Figure 2.13. TGA weight loss curve of $((CH_3)_2NH_2)Rb_4K_4[Cu(H_2O)Sn(C_6H_5)(H_2O)\text{-}P_2W_{19}O_{69}(H_2O)]\bullet 16H_2O$ (**6**). A 14.2885 mg sample is analyzed under an inert atmosphere. The first weight loss event accounts for 16 waters of hydration. The second weight loss event corresponds to the loss of the DMA counterion, the phenyl ring, and the three metal-coordinated water molecules.

2.6 Conclusions

In summary, the generic difficulty of both controlled and selective synthesis of a series of POMs, a major goal for the realization of many applications based on a particular multifunctional POM structure, has been overcome. A sandwich-type polyoxometalate with three different metals in the belt with the general formula $\{M_aM_bM_c(PW_9)_2\}$ is reported. The compound is synthesized in a rational way through a new route by the controlled decomposition of one of the belt positions in the sandwich. The selective removal of a $[O=W(OH_2)]^{4+}$ unit is important because the direct synthesis of these compounds by the classical self-assembly process is prohibited by practical synthetic considerations. The steric nature of the phenyltin unit removes refinement of crystallographic disorder allowing for clear crystallographic determination of the units in the belt. Spectroscopic methods (^{31}P and ^{1}H NMR) confirm that these compounds maintain their structures in aqueous solution. The 4 POMs are sequentially-prepared by selective derivatization and are all refined crystallographically disorder-free with respect to the polyanion.

CrystEngComm, **2011**, *13*, 738-740 – Portions of this document have been reproduced by permission of The Royal Society of Chemistry (RSC)
http://pubs.rsc.org/en/Content/ArticleLanding/2011/CE/C0CE00828A

References

1. R. Neumann, *Inorg. Chem.*, 2010, **49**, 3594.

2. P. Kögerler, B. Tsukerblat, A. Müller, *Dalton Trans.*, 2010, **39**, 21.

3. X. Fang, M. Speldrich, H. Schilder, R. Cao, K. P. O'Halloran, C. L. Hill, P. Kögerler, *Chem. Commun.*, 2010, **46**, 2760.

4. K. Binnemans, *Chem. Rev.*, 2009, **109**, 4283.

5. M.-S. Wang, G. Xu, Z.-J. Zhang, G.-C. Guo, *Chem. Commun.*, 2010, **46**, 361.

6. T. Zhang, J. Brown, R. J. Oakley, C. F. J. Faul, *Current Opinion in Colloid & Interface Science*, 2009, **14**, 62.

7. D. Laurencin, R. Villanneau, H. Gérard, A. Proust, *J. Phys. Chem. A*, 2006, **110**, 6345.

8. B. Hasenknopf, K. Micoine, E. Lacôte, S. Thorimbert, M. Malacria, R. Thouvenot, *Eur. J. Inorg. Chem.*, 2008, 5001.

9. X. Fang, T. M. Anderson, C. L. Hill, *Angew. Chem. Int. Ed.*, 2005, **44**, 3540.

10. B. Bassil, S. S. Mal, M. H. Dickman, U. Kortz, H. Oelrich, L. Walder, *J. Amer. Chem. Soc.*, 2008, **130**, 6696.

11. Y. Kikukawa, K. Yamaguchi, N. Mizuno, *Angew. Chem. Int. Ed.*, 2010, **49**, 6096

12. G. C. Lica, K. P. Browne, Y. Tong, *J. Cluster Sci.*, 2006, **17**, 349.

13. W. H. Casey, J. R. Rustad, L. Spiccia, *Chem. Eur. J.*, 2009, **15**, 4496.

14. P. P. Mishra, J. Jing, L. C. Francesconi, T. Liu, *Langmuir*, 2008, **24**, 938.

15. B. J. Smith, V. A. Patrick, *Aust. J. Chem.*, 2000, **53**, 965.

16. C. Zhang, R. C. Howell, K. B. Scotland, F. G. Perez, L. Todaro, L. C. Francesconi, *Inorg. Chem.*, 2004, **43**, 7691.

17. S. Bareyt, S. Piligkos, B. Hasenknopf, P. Gouzerh, E. Lacôte, S. Thorimbert, M. Malacria, *J. Am. Chem. Soc.*, 2005, **127**, 6788.

18. C. L. Hill, L. Delannoy, D. C. Duncan, I. A. Weinstock, R. F. Renneke, R. S. Reiner, R. H. Atalla, J. W. Han, D. A. Hillesheim, R. Cao, T. M. Anderson, N. M. Okun, D. G. Musaev, Y. V. Geletii, *Comptes Rendus Chimie*, 2007, **10**, 305.

19. N. M. Okun, J. C. Tarr, D. A. Hilleshiem, L. Zhang, K. I. Hardcastle, C. L. Hill, *J. Mol. Cat. A: Chem.*, 2006, **246**, 11.

20. G. Izzet, E. Ishow, J. Delaire, C. Afonso, J.-C. Tabet, A. Proust, *Inorg. Chem.*, 2009, **48**, 11865.

21. C. Besson, S.-W. Chen, R. Villanneau, G. Izzet, A. Proust, *Inorg. Chem. Commun.*, 2009, **12**, 1042.

22. C. Besson, Y. V. Geletii, F. Villain, R. Villanneau, C. L. Hill, A. Proust, *Inorg. Chem.*, 2009, **48**, 9436.

23. V. Lahootun, C. Besson, R. Villanneau, F. Villain, L.-M. Chamoreau, K. Boubekeur, S. Blanchard, R. Thouvenot, A. Proust, *J. Am. Chem. Soc.*, 2007, **129**, 7127.

24. R. Cao, K. O'Halloran, D. A. Hillesheim, K. I. Hardcastle, C. L. Hill, *CrystEngComm*, 2010, **12**, 1518.

25. G. Sazani, M. H. Dickman, M. T. Pope, *Inorg. Chem.*, 2000, **39**, 939.

26. W. H. Knoth, P. J. Domaille, R. D. Farlee, *Organometallics*, 1985, **4**, 62.

27. F. Hussain, U. Kortz, R. J. Clark, *Inorg. Chem.*, 2004, **43**, 3237.

28. W. H. Knoth, P. J. Domaille, R. L. Harlow, *Inorg. Chem.*, 1986, **25**, 1577.

29. Hou, Yu; Xu, Lin; Cichon, Morgan J.; Lense, Sheri; Hardcastle, Kenneth I.; Hill, Craig L., *Inorg. Chem.*, 2010, **49**, 4125-4132.

30. L. Ruhlmann, C. Costa-Coquelard, J. Canny, R. Thouvenot, *Eur. J. Inorg. Chem.* 2007, 1493.

31. L. Ruhlmann, J. Canny, J. Vaissermann, R. Thouvenot, *Dalton Trans.*, 2004, 794.

32. M. T. Pope, S. E. O'Donnell, R. A. Prados, in *Advances in Chemistry Series: Inorganic Compounds with Unusual Properties, Vol. 150* (Ed.: R. B. King), American Chemical Society, Washington, DC, 1976, pp. Chapter 8.

33. B. Keita, I. M. Mbomekalle, Y. W. Lu, L. Nadjo, P. Berthet, T. M. Anderson, C. L. Hill, *Eur. J. Inorg. Chem.*, 2004, 3462.

34. A. Proust, R. Thouvenot, P. Gouzerh, *Chem. Commun.*, 2008, 1837.

35. K. Micoine, B. Hasenknopf, S. Thorimbert, E. Lacôte, M. Malacria, *Org. Lett.*, 2007, **9**, 3981.

36. N. M. Okun, T. M. Anderson, C. L. Hill, *J. Am. Chem. Soc.*, 2003, **125**, 3194.

37. R. Contant, *Can. J. Chem.*, 1987, **65**, 568-573.

38. *Bruker APEX2*, Bruker AXS Inc., Madison, Wisconsin, USA, 2007.

39. *Bruker, SAINT*, Bruker AXS Inc., Madison, Wisconsin, USA, 2007.

40. G. Sheldrich, *Sadabs, 2.10 edition*, 2003.

41. Bruker 2007 program: G. M. Sheldrick, A short history of SHELX, *Acta Crystallogr., Sect. A: Fundam. Crystallogr.*, 2008, **64**, 112-122.

Chapter 3: Multi-d-Electron-Containing Polyoxometalates as Useful Complexes in Emerging Research Areas

3.1 Abstract

The preparation of six new transition-metal-substituted polyoxometalates are presented below. These complexes share the useful feature of containing multiple d^n (where n = 1-9) transition metals in close proximity to one another in the polyoxometalate framework. This feature affects their properties and enhances their behavior. Most notably, a cubane-type Mn_4O_3 cluster is presented that is covalently bound to a polyoxometalate which exhibits single molecule magnet behavior in the solid state. This complex is generated by two synthetic routes: either by the generation of the Mn_4O_3 cluster *in situ* or by the hydrolytic fragmentation of $[Mn^{III}_8Mn^{IV}_4O_{12}(CH_3COO)_{16}(H_2O)_4]$ in solution. Also presented here is the conventional $Mn_4(P_2W_{15}O_{56})_2$ complex that results when only Mn(II) is used as the starting material, an Fe-O-Fe dimer encapsulated by two polyoxometalates, and a $Pd_3(SiW_9O_{33})_2$ sandwich-type structure. Portions of this chapter were written by collaborating authors who conducted the magnetic experiments and interpreted the resulting data.

3.2 Introduction

Transition-metal-substituted derivatives of polyoxometalates (POMs) are among the most heavily studied and used class of POMs in recent years. The presence of a

d^n (where n = 1-9) transition metal in a POM opens up new electrochemical processes and methods of characterization that are unavailable to traditional polyoxometalate frameworks that contain only d^0 metal ions. Furthermore, the incorporation of multiple transition metals increases the complexity of their properties and reactivity. The properties of such complexes can be modified by the choice of POM framework, heteroatom, or counter cations. There are a few particular areas of research interest in both pure and applied contexts that rely on multi-d-electron-containing polyoxometalates which will be described below.

The first research area is water oxidation catalysis based on polyoxometalate frameworks. Several of these catalysts are known and typically contain a M_4 moiety. The first such catalyst that was reported contained a Ru_4 in a pseudo-cubane-type geometry which was sandwiched between two $[SiW_{10}O_{36}]^{8-}$ units.[1] The second reported POM-based water oxidation catalyst had a Co_4 in a planar configuration sandwiched between two $[PW_9O_{34}]^{9-}$ units.[2] From this initial set of examples it appears that a M_4 moiety is important in water oxidation catalysis because the oxidation of water to O_2 is a 4-electron process which can be achieved with 4 transition metals working in conjunction. This reactivity model is substantiated by the thorough investigation of the oxidation states relevant to catalytic turnover of these water oxidation catalysts.[3]

The second area of research that makes use of multi-d-electron-containing polyoxometalates is the stabilization of single molecule magnets. Magnetic properties of POMs have recently come to attention[4-6] and are a unique chance for POMs to contribute to the well-established field of single molecule magnets. POMs

bring a unique attributes to this area because of their high solubility in water which has historically been limited to polar organics due to the organic ligands that ordinarily stabilize single molecule magnets. It is this area that will be the primary focus of this chapter.

The magnetic characteristics of polynuclear metal complexes can be greatly altered by even small changes in structure or symmetry through ligand substitution. As a notable example, the distortion caused by substituting oximato ligands switches the exchange interactions in an acetate-bridged triangular $[Mn_3O]^{7+}$ complex from antiferromagnetic to ferromagnetic.[7] Ligand substitution may also allow access to different oxidation levels of spin centers by introducing electron-donating or -withdrawing groups that may help in facilitating oxidation or reduction.[8,9] These findings have motivated our co-workers efforts[10,11] to replace bridging carboxylates on pre-formed manganese clusters with lacunary polyoxometalates.[12-14] Often highly charged, these inorganic anion ligands can show greater affinity to metal ions or coordination clusters than carboxylate and alkoxide groups. In addition, their confined ligation environments and rich redox properties, distinct from most organic ligands, qualify them for both creating unusual magnetic clusters and imparting structural and magnetic perturbations to established cluster types.

Herein, we demonstrate how to graft high-spin coordination clusters, in particular single-molecule magnets (SMMs), onto POMs. Only very few POM clusters incorporating 3d[15-17] and 4f[18] spin centers have been reported to exhibit slow magnetization relaxation characteristic for SMMs. However, a broader

approach based on replacing organic ligands of high-spin SMMs with POMs has been largely unexplored. Ligand metathesis on the numerous known classes of SMMs[19,20] should provide new insights into the control of the spin states, magnetization dynamics, and related quantum phenomena of SMMs.

We focus on a class of mixed-valence cubane manganese clusters of the type $[Mn^{III}_3Mn^{IV}O_4]^{5+}$, which has been extensively studied both as a model system of the oxygen-evolving complex in photosystem II[21-25] and as an archetypal family of SMMs with a spin-9/2 ground state that is energetically well separated from other multiplet states.[26] The $\{Mn^{III}_3Mn^{IV}\}$ cubane clusters exhibit slow relaxation and quantum tunneling of the magnetization that can even be fine-tuned through weak inter-cluster interactions.[27,28] We demonstrate here that the attachment of such a high-spin cluster to an inorganic polyoxoanion can dramatically change its magnetic properties.

3.3 Results and Discussion

The well-known single molecule magnet, $[Mn^{III}_8Mn^{IV}_4O_{12}(CH_3COO)_{16}(H_2O)_4]$ (**7**), $\{Mn_{12}O_{12}\}$,[29] was synthesized and characterized by X-ray crystallography (Figure 3.1.) This complex was used as a precursor to generate a cubane-type Mn_4 cluster *in situ* for the attachment to a POM.

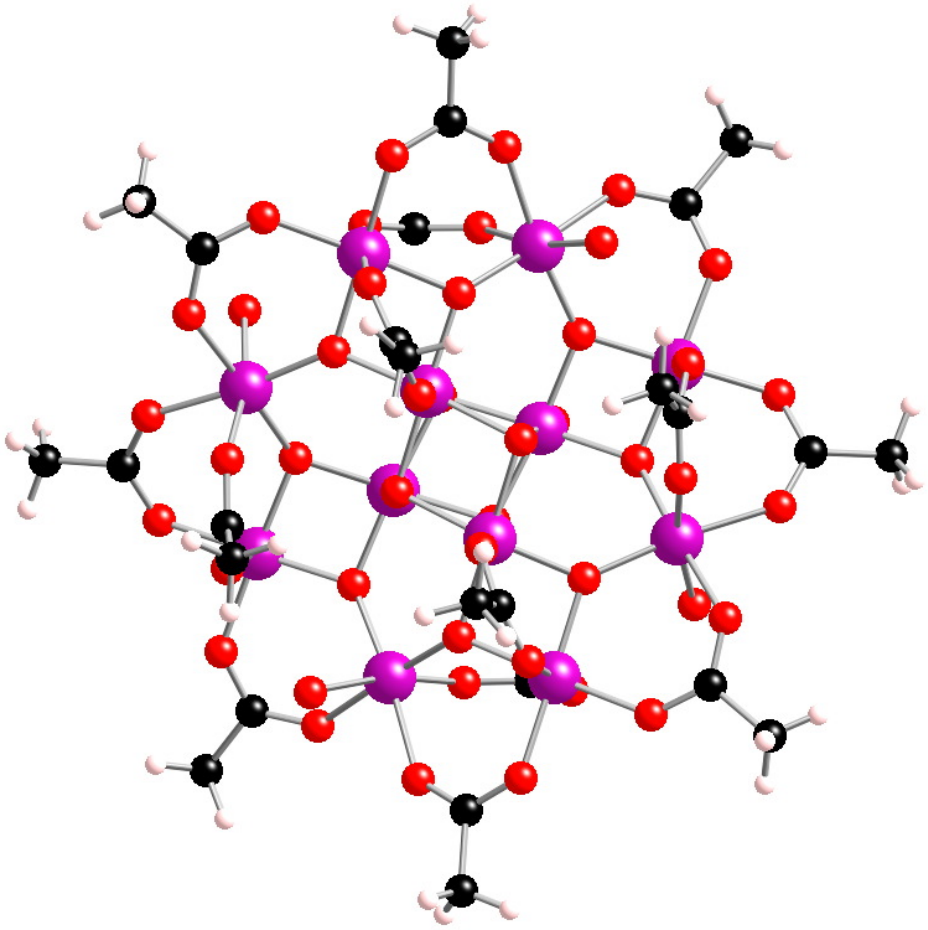

Figure 3.1. Ball-and-stick representation of **7** derived from X-ray data.

The $\{Mn^{III}_3Mn^{IV}\}$ cubane group is produced *in situ* by fragmentation of the prototypal $\{Mn_{12}\}$ complex, in the presence of $[\alpha\text{-}P_2W_{15}O_{56}]^{12-}$ in 3:2 (v/v) CH_3COOH/H_2O, resulting in the complex anion $[(\alpha\text{-}P_2W_{15}O_{56})Mn^{III}_3Mn^{IV}O_3(CH_3COO)_3]^{8-}$ (**8**), which is isolated as $[(CH_3)_2NH_2]_{5.33}H_2Mn^{II}_{0.33}$**8**$\cdot 16H_2O$ (**8a**). In addition to the dimethylammonium counter cations, hydrated Mn(II) ions are also located in the crystal lattice of **8a**, indicating that the transformation from **7** to the $\{Mn^{III}_3Mn^{IV}\}$ cubane may involve disproportionation reactions of Mn^{III} that are also observed in the formation of

other cubane-Mn_4 complexes.[30]

Single-crystal X-ray diffraction identifies **8** as a hybrid assembly of the inorganic polyoxoanion $[\alpha\text{-}P_2W_{15}O_{56}]^{12-}$ and a distorted cubane $[Mn_4O_4(\eta^2{:}\mu_2\text{-}OOCCH_3)_3]^{2+}$ cluster (Figure 3.2) which closely resembles previously reported cubane fragments $[Mn_4(\mu_3\text{-}O)_3(\mu_3\text{-}X)]^{6+}$ (X = halides, OH^-, CH_3O^-, CH_3COO^-, NO_3^- etc.)[31-34] that are surrounded exclusively by organic ligands.

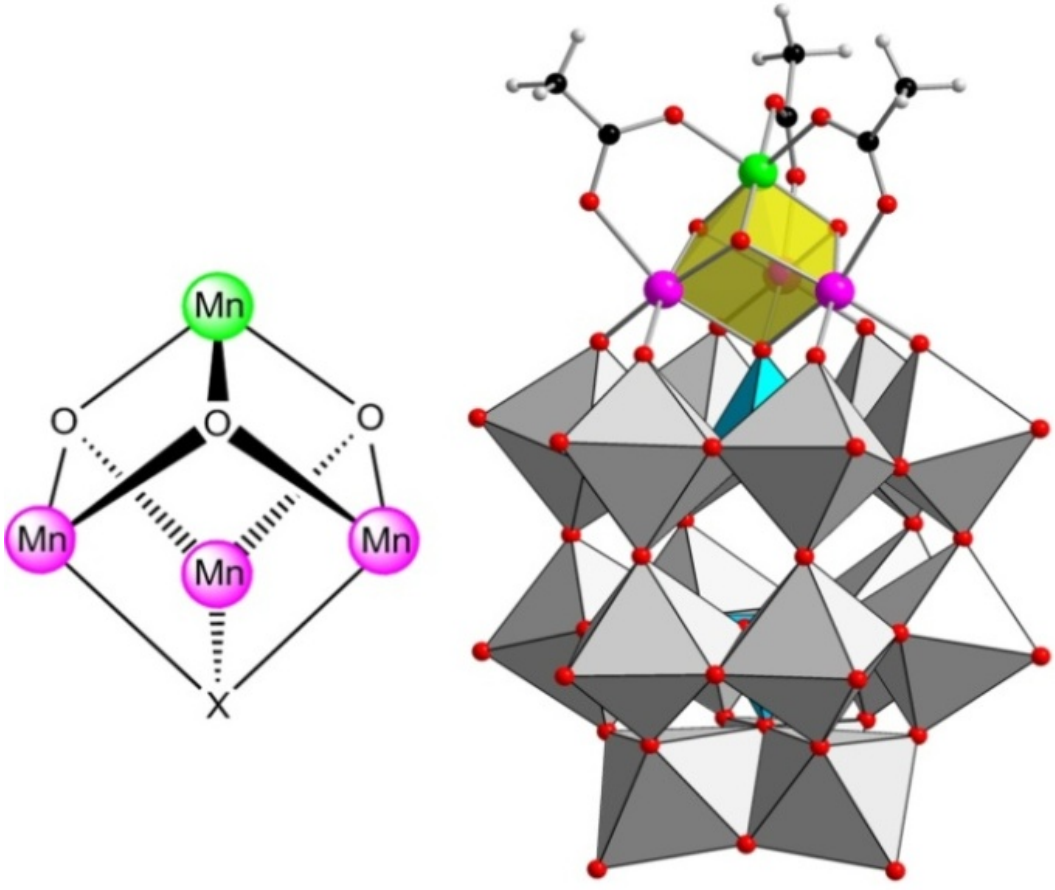

Figure 3.2. Left: The cubane $[Mn^{III}_3Mn^{IV}O_3X]^{6+}$ motif (X: monoanion ligand) common to many Mn_4 SMMs. Right: Structure of polyanion complex **8** (plotted at 50% probability). Mn^{III}, purple; Mn^{IV}, green; O, red; C, black; WO_6, gray octahedra; PO_4, blue tetrahedra.

The Mn_4 core in **8** represents a $Mn^{III}_3Mn^{IV}$ trigonal pyramid with an Mn^{IV} apex. The Mn oxidation states are established by bond valence sum analysis (2.94–3.03 for Mn^{III}; 3.96 for Mn^{IV}) and the presence of Jahn–Teller (JT) elongation axes for high-spin Mn^{III} (d^4) ions. The bond valence sum analysis was performed using the equation $s = \exp[(r_0-r)/B]$. where $B = 0.37$ and r_0 is obtained from published tables.[35] The terminal phosphate oxo ligand of the $[\alpha\text{-}P_2W_{15}O_{56}]^{12-}$ fragment assumes the role of the X group, bridging the three Mn^{III} ions and defining the intersection point of their JT axes.

A $\eta^2{:}\mu_2\text{-}CH_3COO^-$ group bridges each Mn^{III}/Mn^{IV} pair, whereas the heptadentate POM anion chelates and bridges the three Mn^{III} ions. The cluster anion **8** is of virtual C_{3v} symmetry ($Mn^{III}\cdots Mn^{III}$ distances: 3.148(8)–3.156(5) Å; $Mn^{III}\cdots Mn^{IV}$: 2.795(7)–2.804(6) Å), with the C_3 axis passing through the Mn^{IV} and two P sites. The compound **8a** crystallizes in the hexagonal space group $P6_3/m$, with the anion lying on the mirror plane. A hexahydrated Mn^{II} cation (bond valence sum: 1.84) sits on the 6_3 axis, surrounded by three cluster anions **8**, with the shortest $Mn^{II}\cdots Mn^{III}$ distance of 7.71(1) Å; therefore we consider it as a magnetically and structurally isolated counter ion.

The local environments of the Mn^{III} and Mn^{IV} sites render them spin-3/2 ($^5B_{1g}$) and spin-2 ($^4A_2$) centers, respectively.[36,37] In several aspects, the magnetic properties of **8a** are consistent with the behavior expected for $\{Mn^{III}_3Mn^{IV}\}$ cubane-type SMMs (Figure 3.3).

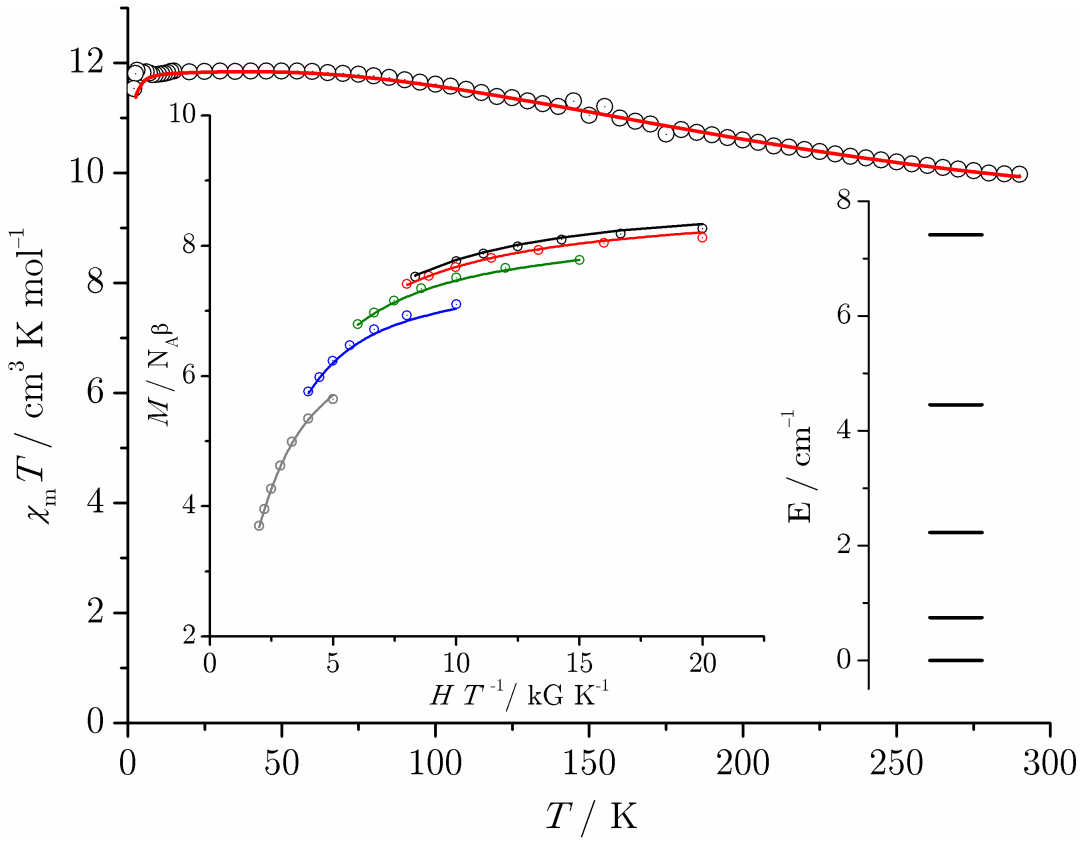

Figure 3.3. Temperature-dependence of xT for **8a** (0.1 T). Experimental data: open circles, best fit: red graph. Inset: Reduced magnetization data (1.8-5 K) with calculated curves based on a complete Hamiltonian (see text). Right: Zero-field splitting of the spin-9/2 ground state.

The temperature-dependence of the low-field susceptibility can be explained (see below) by antiferromagnetic coupling between the Mn^{IV} and Mn^{III} centers and ferromagnetic coupling between the Mn^{III} centers, resulting in an S = 9/2 ground state. Also, the deviation from isotropic Brillouin-type field-dependent magnetization curves at low temperatures (1.8-5 K) indicate strong zero-field splitting due to ligand field effects that are primarily associated with the tetragonally elongated JT-distorted Mn^{III} sites. However, no signs of slow

relaxation phenomena are observed. In particular, no out-of-phase *x*'' component is seen in the ac susceptibility (1-1150 Hz) down to 1.8 K, in striking contrast to $\{Mn^{III}_3Mn^{IV}\}$-type SMMs. To explain this discrepancy, we deviated from the conventionally used simplified spin-only models and employed a comprehensive Hamiltonian to model the observed data, based on single-ion effects (interelectronic repulsion, H_{ee}; spin-orbit coupling, H_{SO}; ligand field effects, H_{lf}; and the applied magnetic field, H_{mag}) and Heisenberg-type exchange coupling (H_{ex}):

$$\hat{H} = \hat{H}_{\mathrm{ee}} + \hat{H}_{\mathrm{lf}} + \hat{H}_{\mathrm{so}} + \hat{H}_{\mathrm{mag}} + \hat{H}_{\mathrm{ex}}$$

The influence of the tetragonal ligand field with reference to the rotation axis for the angular part of the wave function is described by[38,39]

$$H_{\mathrm{lf}}^{\mathrm{tet}} = B_0^2 \sum_{i=1}^{N} C_0^2(i) + B_0^4 \sum_{i=1}^{N} C_0^4(i) + B_4^4 \sum_{i=1}^{N} \left(C_4^4(i) + C_{-4}^4(i) \right)$$

Standard literature values were chosen as initial values for the real ligand field parameters B^k_q (Wybourne notation).[40] Note that the number of independent lf parameters is limited by the symmetry-determined ratios B^k_q/B^k_0.[38] Based on the approximate C_{3v} symmetry of **8**, the exchange interactions are grouped in contacts of the apical Mn^{IV} center and the Mn^{III} centers (J_1, each mediated by one μ_2-carboxylate and two μ_3-oxo ligands) and Mn^{III}-Mn^{III} contacts (J_2, each mediated by one μ_3-oxo, one μ_4-oxo, and, to a much lesser extent, several O-W-O-W-O bridges):

$$H_{\text{ex}} = -2\left[J_1(\hat{\boldsymbol{S}}_1 \cdot \hat{\boldsymbol{S}}_3 + \hat{\boldsymbol{S}}_1 \cdot \hat{\boldsymbol{S}}_2 + \hat{\boldsymbol{S}}_1 \cdot \hat{\boldsymbol{S}}_4) + J_2(\hat{\boldsymbol{S}}_2 \cdot \hat{\boldsymbol{S}}_3 + \hat{\boldsymbol{S}}_2 \cdot \hat{\boldsymbol{S}}_4 + \hat{\boldsymbol{S}}_3 \cdot \hat{\boldsymbol{S}}_4) \right]$$

Using our computational framework CONDON,[41] a complete basis set (full d manifolds, i.e. 210 for Mn^{III} ($3d^4$) and 120 for Mn^{IV} ($3d^3$)) is required to accurately describe the magnetic dipole orientation with respect to the local symmetry elements. Refining the B^k_0 values and J_1 and J_2 by a least-squares fit fully reproduces all data (SQ = 0.57 %) and yields B^2_0 = –5366 cm^{-1}, B^4_0 = 17183 cm^{-1}, B^4_4 = 1848 cm^{-1}, J_1 = –31.3 cm^{-1}, and J_2 = 10.2 cm^{-1}. The signs of the refined B^k_0 values agree with PCEM results.[16] The calculated ligand field splits the tenfold degenerate ground state into five doublets (Figure 3.2), which corresponds to the splitting of an S = 9/2 state into states with m_S equal to ±1/2 to ±9/2 in a spin-only model approach.

The extent of this splitting can be related to the (empirical) axial ZFS parameter D that is generally determined using the phenomenological ground-state-only expression:

$$\hat{H} = D\hat{S}_z^2 + g_{\text{iso}}\mu_{\text{B}}\mathbf{S}\cdot\mathbf{B}$$

and here amounts to D = +0.36 cm^{-1}. Whereas the absolute value of D is entirely in line with those of previously reported $\{Mn^{III}_3Mn^{IV}\}$-type SMMs, we unambiguously obtain a positive sign, i.e. not the negative sign required for the existence of a parabolic energy barrier between the $m_S = \pm S$ states that characterizes SMMs and causes hysteretic metastability upon external field change. This result contradicts previous assumptions that axial elongation of the Mn^{III} sites in $[Mn_4(\mu_3\text{-}O)_3(\mu_3\text{-}X)]^{6+}$ results in negative single-ion D values. For

8a, in contrast, the levels with an $m_S = \pm 1/2$ character are energetically lowest which does not result in a thermal barrier between m_S states and, thus, no frequency dependence of x' (correspondingly, x'' = 0). We note that **8** to our knowledge represents the first example of a $\{Mn^{III}_3Mn^{IV}\}$ cubane cluster that exhibits an inverse order of the zero-field split substates belonging to the ground state. Attachment to the $\{P_2W_{15}\}$ polyanion ligand here effectively 'switches off' the slow thermal relaxation behavior otherwise characteristic for the $\{Mn^{III}_3Mn^{IV}\}$ cluster family.

Conventional $[Mn_4(\mu_3\text{-}O)_3(\mu_3\text{-}X)]$-containing clusters with all-organic ligand peripheries usually are of limited solubility in common solvents, complicating their characterization in solution.[31-34] Introducing highly charged inorganic POM ligands will in turn enhance the solubility of these magnetic clusters in polar media, particularly in water. This will allow their stability and oxidation reactivities to be assessed under biologically relevant conditions. In addition, POM substitution is expected to thermodynamically stabilize the structure. Previous studies suggest that the bridging $\mu_3\text{-}X^-$ ion in $[Mn_4(\mu_3\text{-}O)_3(\mu_3\text{-}X)]$ is generally labile and amenable to substitution.[35] The dissociation of the POM ligand from the magnetic cluster core in **8**, on the other hand, is very unlikely as it requires simultaneous breaking of multiple strong Mn^{III}–O bonds (ca. 1.90 Å). ^1H and ^{31}P NMR of aqueous solutions of **8a** both point to the structural integrity of **8**.

Planar-type $Mn_4(P_2W_{15}O_{56})_2$

In contrast to the cubane-type Mn_4 cluster, a conventional Mn_4 sandwich-type complex with the manganese ions in a planar arrangement is generated when only a Mn(II) source (manganese(II) acetate) is used. The X-ray structure reveals two $[P_2W_{15}O_{56}]^{6-}$ units connected through two crystallographically-independent Mn(II) centers, Mn1 and Mn2 (Figures 3.4 and 3.5.) Mn1 and Mn2 are both determined to be in the Mn(II) oxidation state by bond valence sum (BVS) calculations. The complex is formulated as $K_2Na_{14}[Mn_4(H_2O)_2(P_2W_{15}O_{56})_2]$ (**9**) based on elemental analysis and X-ray diffraction data.

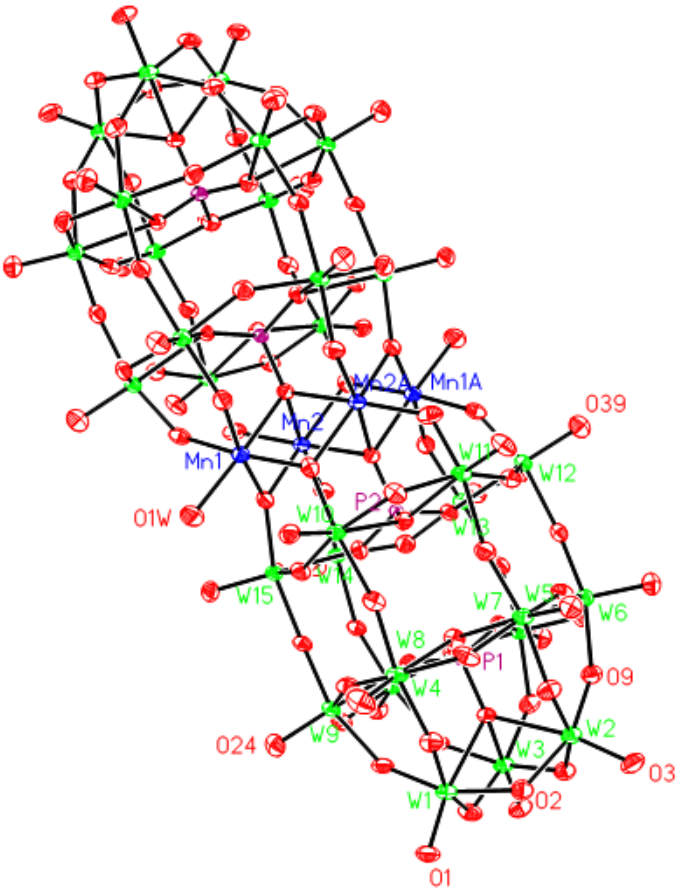

Figure 3.4. Thermal ellipsoid plot and numbering scheme for the polyanion of **9** (plotted at 50% probability).

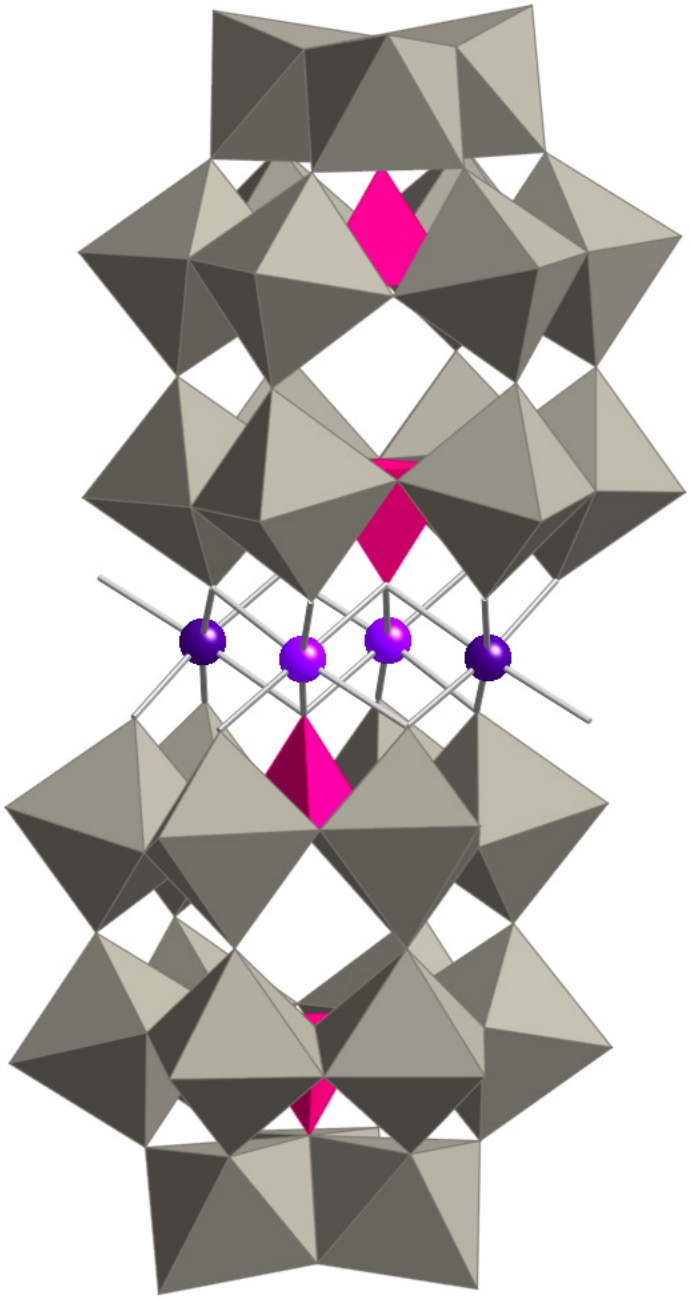

Figure 3.5. Combination polyhedral/ball-and-stick representation of the polyanion of **9**. Mn1 in dark purple, Mn2 in light purple, [WO_6] units in gray, P in purple tetrahedra.

Fe-O-Fe dimers

The Fe-O-Fe unit is a common structural motif in Fe-containing enzymes.[42] An enormous number of μ-oxo-bridged Fe complexes have been reported[43] and mixed-valence Fe clusters exhibit interesting magnetic and crystallographic properties.[44] The interesting feature of this POM-based complex is the single Fe-O-Fe bridging unit. Iron-substituted POMs have been reported before but all contain multiple Fe-O-Fe bridging units.[45] This structural feature is embedded in a polyoxometalate system through the dimerization of two Fe-substituted Keggin units. This is achieved synthetically by the addition of Fe(III) to an aqueous solution of $[PW_{11}O_{39}]^{7-}$ and the pH is adjusted to ~7. It is important to note that without this pH adjustment only the Fe-substituted Keggin species exists in solution. The use of suitable crystallization conditions produces two different crystalline forms of this polyanion. The complex $((CH_3)_2N)_4Na_6[O(FePW_{11}O_{39})_2]$ (**10**) is obtained when a small amount of dimethylammonium chloride is added (Figure 3.6). On the other hand, the complex $((CH_3)_2N)_7Na_3[O(FePW_{11}O_{39})_2]$ (**11**) is obtained when a large amount of dimethylammonium chloride is added (Figure 3.7.) The two complexes are isostructural with one important difference: the Fe-O-Fe bond angle is measurably different. In the polyanion of **10**, the bond angle is 149.5(15)^o while in **11** it is 166.5(7)^o. The difference is attributed to packing forces and is a common aspect of singly-bridged polyoxometalate species.

Table 3.1. Bond distances and angles of the Fe centers in complexes **11** and **12**.

	11	**12 (Fe1)**	**12 (Fe2)**
$Fe\text{-}O_{eq.}$ (Å)	1.93(2) 1.97(2) 2.00(2) 2.02(2)	1.982(11) 1.986(11) 2.029(11) 2.038(11)	1.983(11) 1.988(11) 2.016(11) 2.020(11)
$Fe\text{-}O_{bridging}$ (Å)	1.756(7)	1.785(10)	1.770(10)
Fe-O-Fe (°)	149.5(15)	166.5(7)	

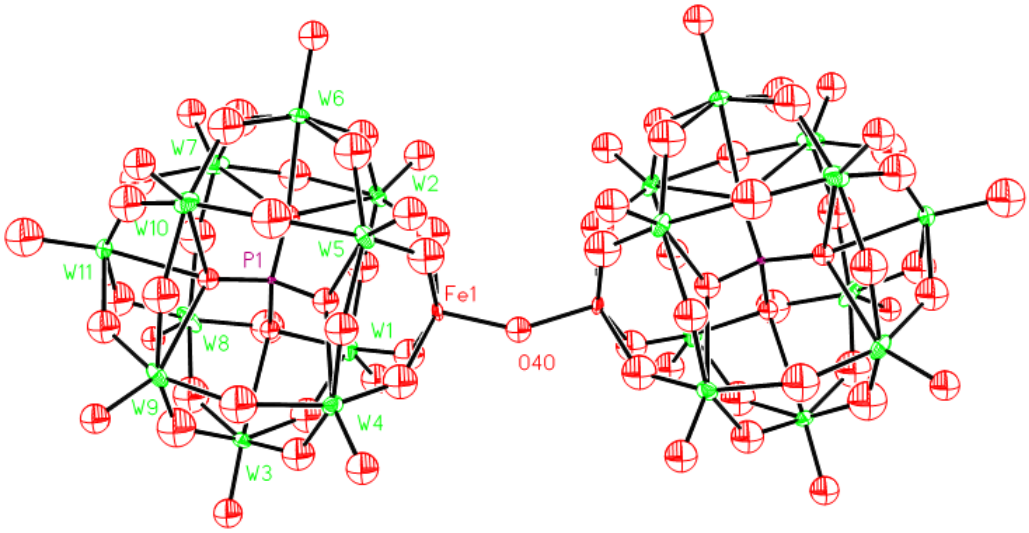

Figure 3.6. Thermal ellipsoid plot and numbering scheme for the polyanion of **10** (plotted at 50% probability).

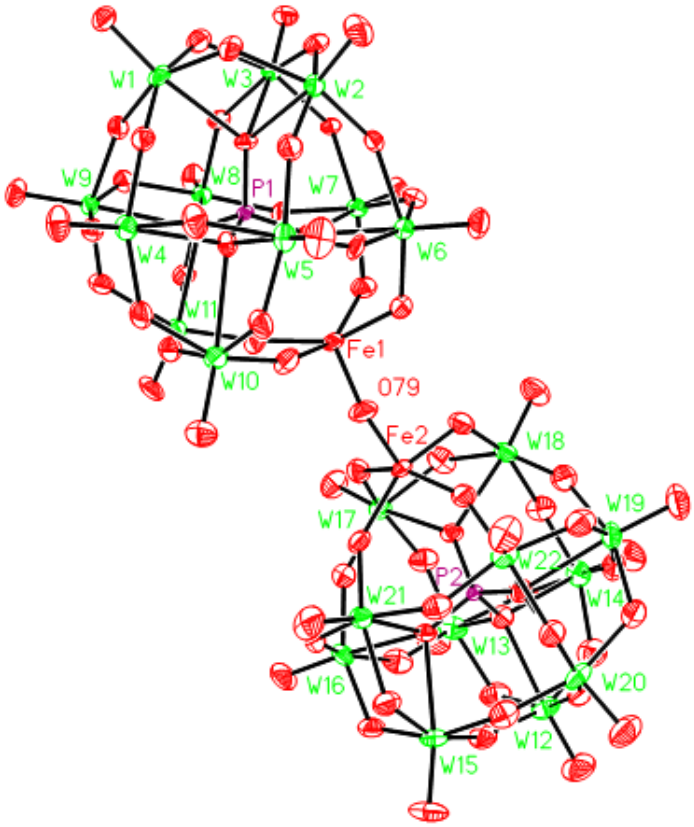

Figure 3.7. Thermal ellipsoid plot and numbering scheme for the polyanion of **11** (plotted at 50% probability).

Pd_3-sandwich type complexes

There is a considerable research interest in Pd-substituted polyoxometalates. Such complexes have been the focus of numerous articles recently with a broad range of possible applications.[46,47] POMs can be regarded as soluble models of metal-oxide surfaces which make them great candidates to study Pd at the atomic scale. The strategy employed here is the addition of the sodium or potassium salt of $[SiW_9O_{34}]^{10-}$ to a sodium acetate buffered solution of Pd(II) and use of the proper crystallization conditions. The complex $Cs_9Na_5[Pd^{II}_3(SiW_9O_{34})_2]$ (**12**) is obtained when CsCl is added to the crystallization solution (Figure 3.8.) On the other hand, $K_7Na_5[Pd^{II}_3(SiW_9O_{34})_2]$ (**13**) is obtained when the potassium salt of $[SiW_9O_{34}]^{10-}$ is used and KCl is added to the crystallization solution (Figure 3.9.) Complex **13** crystallizes in a high symmetry space group, *P6₃/m*, an aspect which often diminishes the crystallographic data quality. As a consequence, adequate refinement of these high symmetry structures is quite difficult or impossible to achieve. The inclusion of the K1 atom in one-third occupancy in each of the symmetry-equivalent positions in the belt was the most chemically appropriate assignment that matched the crystallographic data.

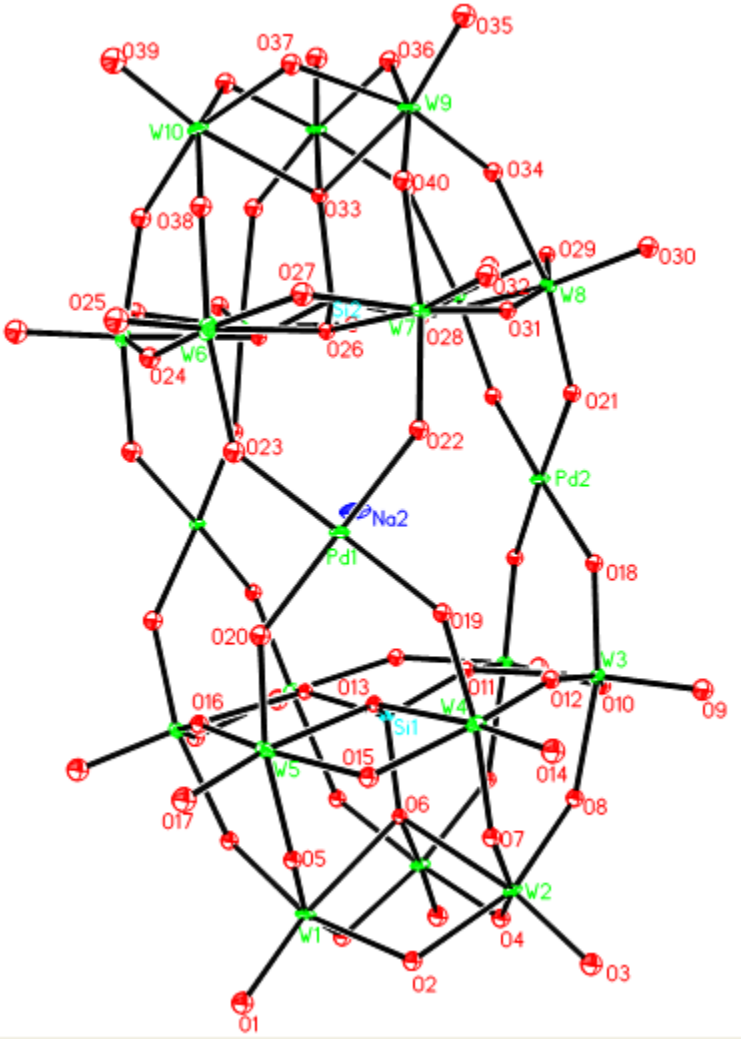

Figure 3.8. Thermal ellipsoid plot and numbering scheme for the polyanion of **12** (plotted at 50% probability).

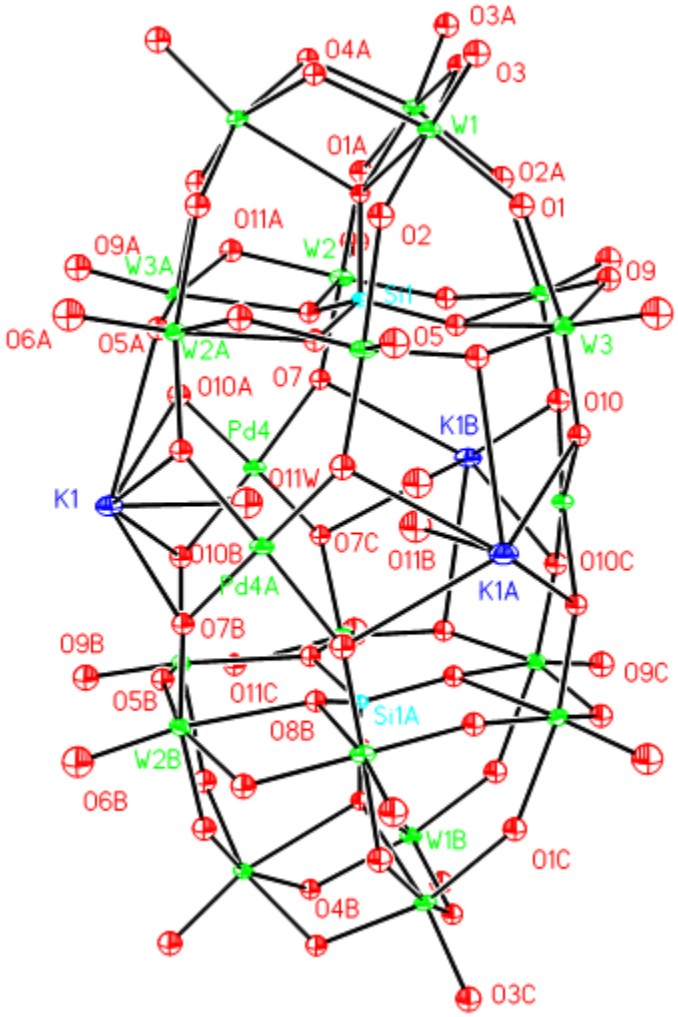

Figure 3.9. Thermal ellipsoid plot and numbering scheme for the polyanion of **13** (plotted at 50% probability).

3.4 Experimental

General methods and materials

Samples of $Mn(CH_3COO)_2 \cdot 4H_2O$, $KMnO_4$, and $Fe(NO_3)_3 \cdot 9H_2O$ were purchased from Aldrich and used as received. Samples of $Na_2WO_4 \cdot 2H_2O$ (95%), $PdSO_4 \cdot 2H_2O$ (99%), and $(CH_3)_2NCl$ were purchased from Alfa Aesar and used without further purification. Elemental analyses of C, H and N were performed by Atlantic Microlab (Norcross, Georgia), and heavy atoms (K, Rb, Cu, Sn, P, and W) were performed by Columbia Laboratory (Tucson, Arizona) and (ICP-OES) were obtained from Zentralabteilung für Chemische Analysen, Forschungszentrum Jülich GmbH, D-52425 Jülich, Germany. Infrared spectra (2% sample in KBr) were recorded on a Thermo Nicolet 6700 instrument and a Bruker Tensor 27 instrument. Atmosphere compensation (CO_2 and H_2O) and baseline corrections (rubberband method) were carried out after spectrum collection. ^{31}P NMR measurements were made in 100% D_2O on a Varian INOVA 400 MHz spectrometer and a Varian VXR-400 MHz instrument, and peaks were referenced to external 85% H_3PO_4. Typical sample concentrations were 0.2 – 0.5 mM. Thermogravimetric data were collected on a TGA 1000 instrument. Magnetic data of **8a** were recorded on a Quantum Design MPMS-5XL SQUID magnetometer (1.8-290 K) and corrected for diamagnetic and temperature-independent paramagnetic contributions ($x_{dia/TIP}$(**8a**) = -3.52×10^{-9} m^3mol^{-1}). Furthermore, the field- and temperature-dependent contributions of the Mn(II) counter ions (1/3 per formula unit) were simulated and subtracted from the data for **8a**.

Synthesis of $Na_{12}[\alpha\text{-}P_2W_{15}O_{56}]\cdot 18H_2O$

This procedure is an adaptation of the published procedure with additional notes which improve the synthesis. In a 600-mL beaker a sample of 38.5 g ($8 * 10^{-3}$ mol) of $K_6[\alpha\text{-}P_2W_{18}O_{62}]$ was dissolved in 125 mL of water (with gentle heating until the compound dissolved and then cooled to room temperature) and 35 g (0.25 mol) of $NaClO_4\cdot H_2O$ was added. After vigorous stirring for 20 min, the mixture was cooled on an ice bath, and the potassium perchlorate was removed by filtering on a coarse filter paper after about 3 hr. A solution of 10.6 g (0.1 mol) of Na_2CO_3 in 100 mL of water (with gentle heating until the compound dissolved and then cooled to room temperature) was added to the filtrate over a period of 20 seconds. The yellow solution became colorless when about half the base was added. A fine white precipitate appeared almost immediately afterward and was decanted and then filtered on a medium porosity sintered glass frit and dried under suction for about 3 hr. Without disturbing the cake that had formed on the frit, the product was then washed for 1 to 2 min with a solution of 4 g NaCl in 25 mL water, dried under suction for about 3 hr, washed for 2 to 3 min with 25 mL ethanol, and air dried under suction for 3 h, washed again with ethanol and dried under suction, and finally dried in a vacuum chamber at room temperature for about 4 hr. Yield: 22 g (62%). IR: 1130, 1075, 1008 cm^{-1}. ^{31}P NMR in pure D_2O was +0.1, -14.1 ppm. In 1M acetic acid/lithium acetate buffer: +0.1, -13.3 ppm.

Synthesis of [(α-$P_2W_{15}O_{56}$)$Mn^{III}_3Mn^{IV}O_3(CH_3COO)_3$] (8a) by the generation of the Mn_4O_3 cluster *in situ*.

A sample of $Mn(CH_3COO)_2 \cdot 4H_2O$ (0.37 g, 1.5 mmol, 6.5 eq.) was dissolved in a solution of 30 mL water and 10 mL glacial acetic acid. Solid $KMnO_4$ (0.08 g, 0.51 mmol, 2.2 eq.) was added under vigorous stirring. The average oxidation state of Mn was +3.3. The solution turned dark black but still homogeneous. After stirring for approx. 1 min, solid $Na_{12}[\alpha\text{-}P_2W_{15}O_{56}]$ (1.0 g, 0.23 mmol, 1 eq.) was added and the solution became slightly cloudy and lighter brown. The solution was stirred at room temperature for 1 hour, during which time an appreciable amount of brown/black solid (manganese oxide) formed. The solution was filtered on coarse filter paper and then fine filter paper. The clear black solution was allowed to evaporate at room temperature for several days, with periodic filtering of manganese oxide that had formed. After 6 days brown needles had developed. One was selected for X-ray crystallography and determined to be the same structure as that derived from $Mn_{12}O_{12}$. A comparison of ^{31}P NMR and IR spectra confirmed this assignment. ^{31}P NMR: -12.0 ppm. IR (KBr pellet): 1623(m), 1553(m), 1466(m), 1388(m), 1341(m), 1085(s), 1009(m), 944(s), 913(s), 801(vs, br), 711(s), 684(s), 625(m), 578(sh), 524(m).

Synthesis of [(α-$P_2W_{15}O_{56}$)$Mn^{III}_3Mn^{IV}O_3(CH_3COO)_3$] (8a) by fragmentation of $Mn_{12}O_{12}$.

In a 100 mL beaker, a sample of **7**$\cdot 4H_2O \cdot 2CH_3COOH$ (0.21 g, 0.1 mmol) was suspended in a mixture of CH_3COOH (36 mL) and H_2O (24 mL). After vigorous

stirring for 1 hr, solid $Na_{12}[\alpha\text{-}P_2W_{15}O_{56}]\cdot 18H_2O$ (0.86 g, 0.2 mmol) was then added to the above solution. After stirring for 1/2 hr at room temperature, the mixture was heated to 80 °C for another 1 hr and filtered. Dimethylamine hydrochloride (0.30 g) was then added to the solution. Any insoluble material precipitated overnight was removed by centrifugation. Slow evaporation of the dark red solution afforded dark red needle crystals. Yield: 0.23 g, 24.4% based on W. Elemental analysis, calcd. for $C_{16.67}H_{85.67}Mn_{4.33}\ N_{5.33}O_{81}P_2W_{15}$: C 4.24, H 1.83, N 1.58, Mn 5.05, P 1.31, W 58.5, Na, 0.0 %. Found: C 4.33, H 1.99, N 1.44, Mn 5.06, P 1.26, W 56.8, Na <0.02 %. Selected IR bands for **8** (KBr pellet, 2000–500 cm^{-1}): 1623(m), 1553(m), 1466(m), 1388(m), 1341(m), 1085(s), 1009(m), 944(s), 913(s), 801(vs, br), 711(s), 684(s), 625(m), 578(sh), 524(m).

Synthesis of $K_2Na_{14}[Mn_4(H_2O)_2(P_2W_{15}O_{56})_2]$ (9)

A sample of $Mn(CH_3COO)_2\cdot 4H_2O$ (0.15 g, 0.59 mmol, 2.1 eq.) was dissolved in 30 mL water and added $Na_{12}[\alpha\text{-}P_2W_{15}O_{56}]\cdot 18H_2O$ (1.20 g, 0.28 mmol, 1.0 eq.) under vigorous stirring. The solution gradually changed from pink/colorless to bright red and then finally to dark brown/red. After stirring at room temperature for 1 hour, the solid NaCl (2.0 g) was added and the solution was filtered on coarse and then fine filter paper. The solution was allowed to stand for 3 days at room temperature. After 3 days black prisms had developed and were isolated. The product was confirmed to be **9** by X-ray crystallography.

Synthesis of $((CH_3)_2N)_4Na_6[O(FePW_{11}O_{39})_2]$ (10)

A sample of $K_7[PW_{11}O_{39}]$ (1.0 g, 0.306 mmol, 1.0 eq.) was dissolved in 8.0 mL water and a sample of $Fe(NO_3)_3 \cdot 9H_2O$ (0.136 g, 0.337 mmol, 1.1 eq.) was added under vigorous stirring. The resulting pale yellow solution was stirred vigorously while a solution of KOH (1.0 M, ~13 drops) was added dropwise at a rate of 1 drop / 5 seconds. The final pH was 6.28 as determined by pH probe. The solution was stirred for 5 minutes and then a solution of dimethylamine hydrochloride (4.0 M, 0.40 mL) was added which produced white precipitate that dissolved upon stirring. Then, the solution was filtered on a fine filter paper and allowed to evaporate at room temperature. After 4 days long yellow needles appeared and after 2 more days were harvested. These crystals (0.20 g) were dissolved in 2.0 mL water, heated to dissolve, and then 5 drops RbCl solution (5.0 M) and 5 drops dimethylammonium chloride solution (4.0 M) were added. After 5 days of evaporation lots of yellow prisms had formed and were harvested. The product was determined to be **10** by X-ray crystallography. FT-IR: 1087 (s), 1059 (s), 1012 (sh), 962 (s), 887 (s), 802 (br), 749 (br), 683 (w), 592 (w), 515 (m), 487 (w).

Synthesis of $((CH_3)_2N)_7Na_3[O(FePW_{11}O_{39})_2]$ (11)

A sample of $Rb_6K_5[Sn(C_6H_5)(H_2O)P_2W_{19}O_{69}(H_2O)]$ (0.50 g, 1 eq.) was dissolved in 10 mL of water and a sample of $Fe(NO_3)_3 \cdot 9H_2O$ (0.040 g, 1.1 eq.) was added under vigorous stirring. The resulting pale yellow solution was stirred vigorously while a solution of KOH (1.0 M, ~8 drops) was added dropwise at a rate of 1 drop / 5 seconds. The final pH was 6.50 as determined by pH probe and the solution was

paler yellow. The solution was stirred for 1 hour and then a solution of dimethylamine hydrochloride (4.0 M, 0.50 mL) was added under stirring which produced a white cloudiness that went away upon stirring. Subsequently, the solution was filtered on a fine filter paper and allowed to evaporate at room temperature. Over a period of several days, the solution gradually became darker yellow/gold in color, and after 7 days long yellow prisms appeared which were removed and determined to be $[((C_6H_5)Sn)_3(PW_9O_{34})_2]$ by X-ray crystallography. The remaining filtrate continued to evaporate and after 5 additional days produced darker yellow prisms which were determined to be **11** by X-ray crystallography. FT-IR: 1084 (s), 1058 (s), 1015 (sh), 962 (s), 885 (s), 802 (br), 747 (w), 726 (w), 670 (w), 591 (w), 513 (m), 489 (w).

Synthesis of $Cs_8Na_6[Pd^{II}_3(SiW_9O_{34})_2]$ (12)

A sample of $PdSO_4 \cdot 2H_2O$ (0.25 g, 3.0 eq.) was suspended in 20 mL water and the solution turned cloudy brown. A solution of CsCl (1.0 M, 0.20 mL) was added and the pH was measured to be 1.65. A sample of $Na_{10}[A\text{-}\alpha\text{-}SiW_9O_{34}]$ (1.01 g, $3.32 * 10^{-4}$ mol, 1.0 eq.) was added under vigorous stirring and the solution became even more cloudy brown. The solid POM took about 1 minute to completely dissolve. A solution of KOH was added slowly (0.33 M, ~10 drops) under vigorous stirring at a rate of about 1 drop / 5 seconds. The final pH was 5.11 as measured by pH probe. The solution was filtered on a fine filter paper and allowed to evaporate at room temperature. The next day large, dark brown cube-shaped crystals appeared which were determined to be **12** by X-ray crystallography. FT-IR: 998 (s), 937 (s), 884 (s,

br), 779 (s, br), 670 (br, w), 547 (w), 529 (w), 440 (w). Yield: 0.20 g. UV-vis: λ = 452, ε = 559 in water.

Synthesis of $K_{11}Na_3[Pd^{II}_3(SiW_9O_{34})_2]$ (13)

A sample of $PdSO_4 \cdot 2H_2O$ (0.141 g, 2.0 eq.) was suspended in 30 mL water and the solution turned cloudy brown. A sample of $K_{10}[A\text{-}\alpha\text{-}SiW_9O_{34}]$ (0.60 g, $1.97 * 10^{-4}$ mol, 1.0 eq.) was added under vigorous stirring and the solution became even more cloudy brown. The solid POM took about 1 minute to completely dissolve and the pH was 2.93 as measured by pH probe. A solution of KOH was added slowly (0.30 M, ~47 drops) under vigorous stirring at a rate of about 1 drop / 5 seconds at first then at pH = 4 sped up the addition to 1 drop / 1 second. The final pH was 5.10 as measured by pH probe. A saturated solution of KCl was added (6 drops) and the solution was heated to 50 ^{o}C for 3 minutes under vigorous stirring. The solution was cooled to room temperature and then filtered on a fine filter paper. Thirty minutes later the solution had microcrystals. The solution was allowed to evaporated at room temperature and after 1 day produced many tiny brown crystals which were determined to be **13** by X-ray crystallography. FT-IR: 997 (s), 966 (sh), 928 (m), 878 (m), 776 (s), 680 (m), 660 (m), 531 (m), 481 (w), 445 (w).

X-ray crystallography

The complete datasets for complexes **7-13** were collected at Emory University. Single crystals suitable for X-ray analysis, were each coated with Paratone-N oil, suspended in a small fiber loop, and placed in a cooled gas stream on a Brüker D8

SMART APEX CCD sealed tube diffractometer. Diffraction intensities were measured using graphite monochromated Mo Kα radiation (λ = 0.71073 Å) at 173(2) K and a combination of φ and ω scans with 10 s frames traversing about ω at 0.5° increments. Data collection, indexing, and initial cell refinements were carried out using SMART;[48] frame integration and final cell refinements were done using SAINT.[49] The molecular structure of each complex was determined using Direct Methods and Fourier techniques and refined by full-matrix least squares. A multiple absorption correction, including face index, for each dataset at 173(2) K was applied using the program SADABS.[50] The largest residual electron density for each structure was located close to (less than 1.0 Å from) W atoms and was most likely due to imperfect absorption corrections frequently encountered in heavy-metal atom structures.

(b) Refinement details. The structures of **7-13** were solved using Direct Methods and difference Fourier techniques. All the heavy atoms were refined anisotropically. Some of the potassium ions and solvent water molecules were refined with partial occupancies; not all the counter cations and solvent water molecules could be located in difference Fourier maps because of disorder. The acetate H atoms were modeled according to idealized positions. Scattering factors and anomalous dispersion corrections are taken from the *International Tables for X-ray Crystallography*. Structure solution, refinement, graphic and generation of publication materials were performed by using SHELXTL, V6.14 software.[51] Crystal data for **8a**, M = 4715.00 g mol^{-1}, space group $P6_3/m$, a = 30.731(1), c = 18.522(1) Å, V = 15148(2) Å^3, T = 173(2) K, Z = 6, D_c = 3.101 Mg m^{-3}, F(000) = 12716, μ(Mo-

Kα) = 17.661 mm^{-1}, crystal size 0.24 × 0.03 × 0.03 mm^3. ρ(max./min.): 2.18 and –1.66 e $Å^{-3}$. The refinement converges to $R1$ = 0.0532, $wR2$ = 0.1135 and GOF = 1.019 for 7522 reflections with $I > 2\sigma(I)$.

Table 3.2. Crystal data and structural refinement for **8** and **9**.

complex	**8**	**9**
molecular formula	$C_{16.67}H_{85.67}Mn_{4.33}N_{5.33}Na_0O_{81}P_2W_{15}$	$K_2Mn_4Na_{14}O_{130}P_4W_{30}$
formula wt. (g mol^{-1})	4715.00	8362.20
temperature (K)	173(2)	173(2)
radiation (λ, Å)	0.71073	0.71073
crystal system	hexagonal	triclinic
space group	*P6₃/m*	$P\bar{1}$
a (Å)	30.7308(12)	12.9111(14)
b (Å)	30.7308(12)	14.8440(17)
c (Å)	18.5220(15)	19.7129(2)
α (°)	90.00	92.028(6)
β (°)	90.00	90.978(7)
γ (°)	120.00	100.750(6)
Volume (Å^3)	15148.4(15)	3708.1(7)
Z	6	4
ρ_{calcd} (g cm^{-3})	3.101	3.745
μ (mm^{-1})	17.661	23.726
F(000)	12716	3623
crystal size (mm^3)	0.24 × 0.03 × 0.03	0.29 × 0.15 × 0.11
θ range	1.34 to 23.26º	1.61 to 36.86º
reflections collected	63115	119076
independent reflections	7522 [R(int) = 0.0847]	35651 [R(int) = 0.0894]
max./min. transmission	0.1009 and 0.6194	0.1800 and 0.0553
refinement method	full-matrix least-squares on F^2	full-matrix least-squares on F^2
data/restraints/param.	7522/0/516	35651/0/834
goodness-of-fit on F^2	1.019	1.019
final R indices [R > 2σ (I)]	R1[a] = 0.0532 wR2[b] = 0.1135	R1[a] = 0.0731 wR2[b] = 0.1918
R indices (all data)	R1[a] = 0.1131 wR2[b] = 0.1383	R1[a] = 0.1086 wR2[b] = 0.2147
largest diff. peak and hole (e Å^{-3})	2.182 and -1.662	8.415 and -3.693

[a] $R_1 = \Sigma||F_o| - |F_c|| / |F_o|$

[b] $wR_2 = \{\Sigma[w(F_o^2 - F_c^2)^2] / \Sigma[w(F_o^2)^2]\}^{0.5}$

Table 3.3. Crystal data and structural refinement for **10** and **11**.

complex	**10**	**11**
molecular formula	$C_8H_{32}Fe_2N_4Na_6O_{82.5}P_2W_{22}$	$C_{13}H_{52}Fe_2Na_3N_{6.5}O_{80}P_2W_{22}$
formula wt. (g mol^{-1})	5814.68	5797.95
temperature (K)	173(2)	173(2)
radiation (λ, Å)	0.71073	0.71073
crystal system	monoclinic	triclinic
space group	$P2_1/m$	$P\bar{1}$
a (Å)	11.4350(8)	12.043(7)
b (Å)	42.411(3)	19.117(11)
c (Å)	11.7629(8)	22.531(14)
α (°)	90.00	95.857(9)
β (°)	118.5790(10)	93.902(10)
γ (°)	90.00	90.679(9)
Volume ($Å^3$)	5009.6(6)	5147(5)
Z	2	2
ρ_{calcd} (g cm^{-3})	3.855	3.741
μ (mm^{-1})	25.564	24.863
F(000)	5044	5051
crystal size (mm^3)	0.24 × 0.13 × 0.02	0.22 × 0.16 × 0.14
θ range	0.96 to 30.38º	0.91 to 30.32º
reflections collected	93156	96348
independent reflections	14763 [R(int) = 0.0824]	28917 [R(int) = 0.0582]
max./min. transmission	0.6289 to 0.0636	0.1285 to 0.0734
refinement method	full-matrix least-squares on F^2	full-matrix least-squares on F^2
data/restraints/param.	14763/0/353	28917/1/1034
goodness-of-fit on F^2	1.111	1.032
final R indices [R > 2σ (I)]	$R1^a$ = 0.0793 $wR2^b$ = 0.1829	$R1^a$ = 0.0540 $wR2^b$ = 0.1351
R indices (all data)	$R1^a$ = 0.1061 $wR2^b$ = 0.1967	$R1^a$ = 0.0785 $wR2^b$ = 0.1484
largest diff. peak and hole (e $Å^{-3}$)	5.932 and -4.705	7.206 and -3.674

$^a R_1 = \Sigma||F_o| - |F_c|| / |F_o|$

$^b wR_2 = \{\Sigma[w(F_o^2 - F_c^2)^2] / \Sigma[w(F_o^2)^2]\}^{0.5}$

Table 3.4. Crystal data and structural refinement for **12** and **13**.

complex	**12**	**13**
molecular formula	$Cs_8Na_6O_{79.40}Pd_3Si_2W_{18}$	$K_{11}Na_3O_{104.50}Pd_3Si_2W_{18}$
formula wt. (g mol^{-1})	6156.30	5832.76
temperature (K)	173(2)	173(2)
radiation (λ, Å)	0.71073	0.71073
crystal system	monoclinic	hexagonal
space group	*P2$_1$/m*	*P6$_3$/m*
a (Å)	14.382(3)	12.4313(16)
b (Å)	18.665(4)	12.4313(16)
c (Å)	17.823(4)	33.607(9)
α (^{o})	90.00	90.00
β (^{o})	107.064(3)	90.00
γ (^{o})	90.00	120.00
Volume (Å^3)	4573.7(16)	4497.8(14)
Z	2	2
ρ_{calcd} (g cm^{-3})	4.470	4.307
μ (mm^{-1})	26.395	24.176
F(000)	5278	5130
crystal size (mm^3)	0.39 × 0.15 × 0.11	0.20 × 0.17 × 0.10
θ range	1.84 to 32.61°	2.42 to 30.24
reflections collected	98771	82930
independent reflections	16220 [R(int) = 0.0542]	4113 [R(int) = 0.0321]
max./min. transmission	0.1577 and 0.0342	0.1960 and 0.0835
refinement method	full-matrix least-squares on F^2	full-matrix least-squares on F^2
data/restraints/param.	16220/0/403	4113/0/142
goodness-of-fit on F^2	1.034	1.579
final R indices [R > 2σ (I)]	R1^a = 0.0391 wR2^b = 0.0939	R1^a = 0.0804 wR2^b = 0.3446
R indices (all data)	R1^a = 0.0510 wR2^b = 0.0997	R1^a = 0.0871 wR2^b = 0.3508
largest diff. peak and hole (e Å^{-3})	7.093 and -4.971	7.878 and -5.167

$^a R_1 = \Sigma||F_o| - |F_c|| / |F_o|$

$^b wR_2 = \{\Sigma[w(F_o^2 - F_c^2)^2] / \Sigma[w(F_o^2)^2]\}^{0.5}$

1.5 Characterization data for complex 8a

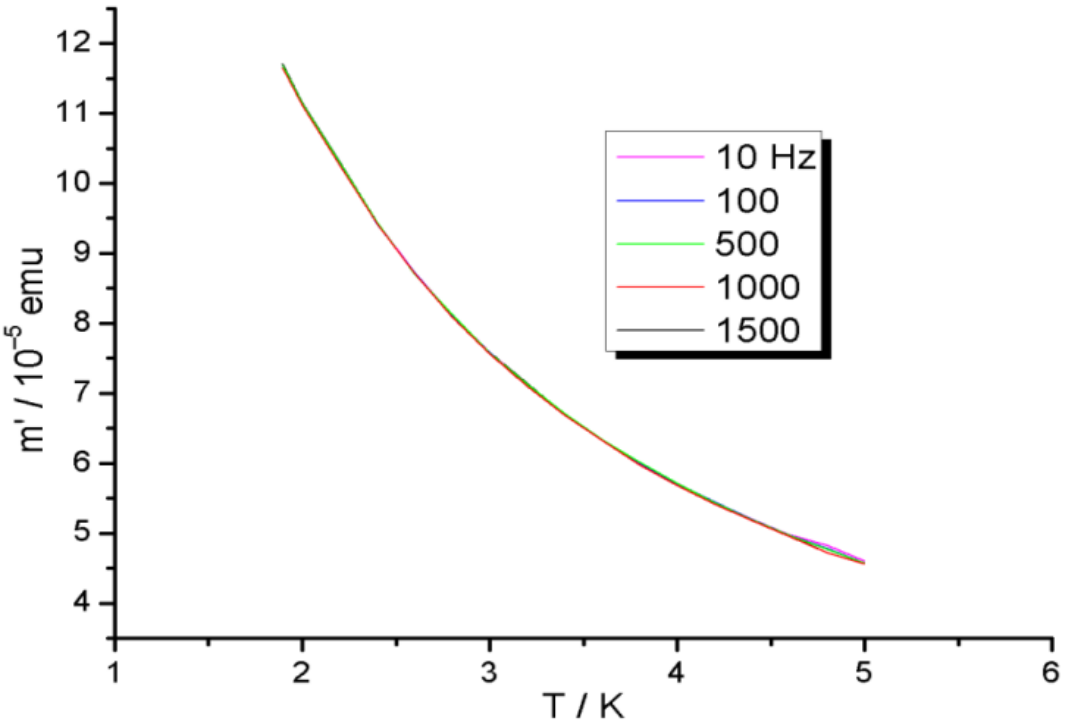

Figure 3.10. In-phase ac magnetization component m' of **8a** (24.06 mg) for frequencies ranging from 10 to 1500 Hz between 1.8 and 5 K in the absence of a dc bias field, illustrating the lack of frequency dependency. No out-of-phase component m'' is observed for the same parameter range.

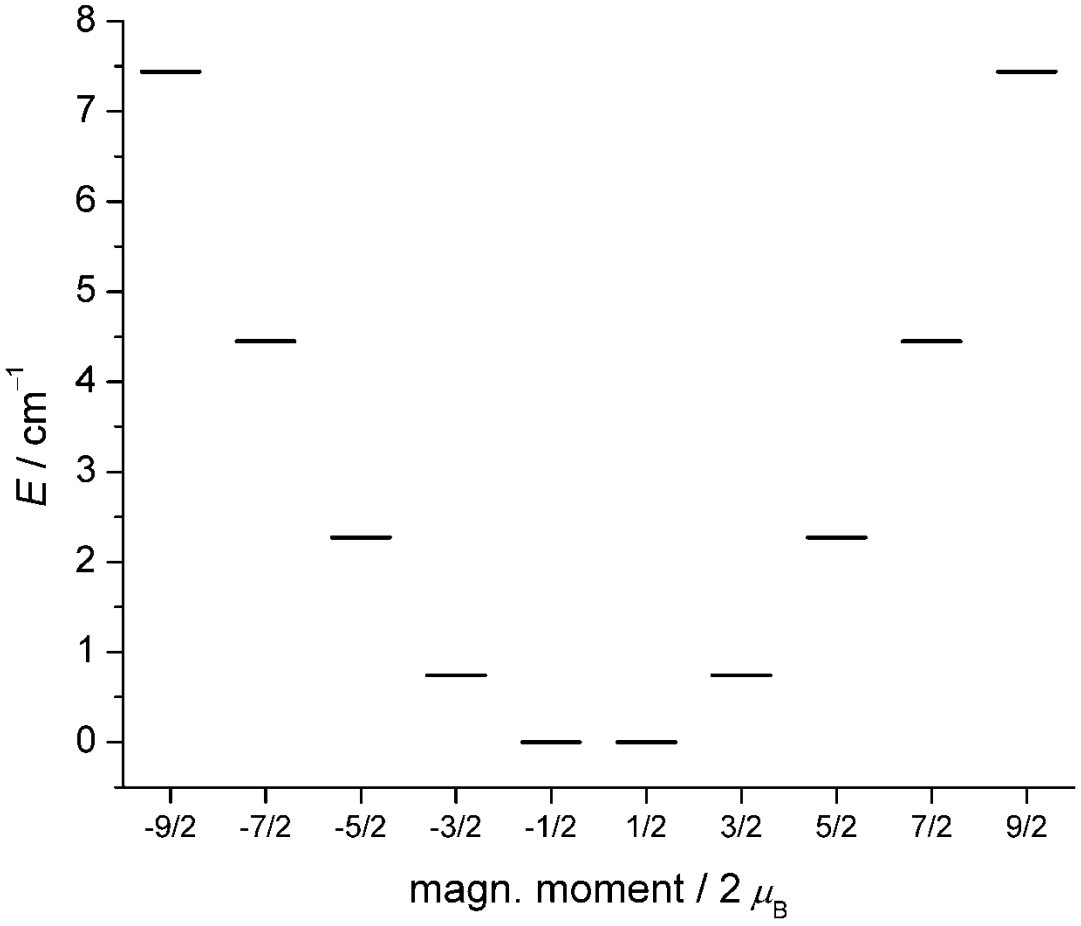

Figure 3.11. Calculated energies of the zero field-split substates belonging to the ground state of **8a**.

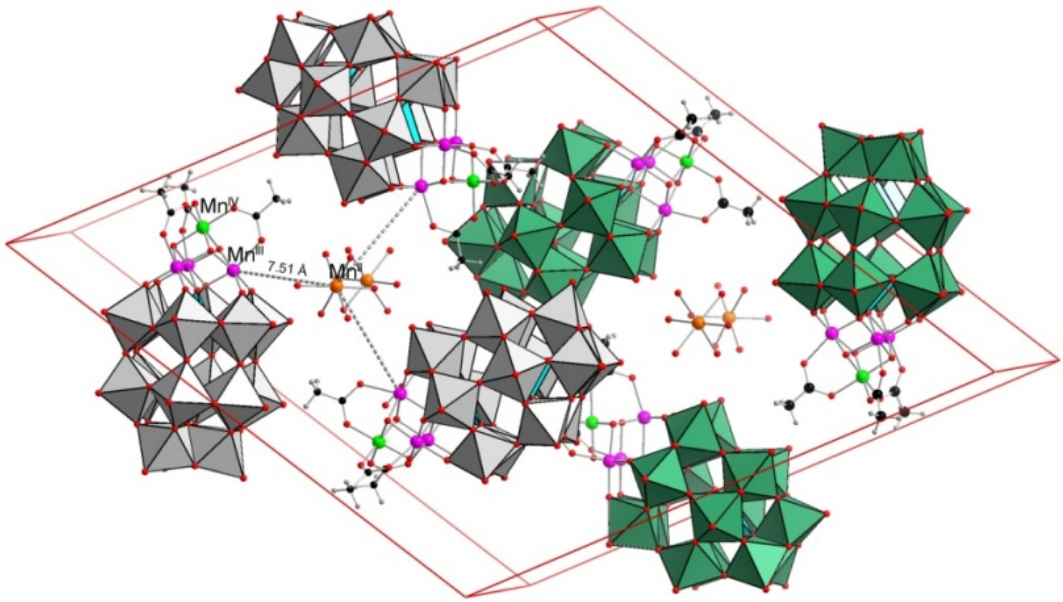

Figure 3.12. Arrangement of cluster anions in a unit cell of **8a**. Grey and green polyhedra distinguish the front and rear cluster trimers that are centered around Mn^{II} counter ions (orange spheres). The Mn^{II} ions are positioned on 6_3 axes and disordered equally over two positions related by a mirror plane. Compound **8a** crystallizes in space group $P6_3/m$.

Solution NMR results: ^{1}H NMR shows a single methyl resonance for the three acetate groups of **2** at 1.84 ppm, consistent with effective C_{3v} symmetry. ^{31}P NMR, also as expected, only has a very broad signal at –11.9 ppm that attributed to the distal P atom, while the proximal P signal is too broadened to be observed due to its close proximity to the paramagnetic Mn centers, a situation that has been seen in other Mn-substituted Dawson systems.[52] No noticable changes have been observed for both spectra after 2 days.

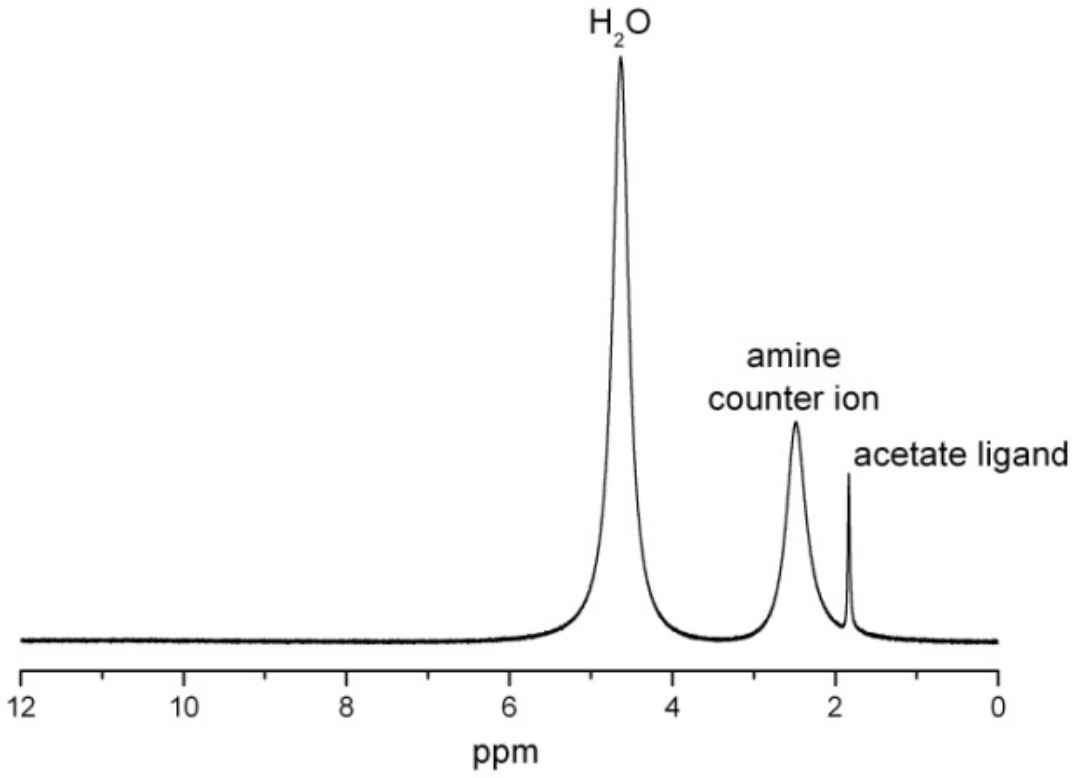

Figure 3.13. ^{1}H NMR spectrum of **8a** in D_2O.

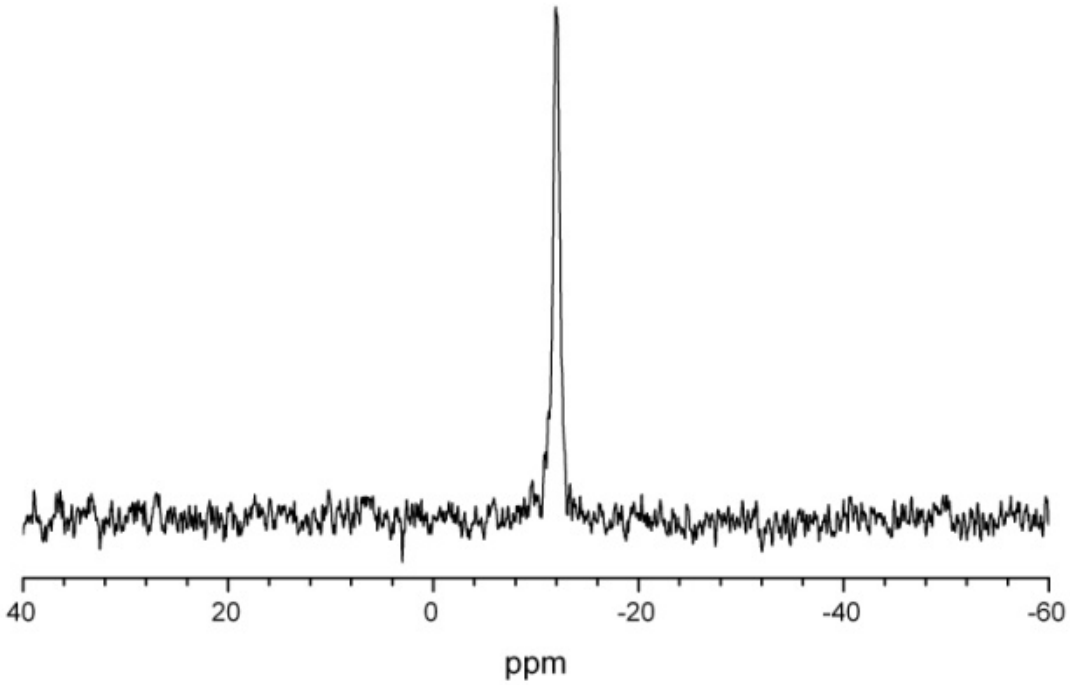

Figure 3.14. ^{31}P NMR spectrum of **8a** in D_2O.

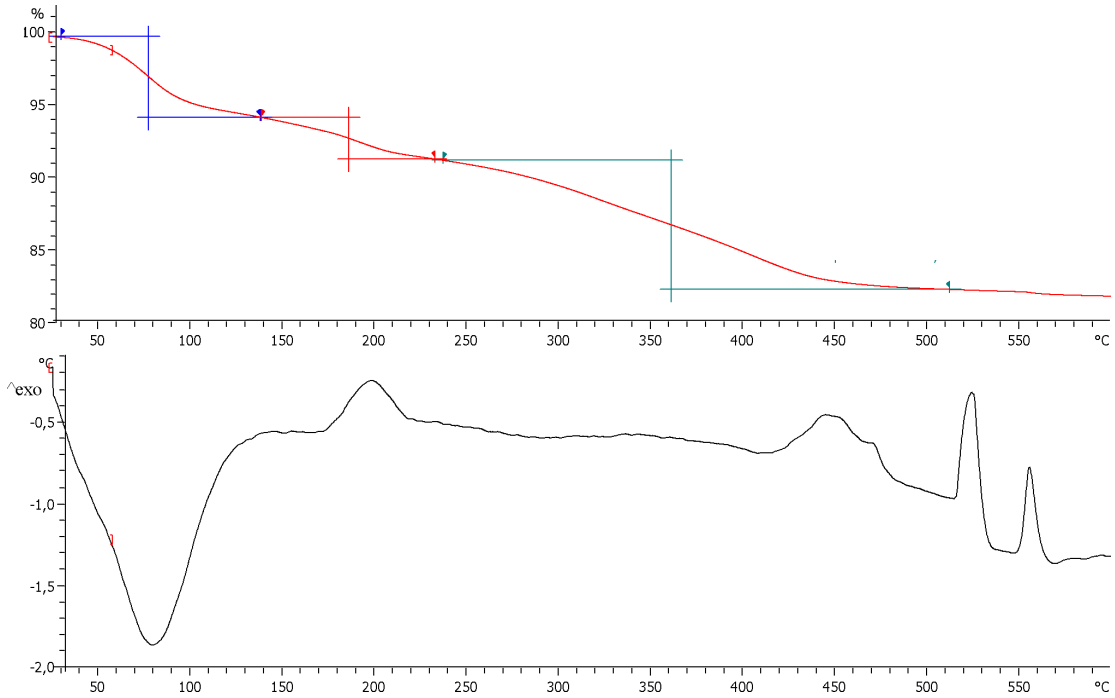

Figure 3.15. TGA and simultaneous DTA graphs of **8a** (10 K/min, 60 ml N_2/min).

Magnetic simulations: Using our computational framework CONDON, the magnetic properties of **8a** were simulated based on all relevant influences on the molecular spin structure. Note that due to the inclusion of angular momentum contributions, the resulting magnetic states are not adequately characterized any longer by spin quantum numbers (e.g. S, m_S). In the case of **8a**, magnetic moments of single d^3 and d^4 ions are determined as a function of spin-orbit coupling, interelectronic repulsions, and ligand field effects, employing the full basis set of all microstates. The individual single-ion magnetic moments then are coupled to the molecular moment of the $Mn^{III}_3Mn^{IV}$ cluster structure using a Heisenberg-type superexchange formalism as a function of an applied external field whereby all perturbations are taken into account simultaneously. Standard spectroscopic values are chosen for the spin-orbit coupling constant ζ (Mn^{IV}: ζ = 170 cm^{-1}; Mn^{III}: ζ = 190 cm^{-1}) and Racah parameters $C = 4B$ and B (Mn^{IV}: B = 700 cm^{-1}; Mn^{III}: B = 800 cm^{-1}). The full Hamiltonian is defined as follows and augmented by the Heisenberg exchange Hamilton.

$$\begin{aligned}\hat{H} \;=\; & \underbrace{\sum_{i=1}^{N}\left[-\frac{\hbar^2}{2m_e}\nabla_i^2 + V(r_i)\right]}_{\hat{H}^{(0)}} + \underbrace{\sum_{i>j}^{N}\frac{e^2}{r_{ij}}}_{\hat{H}_{\mathrm{ee}}} + \underbrace{\sum_{i=1}^{N}\zeta(r_i)\,\kappa\;\hat{\boldsymbol{l}}_i\cdot\;\hat{\boldsymbol{s}}_i}_{\hat{H}_{\mathrm{so}}} + \\ & \underbrace{\sum_{i=1}^{N}\sum_{k=0}^{\infty}\left\{B_0^k C_0^k(i) + \sum_{q=2}^{k}\left[B_q^k\left(C_{-q}^k(i) + (-1)^q C_q^k(i)\right)\right]\right\}}_{\hat{H}_{\mathrm{LF}}} + \\ & \underbrace{\sum_{i=1}^{N}\mu_B(\kappa\;\hat{\boldsymbol{l}}_i + 2\;\hat{\boldsymbol{s}}_i)\cdot\;\boldsymbol{B}}_{\hat{H}_{\mathrm{mag}}}\end{aligned}$$

3.6 Conclusions

In summary, 6 new polyoxometalates have been formed and characterized which all contain multiple d-electron-containing-transition metals in close proximity to one another. The different types of metals and coordination geometries offer diverse possible uses and applications. Most interestingly, the existing SMM motif, $[Mn_4(\mu_3\text{-}O)_3(\mu_3\text{-}X)]$, can be integrated into lacunary $\{P_2W_{15}\}$ framework while retaining the SMM core geometry, a process that formally can be considered ligand metathesis. For the resulting $\{Mn_4P_2W_{15}\}$ cluster, **8,** this step is accompanied by an unexpected change in the order of the lowest magnetic levels affected by strong zero-field splitting, transforming an SMM group into a high-spin cluster with no observable slow relaxation. Further plans with our collaborators include studies to identify the cause of the switching phenomenon, and to this end, the exploration of grafting other SMM types onto different lacunary POMs. For the iron system, two Fe-substituted Keggin structures were dimerized through an oxo atom to form a Fe-O-Fe unit with different Fe-O-Fe angles depending on the crystallization conditions. For the palladium species, two different Pd_3-sandwich type complexes were formed with different alkali metals in the belt depending on synthetic conditions. All of these systems demonstrate the unique ability of POMs to bring together multiple d-electron-transition metals within close proximity to one another.

Chem. Commun., **2010**, *46*, 2760-2762 – Portions of this document have been reproduced by permission of The Royal Society of Chemistry (RSC) http://pubs.rsc.org/en/Content/ArticleLanding/2010/CC/B925947C

Acknowledgments

We would like to thank collaborators Xikui Fang (Ames Lab, IA) and Paul Kögerler (Institut für Anorganische Chemie, Germany). We are grateful to Dr. Gordon Miller for allowing us access to X-ray facilities. Ames Laboratory is operated for the U.S. Department of Energy by Iowa State University under Contract No. DE-AC02-07CH11358. PK thanks RWTH Aachen University for a seed fund.

References

1. Y. V. Geletii, Z. Huang, Y. Hou, D. G. Musaev, T. Lian and C. L. Hill, *J. Am. Chem. Soc.* 2009**, 131**, 7522-7523.

2. Q. Yin, J. M. Tan, C. Besson, Y. V. Geletii, D. G. Musaev, A. E. Kuznetsov, Z. Luo, K. I. Hardcastle and C. L. Hill, *Science*, 2010, **328**, 342.

3. C. Besson, Z. Huang, Y. V. Geletii, S. Lense, K. I. Hardcastle, D. G. Musaev, Y. Lian, A. Proust and C. L. Hill, *Chem. Commun.*, 2010, **46**, 2784-2786.

4. Z. Luo, P. Kögerler, R. Cao and C. L. Hill, *Inorg. Chem*., 2009, **48**, 7812-7817.

5. Z. Luo, P. Kögerler, R. Cao and C. L. Hill, *Polyhedron*, 2008, **28**, 215-220.

6. Z. Luo, P. Kögerler, R. Cao, I. Hakim and C. L. Hill, *Dalton Trans.*, 2008, 54-58.

7. T. C. Stamatatos, D. Foguet-Albiol, C. C. Stoumpos, C. P. Raptopoulou, A. Terzis, W. Wernsdorfer, S. P. Perlepes and G. Christou, *J. Am. Chem. Soc.*, 2005, **127**, 15380.

8. H. J. Eppley, H. L.Tsai, N. de Vries, K. Folting, G. Christou and D. N. Hendrickson, *J. Am. Chem. Soc.*, 1995, **117**, 301.

9. M. Soler, W. Wernsdorfer, K. A. Abboud, J. C. Huffman, E. R. Davidson, D. N. Hendrickson and G. Christou, *J. Am. Chem. Soc.*, 2003, **125**, 3576.

10. X. Fang and P. Kögerler, *Chem. Commun.*, 2008, 3396

11. X. Fang and P. Kögerler, *Angew. Chem., Int. Ed.*, 2008, **47**, 8123.

12. M. T. Pope, in *Comprehensive Coordination Chemistry II*, Elsevier, New York, 2004, vol. 4, pp. 635–678.

13. C. L. Hill, in *Comprehensive Coordination Chemistry II*, Elsevier, New York, 2004, vol. 4, pp. 679–759

14. A. Proust, R. Thouvenot and P. Gouzerh, *Chem. Commun.*, 2008, 1837.

15. C. Ritchie, A. Ferguson, H. Nojiri, H. N. Miras, Y.-F. Song, D.-L. Long, E. Burkholder, M. Murrie, P. Kögerler, E. K. Brechin and L. Cronin, *Angew. Chem., Int. Ed.*, 2008, **47**, 5609.

16. J. Compain, P. Mialane, A. Dolbecq, I. M. Mbomekalle, J. Marrot, F. Secheresse, E. Riviere, G. Rogez and W. Wernsdorfer, *Angew. Chem., Int. Ed.*, 2009, **48**, 3077.

17. A. Giusti, G. Charron, S. Mazerat, J.-D. Compain, P. Mialane, A. Dolbecq, E. Rivière, W. Wernsdorfer, R. N. Biboum, B. Keita, L. Nadjo, A. Filoramo, J.-P. Bourgoin and T. Mallah, *Angew. Chem., Int. Ed.*, 2009, **48**, 4949.

18. M. A. AlDamen, J. M. Clemente-Juan, E. Coronado, C. Marti-Gastaldo and A. Gaita-Arino, *J. Am. Chem. Soc.*, 2008, **130**, 8874.

19. G. Aromí and E. K. Brechin, *Struct. Bonding*, 2006, **122**, 1.

20. D. Gatteschi and R. Sessoli, *Angew. Chem., Int. Ed.*, 2003, **42**, 268.

21. S. Wang, H.-L. Tsai, K. S. Hagen, D. N. Hendrickson and G. Christou, *J. Am. Chem. Soc.*, 1994, **116**, 8376.

22. J. S. Bashkin, H.-R. Chang, W. E. Streib, J. C. Huffman, D. N. Hendrickson and G. Christou, *J. Am. Chem. Soc.*, 1987, **109**, 6502.

23. Q. Li, J. B. Vincent, E. Libby, H.-R. Chang, J. C. Huffman, P. D. W. Boyd, G. Christou and D. N. Hendrickson, *Angew. Chem., Int. Ed. Engl.*, 1988, **27**, 1731.

24. S. Wang, K. Folting, W. E. Streib, E. A. Schmitt, J. K. McCusker, D. N. Hendrickson and G. Christou, *Angew. Chem., Int. Ed. Engl.*, 1991, **30**, 3050.

25. D. N. Hendrickson, G. Christou, E. A. Schmitt, E. Libby, J. S. Bashkin, S. Wang, H.-L. Tsai, J. B. Vincent, P. D. W. Boyd, J. C. Huffman, K. Folting, Q. Li and W. E. Streib, *J. Am. Chem. Soc.*, 1992, **114**, 2455.

26. S. M. J. Aubin, M. W. Wemple, D. M. Adams, H.-L. Tsai, G. Christou and D. N. Hendrickson, *J. Am. Chem. Soc.*, 1996, **118**, 7746, and references therein.

27. W. Wernsdorfer, N. Aliaga-Alcalde, D. N. Hendrickson and G. Christou, *Nature*, 2002, **416**, 406.

28. S. Hill, R. S. Edwards, N. Aliaga-Alcalde and G. Christou, *Science*, 2003, **302**, 1015.

29. T. Lis and B. Jezowska-Trzebiatowska, *Acta Cryst.* 1977, **B33**, 2112.

30. S. Wang, H.-L. Tsai, E. Libby, K. Folting, W. E. Streib, D. N. Hendrickson and G. Christou, *Inorg. Chem.*, 1996, **35**, 7578.

31. M. W. Wemple, H.-L. Tsai, K. Folting, D. N. Hendrickson and G. Christou, *J. Am. Chem. Soc.*, 1995, **117**, 7275.

32. M. W. Wemple, D. M. Adams, K. S. Hagen, K. Folting, D. N. Hendrickson and G. Christou, *J. Chem. Soc. Chem. Commun.*, 1995, 1591.

33. G. Aromí, M. W. Wemple, J. S. Aubin, K. Folting, D. N. Hendrickson and G. Christou, *J. Am. Chem. Soc.*, 1998, **120**, 5850.

34. G. Aromí, S. Bhaduri, P. Artus, K. Folting and G. Christou, *Inorg. Chem.*, 2002, **41**, 805.

35. W. Liu and H. H. Thorp, *Inorg. Chem.*, 1993, **32**, 4102.

36. O. Kahn, *Molecular Magnetism*, Wiley-VCH, 1983.

37. B. N. Figgis and M. A. Hitchman, *Ligand Field Theory and its Applications*, Wiley-VCH, 2000.

38. C. Görller-Walrand and K. Binnemans, in *Handbook on the Physics and Chemistry of Rare Earths*, Vol. 23 (Ed.: J. K. A. Gschneidner and L. Eyring), Elsevier, 1996, p. 121.

39. B. G. Wybourne, *Spectroscopic Properties of Rare Earths*, Wiley, 1965.

40. E. König and S. Kremer, *Magnetism Diagrams for Transition Metal Ions*, Plenum Press, 1979.

41. H. Schilder and H. Lueken, *J. Magn. Magn. Mater.*, 2004, **281**, 17.

42. Y.-M. Lee, S. Hong, Y. Morimoto, W. Shin, S. Fukuzumi and W. Nam. *J. Am. Chem. Soc.*, 2010, **132**, 10668.

43. S. C. Payne, K. S. Hagen, *J. Am. Chem. Soc.*, 2000, **122**, 6399.

44. K. S. Hagen, S. G. Naik, B. H. Huynh, A. Masello, G. Christou, *J. Am. Chem. Soc.*, 2009, **131**, 7516.

45. L.-H. Bi, U. Kortz, S. Nellutla, A. C. Stowe, J. van Tol, N. S. Dalal, B. Keita, and L. Nadjo, *Inorg. Chem.*, 2005, **44**, 896.

46. L.-H. Bi, U. Kortz, B. Keita, L. Nadjo, H. Borrmann, *Inorg. Chem.* 2004, **43**, 8367.

47. L.-H. Bi, M. Reicke, U. Kortz, B. Keita, L. Nadjo, R. J. Clark, *Inorg. Chem.* 2004, **43**, 3915.

48. *Bruker APEX2*, Bruker AXS Inc., Madison, Wisconsin, USA, 2007.

49. *Bruker, SAINT*, Bruker AXS Inc., Madison, Wisconsin, USA, 2007.

50. G. Sheldrich, *Sadabs, 2.10 edition*, 2003.

51. Bruker 2007 program: G. M. Sheldrick, A short history of SHELX, *Acta Crystallogr., Sect. A: Fundam. Crystallogr*., 2008, **64**, 112-122.

52. T. L. Jorris, M. Kozik, N. Casan-Pastor, P. J. Domaille, R. G. Finke, W. K. Miller, L. C. W. Baker, *J. Am. Chem. Soc.*, 1987, **109**, 7402.